Universidad de Málaga

Escuela Técnica Superior de Ingeniería de Telecomunicación

UNIVERSIDAD DE MÁLAGA

Programa de Doctorado en Ingeniería de Telecomunicación

TESIS DOCTORAL

A Broadband Cavity-Backed Slot for Series-Fed Arrays

Autor:

Alberto Hernández Escobar

Directores:

Elena Abdo Sánchez

Carlos Camacho Peñalosa

Acknowledgements

First of all, my most sincere gratitude to Prof. Jaime Esteban from the Universidad Politécnica de Madrid for his advice in multiple topics, collaboration, and invaluable assistance in the measurement of the prototypes. Because part of this work is also his.

In addition, I want to express my gratitude to both of my supervisors, Elena Abdo Sánchez and Carlos Camacho Peñalosa. It has been a real pleasure to work and learn alongside them all these years. Also, I want to thank Teresa Martín Guerrero for her cheerfulness and contribution to the work.

This thesis was carried out in the framework of the program for the training of university professors (Programa para la Formación del Profesorado Universitario) by the Spanish Ministerio de Educación, Cultura y Deporte, under grant FPU15/06457. Besides, it was also supported in part by the Spanish Ministerio de Ciencia, Innovación y Universidades (MCIU), the Agencia Estatal de Investigación (AEI), and the Fondo Europeo de Desarrollo Regional (FEDER) (Programa Estatal de I+D+i Orientada a los Retos de la Sociedad) under grant RTI2018-097098-J-I00, in other part by the Spanish Ministerio de Economía y Competitividad, under project ADDMATE TEC2016-76070-CR3-3-R, and in other part by the European Union's Horizon 2020 research and innovation programme under the Marie Sklodowska-Curie, under grant No. 706334.

Lastly, I would to dedicate this paragraph to all my current and past colleagues for their unconditional support and the good time we have spent together. Thank you.

Abstract

In this Ph.D. thesis, an upgraded version of the complementary strip-slot radiating element is proposed. The original radiating element consists of a microstrip-fed slot in transmission configuration. In the proposed modification, the slot is backed by a cavity in order to obtain unidirectional radiation. The presence of this cavity changes the mode of the slot. After a comprehensive study of this particular slot mode, a broadband method to obtain its propagation constant is explored. Then, an equivalent circuit that models a cavity-backed slot fed by a strip is extracted. The equivalent circuit separates the effect of the slot and the feeding and provides physical insight into the radiating element. As in the original complementary strip-slot, the bandwidth of the slot is greatly enhanced by the use of a stub. A complete equivalent circuit is used to propose a design methodology for broadband operation. The potential of the radiating element for building series-fed arrays is highlighted through two different antenna configurations: a phased array and a log-periodic array. Promising experimental results verify the unidirectional radiation and the wide bandwidth of these antennas.

Contents

List of Figures

Chapter 1

Introduction

The objective of this first, introductory chapter is to illustrate the topic of this dissertation. First, the contextual framework of the work is shown. Next, the motivations and origins that have led to starting this research are presented and, then, its main objectives are provided. Lastly, the original contributions of the thesis are discussed as the structure of the content is shown.

1.1 Contextual Framework

Now more than ever, the world needs to be fully interconnected by digital means. The efforts of the past years have allowed reducing what before was inevitable mobility and physical interaction, in addition to increasing the working efficiency of developed countries. However, more work must be done in order to achieve real-time global communications that are accessible to everyone. For this aim, extremely high bitrates are also required in wireless links.

In the latest tendencies in wireless communications, namely, in the fifth generation of mobile communications (5G), the use of higher frequency bands is proposed to increase the bitrate, since more bandwidth is available at such bands. For this reason, the mm-wave band (30 GHz – 300 GHz) has recently gained attention. The initial focus has been on 24, 28, and 39 GHz bands but now even the E-band (60 GHz) and V-band (70/80 GHz) are being considered. Even more promising bands include the W-band (100 GHz) and the D-band (150 GHz). This is just an example of how the traditional narrow-band wireless communications are being discarded in favor of higher-frequency,

wideband systems.

Despite the fact that the antenna design in the context of communication systems is one of the most classic challenges in telecommunication engineering, the antennas for new applications and recently-appeared services may require special attention in their development or further research. These enhanced functionalities can include wide bandwidth, high efficiency, high directivity, small size, low cost, and easy integration.

Slot-like radiators have been traditionally strong candidates when designing high-performance small antennas due to their many advantages, such as lightweight, high cross-polarization discrimination, low profile, and low manufacturing cost. Furthermore, they can be implemented using different technologies such as microstrip or waveguide. For these reasons, they may be a good solution for the antennas of future communication systems.

However, although the bandwidth of these radiators is enough for narrow-band applications, it will be insufficient for more-demanding, high-bitrate systems. Slot radiating elements have a very resonant nature which compromises their impedance bandwidth considerably. There are some techniques to slightly broaden their impedance bandwidth, like using wide slots or decentering the element with respect to their feeding. However, all of them introduce serious drawbacks. The first one worsens its radiation characteristics and the second one makes the slot radiate less power over an even narrower bandwidth.

In [1], a brand new method for increasing the bandwidth of microstrip-fed slots was proposed. The method consists of adding a strip on the microstrip line which completely cancels the reactance of the slot and, thus, increasing its bandwidth. Actually, if the dimensions of the strip are chosen properly, the impedance bandwidth of the resulting radiating element can be theoretically unlimited. This solution does not introduce new drawbacks and, additionally, is simple, easy to implement, and its design is straightforward. This new element has proven to be a solid radiator for building arrays, such as Leaky-Wave Antennas (LWAs) [2] or log-periodic arrays [3].

Microstrip-fed slots, however, radiate towards both half-spaces, since it consists of a slot printed on a single ground plane. This means that there will be at least two main beams when an array made of this element is built. Thus, they can be a poor antenna choice when a single, directional beam is desired that does not waste power on an additional beam. To eliminate one of the beams, it is possible to use a reflector plane behind the slot, as in [3]. However, the optimum distance between the reflector

and the radiator is frequency-dependent, which reduces the bandwidth of the element. Furthermore, this solution increases the size of the antenna significantly and removes its planar profile, which was one of the main advantages of using a microstrip antenna.

An alternative solution is the use of a Cavity-Backed Slot (CBS). These slots are printed on the surface of a closed cavity instead of on a single-layer ground plane. Their radiation is unidirectional because the cavity blocks the radiation towards one half-space. CBSs were studied long before [4] and their use has increased recently due to their good performance and fabrication using post-wall waveguide (also called Substrate Integrated Waveguide [SIW]) [5]. Despite this, its previous analyses did not provide physical insight about how the radiator works, and their design equations were too complex for their practical use or the elaboration of an equivalent circuit. Of course, the bandwidth problem had not been solved for the CBSs as elegantly as in [1], and the addition of the cavity can make the radiator quite bulky at lower frequencies compared to microstrip-fed slots. Still, applying the same matching technique to CBSs is very interesting in order to obtain a wideband, unidirectional slot-like radiating element.

Consequently, the search for novel matching techniques to increase the bandwidth of CBSs seems to be an attractive topic for the antenna community. Applying the matching technique from [1] to this type of slot can, then, be very interesting from a practical point of view. Furthermore, to do this, the understanding and physical insight of these, more complex, slots can help their design and further enhance their radiation properties.

1.2 Genesis

The core of this Ph.D. thesis emerged while trying to obtain a new broadband radiating element that could be useful to design antenna arrays for 5G communication systems and, for that, a unidirectional-radiating element was necessary. There was an attempt of fixing the bilateral problem of the microstrip-fed slot by using stripline instead of microstrip. In this manner, the concept of the complementary strip-slot from [1] was applied to design a stripline-fed slot with a matching stub to obtain unidirectional radiation.

However, it was found out that the impedance of the slot did not behave as expected by the classic slotline theory, which was the model used in the traditional complementary strip-slot. The metallic walls of the stripline were acting as a cavity, and the slot

was, then, a CBS. In this type of slot, the size of the cavity (the distance between the walls of the stripline in this case) has a significant impact on its behavior.

Although it was proved that by properly adjusting the size of the cavity it was possible to obtain a broad matching, the simple transmission-line model lacked the precision to model the slot. A simple and useful model was not found in the literature and, thus, further research of CBSs was needed. At this moment, our understanding of the slot increased considerably. The mode that propagates inside the cavity is the slot mode of a rectangular waveguide, which has a cut-off frequency. Using that mode, it was possible to extract a transmission-line equivalent circuit for the slot which obtained accurate results for different values of the slot length.

This particular mode that was propagating inside the structure sparkled our interest and, thus, a method for obtaining its propagation constant was also developed. Our group had extensive experience in applying an enhanced version of the method proposed by Bianco and Parodi [6] to different structures. This way, a specialized method to obtain more information about the slot mode was obtained.

1.3 Objectives

The first goal was to obtain a unidirectional radiating element for series-fed arrays based on the concept of the complementary strip-slot. Since to achieve the first goal a CBS was used and its model was not straightforward, additional goals included the understanding of the CBS enough to elaborate a transmission-line model. Then, an equivalent circuit and design procedure for the new radiating element had to be developed.

Once the element was completely characterized, the aim was to use the array configurations explored with the complementary strip-slot to obtain single-beam arrays. Due to the element series feeding, the focus was on series-fed arrays.

It is important to point out that a self-imposed requirement was to corroborate the conclusions extracted from theory and electromagnetic simulations with the manufacture of prototypes at each step of the research, in order to prove the concepts with the experimental verification of the designs.

The final object of this research work was to design high-performance antennas using a broadband series-fed CBS and highlight the potential of this matching technique to obtain non-resonant radiators.

1.4 Thesis Outline and Contributions

This section provides a brief explanation of the contents of each chapter and highlights the most relevant contributions of the related work.

Chapter 2 starts with the description of the slot mode of a rectangular waveguide. Afterward, two ways of characterizing the mode are presented. The first one uses a commercial electromagnetic simulator to obtain information from a waveguide segment, which produces fast but inaccurate results at some frequencies. The second one derives from the method proposed by Bianco and Parodi in [6] and uses several slot lengths to obtain the value of the propagation constant of the mode in a very wide bandwidth. A simple structure is proposed and fabricated to apply the method, and measurements are obtained. The main contribution of this chapter is the application of this second method, although the acknowledgment of the slot mode and its simple excitation through a strip is also relevant.

The aforementioned mode is used to elaborate on the operation of the CBS by proposing an equivalent transmission-line circuit in ***Chapter 3***. The main part of the equivalent circuit is composed of a transmission line with the propagation constant of the slot mode and a length equal to the one of the slot. Also, the slot end-effect and its distance to the feeding strip is taken into account. This equivalent circuit is an important contribution that helps to understand the operation of CBSs.

In ***Chapter 4*** the concept of the complementary strip-slot is applied to a CBS to significantly increase its bandwidth. Its design procedure and equivalent circuit are studied. Also, two prototypes were fabricated and measured using different technologies. The proposed bandwidth-enhancing method is compared to a more classic one to highlight its advantages. Lastly, two ways to increase even more the bandwidth of the radiating element are illustrated by two additional designs. One of them is designed to be used in the millimeter-wave band with promising results. The most significant contribution of this chapter is a wideband radiator with good radiation properties and a unidirectional beam while being simple in form and design.

Once the element is studied, array applications are explored. Due to the feeding of the element, series-fed arrays are considered. Hence, the first part of ***Chapter 5*** contains the first and immediate array concept, built by cascading several strip-fed CBS elements. With a simple prototype, a Leaky-Wave Antenna (LWA) with scanning capabilities is fabricated and measured. Full scanning from backward to

forward (including broadside) angles is achieved. The second part of ***Chapter 5*** deals with the idea of a log-periodic array based on the broadband CBS. The challenge here is to adapt the radiating element to reduce the distance between them despite the cavity. Also, the mutual coupling between the elements has to be reduced. A prototype was built to prove the concept.

Finally, ***Chapter 6*** summarises the main results and stresses the most significant contributions derived from this thesis. It concludes with the proposal for guidelines to carry on with this work in the future.

In addition, two appendices are included to expand on the provided contents. Appendix A shows the measurement of the propagation constants of coupled microstrip lines using a method similar to the one proposed in Chapter 2. In Appendix B a new circuit topology for asymmetric structures is studied. The circuit configuration separates the eigenmodes as the lattice network does for symmetric structures. The publications derived from this thesis are enumerated in Appendix C. Lastly, Appendix D contains a summary of the thesis in Spanish.

Chapter 2

The Slot Mode of a Rectangular Waveguide

Leaky-wave antennas (LWA) are popular candidates for high-performance applications due to their many advantages, including high directivity, large bandwidth, frequency-scanning capabilities, and simple fabrication. Among them, slotted waveguides have received significant attention lately [7, 8] since they can be built using the Substrate Integrated Waveguide (SIW) [9], which reduces its weight and cost. In LWAs, it is very important to know and control the propagation characteristics of the leaky mode of the structure. Although several analytical methods and equivalent circuits are used to calculate the attenuation (leakage factor) and phase constants [10–12], their measurements are obtained from the measured radiation patterns [13] in single-frequency points or over a small bandwidth.

Usually, the perturbed TE_{10} mode of the rectangular waveguide propagates along the slotted waveguide as the leaky mode. However, the slot mode has been recently used instead of the TE_{10} as the leaky mode for fixed-beam capabilities [7]. In particular, this mode is one of the focus of this thesis and it is used in the following chapters as the radiation mode of slot antennas.

The slot mode of a rectangular waveguide was found for the first time in [14] as an undesirable mode when the used leaky-wave mode was the perturbed TE_{10} mode of the waveguide [15], but, to the authors' knowledge, no further attempts to analyze it have been made. Since it is difficult to properly excite a slot mode in full-wave simulation using waveports, the extraction of the propagation constant of this mode is

not straightforward, even using commercial electromagnetic simulators. This chapter focuses on the study of this slot mode with the aim of finding a measurement method able to extract its propagation constant.

This chapter is structured as follows. First of all, the mode is characterize using simple methods in Section 2.1. In Section 2.2, a more accurate measurement method for the propagation constant is described and its results shown. Finally, Section 2.3 summarizes the main conclusions of the measurement technique.

2.1 Characterization of the Slot Mode of a Rectangular Waveguide

The presence of a longitudinal slot in a classic rectangular waveguide allows the propagation of the slot mode. The electric field distribution of this mode in a rectangular waveguide is shown in Fig. 2.1. It can be observed that this field distribution closely resembles that of the TEM mode of an ordinary slotline. The slot mode of a rectangular waveguide, however, has a cut-off frequency since there is only one conductor in the structure. This cut-off frequency, f_c, however, is highly dependent on the width of the slot and the dimensions of the section of the waveguide and, to the authors' knowledge, its analytical expression has not been reported in the literature yet.

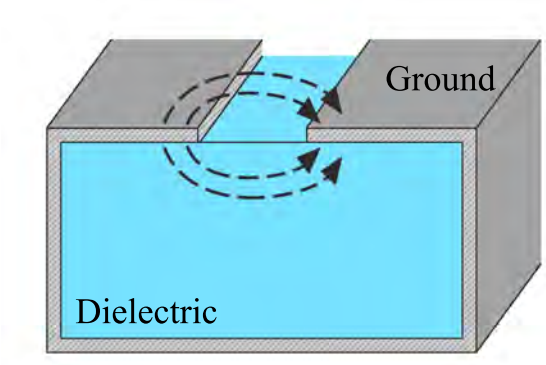

Figure 2.1: Electric field vector distribution of the slot mode in a rectangular waveguide.

As in slotlines, the slot mode of a rectangular waveguide is almost Transverse Electric (TE) in nature [16]. Besides, even in presence of Perfect Electric Conductor (PEC) and lossless dielectrics only, there are losses due to the radiation of the structure. For these reasons, in order to model the frequency-dependent behavior of its propagation constant and impedance, a lossy TE-mode will be considered. The propagation con-

stant and the characteristic impedance of a TE-mode in a lossy medium enclosed by PEC, as shown in [17], are given by

$$\gamma_{CBS} = j\frac{2\pi f\sqrt{\varepsilon_r' - j\varepsilon_r''}}{c}\sqrt{1-\left(\frac{f_c}{f}\right)^2\frac{\varepsilon_r'}{\varepsilon_r' - j\varepsilon_r''}} \tag{2.1}$$

$$Z_0 = \frac{Z_m}{\sqrt{\varepsilon_r' - j\varepsilon_r''}\sqrt{1-\left(\frac{f_c}{f}\right)^2\frac{\varepsilon_r'}{\varepsilon_r' - j\varepsilon_r''}}}, \tag{2.2}$$

where c is the speed of light in vacuum, and the electric permittivity of the medium, ε_r, is split into its real and imaginary parts as follows:

$$\varepsilon_r = \varepsilon_r' - j\varepsilon_r''. \tag{2.3}$$

The value of the impedance Z_m depends on the impedance of free space, the geometry of the section of the structure, the ε_r of the material inside the cavity, and the voltage definition (the possible definitions can be checked in [18]). Therefore, all these parameters will only depend on the dimensions of the transverse section of the structure shown in Fig. 2.1 and the medium inside the cavity. Even though these expressions are only valid for closed structures, they show great concordance with the subsequent results of this chapter.

2.1.1 Simulation Attempts for Characterizing the Mode

In order to characterize the mode, a slotted rectangular waveguide has been simulated using the commercial software HFSS. The simulated structure is shown in Fig. 2.2. The inner height of the waveguide is 8 mm, the inner width 20 mm, and the width of the slot is 1 mm. The length of the waveguide is 80 mm. The waveguide is made of aluminium with a thickness of 6 mm, and its top layer made of a layer of copper with thickness of 0.4 mm. The waveguide is filled with Eccostock SH (ε_r of 1.17 for the 2-10 GHz frequency range according to an in-house previous measurement and estimated loss tangent of 0.003). This bizarre waveguide composition is justified in a later section of the chapter. The structure is fed using waveports, and the propagation constant is computed using the pertinent function of HFSS. However, a disturbing phenomenon is observed: the propagation constant of the mode changes with the port height, ph. This phenomenon is illustrated in Fig. 2.3, where the real part, α, and the imaginary part β of the HFSS-simulated structure is shown. Furthermore, the S-parameters for

each case are different. The only feasible explanation to this is that the calculated propagation constant is not that of the slot mode. Instead, the propagation constant that is being calculated is that of a sort of double-ridge waveguide, since the HFSS waveports build a rectangular waveguide with the metal layer of the slot acting as the ridges. This render the simulation using waveports almost useless for analyzing this mode and, thus, other alternatives are explored in this chapter.

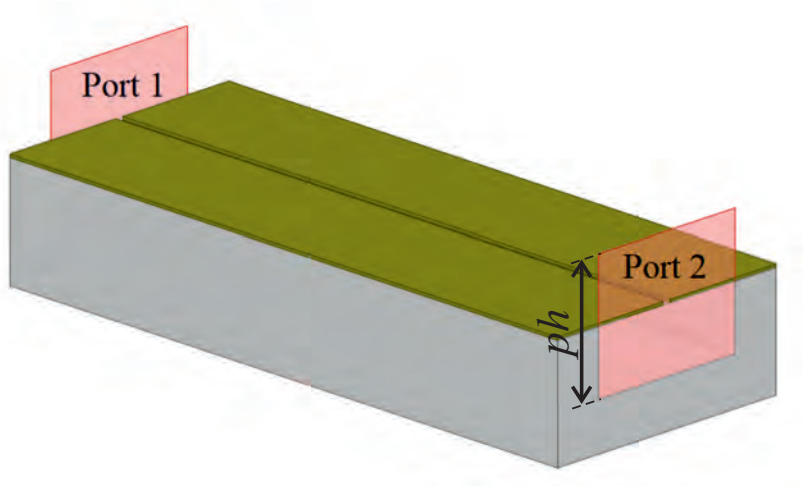

Figure 2.2: Slotted rectangular waveguide simulated in HFSS using waveports.

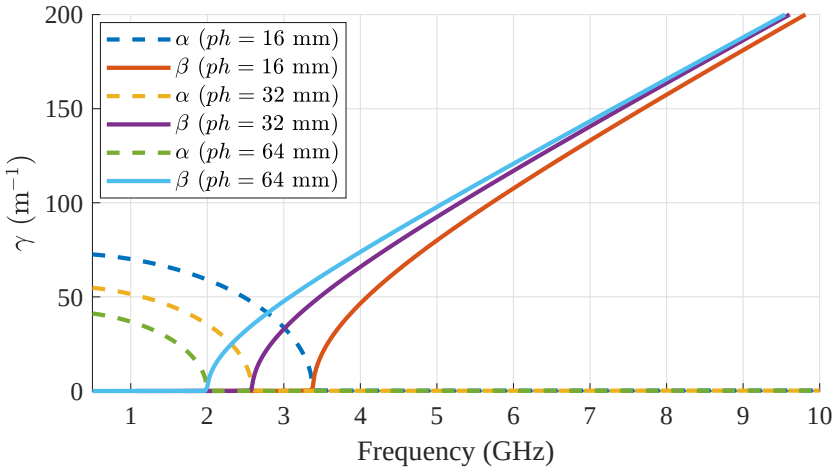

Figure 2.3: Propagation constant of the slot mode of a rectangular waveguide for different port heights using HFSS waveports.

To avoid this problem and properly excite the slot mode, the waveguide has been fed using two lumped ports. To do this, the waveports of Fig. 2.2 have been replaced by lumped ports, placed between the edges of the slot in each of its ends. The dimensions of the structure remain the same. When doing this, there will be an open circuit in each end of the waveguide which will disrupt the desired results. However, more reliable

data can be obtained from this sort of simulation than using waveports. From the S-parameters of the simulated segment, the image parameters can be obtained using, as shown in [19],

$$\gamma_{im} = \cosh^{-1}\left(\frac{1 - S_{11}^2 + S_{21}^2}{2S_{21}}\right) \tag{2.4}$$

$$Z_{im} = Z_{0,ref}\sqrt{\frac{(1+S_{11})^2 - S_{21}^2}{(1-S_{11})^2 - S_{21}^2}}, \tag{2.5}$$

where $Z_{0,ref}$ is the reference impedance used to obtain the S-parameters. Then, from the definition of the image parameters, the impedance of the mode, Z_0, is equal to Z_{im}, and the propagation constant, γ, is γ_{im}/l, where l is the length of the simulated waveguide segment. Fig. 2.4 and Fig. 2.5 show, respectively, the γ and Z_0 obtained for three different waveguide lengths, 40, 80, and 120 mm. However, for shorter lengths, the effect of the open-circuit significantly alters the results and for longer lengths, ripples appear at more frequencies (the effect is more significant in the plot of Z_0). At these frequencies, the length of the waveguide is a multiple of half-wavelength ($\beta l = k\pi$), so the structure gives little information about itself. It is believed that these resonances make the simulation results extremely sensitive to the parasitic effects introduced by the lumped ports and the end-effect of the waveguide. Simulating shorter lines is not recommended since the higher-order modes produced by the lumped-port excitation must attenuate enough to obtain accurate results.

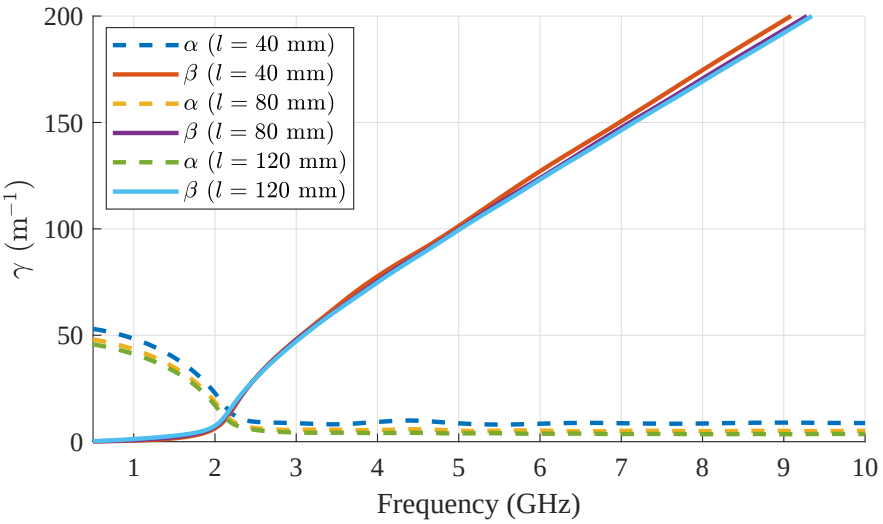

Figure 2.4: Propagation constant of the slot mode of a rectangular waveguide for different segment lengths using HFSS lumped ports.

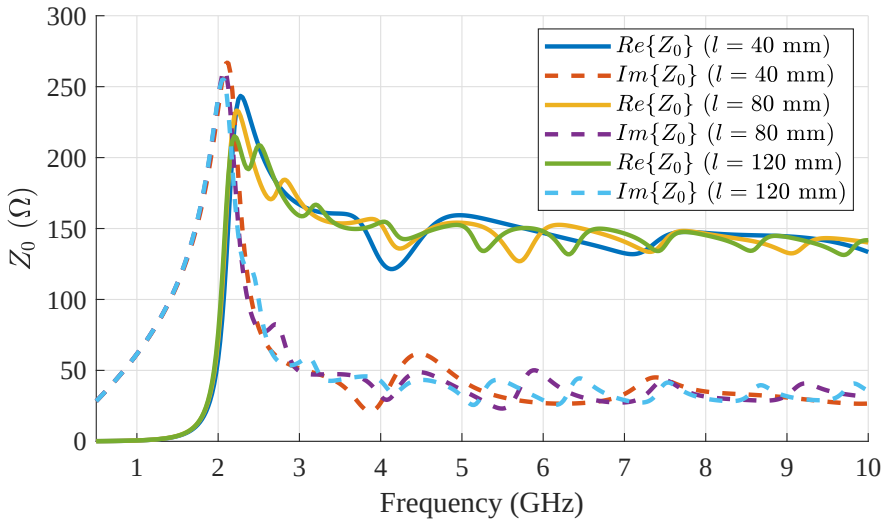

Figure 2.5: Impedance of the slot mode of a rectangular waveguide for different segment lengths using HFSS lumped ports.

2.2 Broadband Determination of the Propagation Constant

The simulation attempts proposed in the previous section to obtain the propagation constant of this mode are not satisfying. The first one, especially, is not useful. The second one, however, has the disadvantage of being inaccurate at some frequencies and somewhat dependant on the length of the simulated segment. Furthermore, if the structure wants to be measured, the implementation of lumped ports entails a challenge which can introduce even more errors. For these reasons, another more reliable method to measure the propagation constant is proposed in this section.

A consolidated method for measuring the propagation constant of the microstrip-line mode is the algorithm proposed by Bianco and Parodi several decades ago [6, 20]. Very recently, a modification of this method was used to propose a broadband determination of the propagation constants of the even and odd modes of coupled lines, which is detailed in the Appendix A. Here, a measurement procedure of the propagation constant of the slot mode in a rectangular waveguide is presented. The propagation constant is obtained from the data of a simulated or measured waveguide with different slot lengths. The proposed method follows the idea of separating the even and odd modes of the structure in order to isolate the contribution of the slot mode, the odd mode in this case. In contrast with other methods in the literature, it allows the measurement of the attenuation and phase constants of leaky modes over a

very broad bandwidth without measuring radiation patterns. This can be especially useful in cases where the substrate permittivity or final dimensions of the structure are not accurately known.

2.2.1 Measurement Technique

The method proposed in [6] is based on the measurement of the reflection coefficient at the input of four identical and equally-terminated waveguides of different lengths. Using the invariance of the cross-ratio of complex numbers under a bilinear transformation, it is possible to extract the propagation constant, γ. The cross-ratio Γ_{1234} can be defined using the four measured reflection coefficients, Γ_1, Γ_2, Γ_3 and Γ_4 as:

$$\Gamma_{1234} = \frac{(\Gamma_1 - \Gamma_2)(\Gamma_3 - \Gamma_4)}{(\Gamma_1 - \Gamma_3)(\Gamma_2 - \Gamma_4)} \tag{2.6}$$

and, then, the following equation can be written:

$$\Gamma_{1234} = \frac{\left(1 - e^{-2\gamma\delta_{21}}\right)\left(e^{-2\gamma\delta_{31}} - e^{-2\gamma\delta_{41}}\right)}{\left(1 - e^{-2\gamma\delta_{31}}\right)\left(e^{-2\gamma\delta_{21}} - e^{-2\gamma\delta_{41}}\right)} \tag{2.7}$$

where δ_{ij} is the difference between the lengths of the i and j waveguides. Solving (2.7) at each frequency point, it is possible to obtain the value of γ over a wide bandwidth. With the statistical improvement proposed in Appendix A, it is possible to increase the accuracy of the method by using a larger number of terminated lines (see Appendix A for more details).

However, in a slotted rectangular waveguide, several modes (e.g. the slot mode or the TE_{10} mode) can propagate at once and, thus, the obtained γ does not necessarily correspond to the desired mode. In order to solve this problem, two-port measurements can be taken and the same strategy that allowed the measurement of the even and odd modes in microstrip coupled lines can be reinterpreted to measure only the slot mode. Indeed, after an analysis of the modes propagating in a slotted rectangular waveguide, the slot mode can be identified with the odd mode of the structure, whereas the TE_{10} mode corresponds to the even mode. The method proposed in Appendix A, designed to calculate the propagation constants of the odd and even modes of coupled lines, can then be applied. Its application to this structure allows obtaining the slot-mode propagation constant as the provided propagation constant for the odd mode. This way, the reflection coefficients in (2.6) must be obtained from two-port measurements

as

$$\Gamma_{slot-mode} = (s_{11} + s_{22})/2 - (s_{12} + s_{21})/2. \tag{2.8}$$

Note that the averages of the S parameters have been used to enforce symmetry, which is not guaranteed in real measurements.

This method has several advantages. For example, it is insensitive to the termination used (as long as it is the same for every line, terminations with a high reflection coefficient are preferred), the characteristic impedance of the waveguide, and the feeding network (as long as it properly feeds the structure). The main drawbacks are the fact that several waveguides must be fabricated and every feeding network and termination must be identical to obtain accurate results, which is not realistic. In Appendix A, these problems were solved by using a destructive method, which consisted in fabricating only the longest line and cutting it before a new measurement to obtain a different length. This approach, however, can only be used when the manufacturing method allows it.

A middle-ground solution between fabricating several waveguides and the destructive method is proposed. The solution lies in the fabrication of a waveguide structure able to have different slot lengths. Its 3D model is shown in Fig. 2.6. The main part of the rectangular waveguide is made of an aluminum U-shaped structure, topped with a copper sheet with the slot printed on it. Another sheet of copper is used for the slot short-circuit. This way, this layer is replaced for each simulation/measurement instead of replicating or destructing the structure, assuring the same connectors and feeding network are used for each case. Thus, it is possible to change the apparent length of the waveguide without having to damage or replicate the whole structure. The waveguide is filled with a solid material to increase the robustness of the structure, but the same principle could also be applied to a hollow waveguide. A challenge found when applying the proposed method to determine the slot-mode propagation constant lies in the choice of the excitation since it must guarantee that the slot-mode is properly excited. For this reason, the waveguide is fed by a microstrip line with a slot mechanized on its ground plane, which is properly aligned with the slot layer used as the cover of the waveguide. The different layers of the structure (from top to bottom: microstrip, short-circuit, slot, dielectric, and waveguide) are fixed using steel screws (represented in Fig. 2.6 as cylinders).

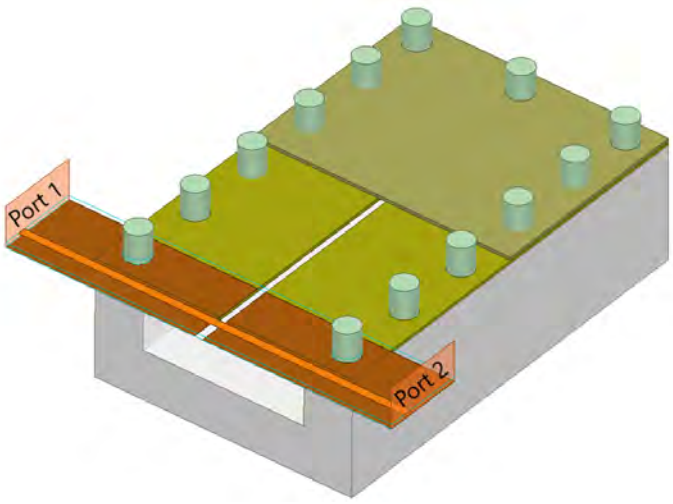

Figure 2.6: 3D model of the proposed structure for fabrication.

2.2.2 Results

The proposed measurement technique has been applied to simulated and measured data in order to prove that it can be used to measure the propagation constant of the slot mode of a rectangular waveguide. Fourteen structures, each one with a different length of the short-circuit layer, were simulated using the commercial software HFSS. For the measured case, thirteen short-circuit layers were fabricated to change the length of the slot. Depending on which short-circuit layer is used, a different slot length is obtained. These lengths are 25.0, 50.9, 76.9, 101.3, 117.3, 131.3, 144.6, 160.0, 172.4, 187.9, 200.6, 222.0, 248.7, and 275.0 mm. The waveguide is the same as that of the simulated in the previous section. To avoid the bending of the slot copper sheet, a piece of low-loss dielectric material (Eccostock SH) is introduced inside the waveguide. The substrate of the feeding microstrip is Rogers RO4350B with $\varepsilon_r = 3.66$, height of 0.51 mm, and copper thickness of 0.0175 mm. The width of the microstrip line is 1 mm (impedance of $Z_0 = 50\ \Omega$) and it is placed on the edge of the waveguide. The steel screws have a diameter of 3 mm and are placed with a separation of 9 mm between them. Fig. 2.7 shows the fabricated structure.

Fig. 2.8 shows the fabricated structure when a longer slot is being measured. From the two-port measurements and simulations of each waveguide length, the reflection coefficients of the slot mode, $\Gamma_{slot-mode}$, in (2.8), are obtained. From the cross-ratio of the reflection coefficients, the propagation constant, γ, is found. The simulation and experimental results are plotted in Fig. 2.9 by showing the propagation constant of the slot mode from its cut-off frequency up to 10 GHz. This method, however, cannot

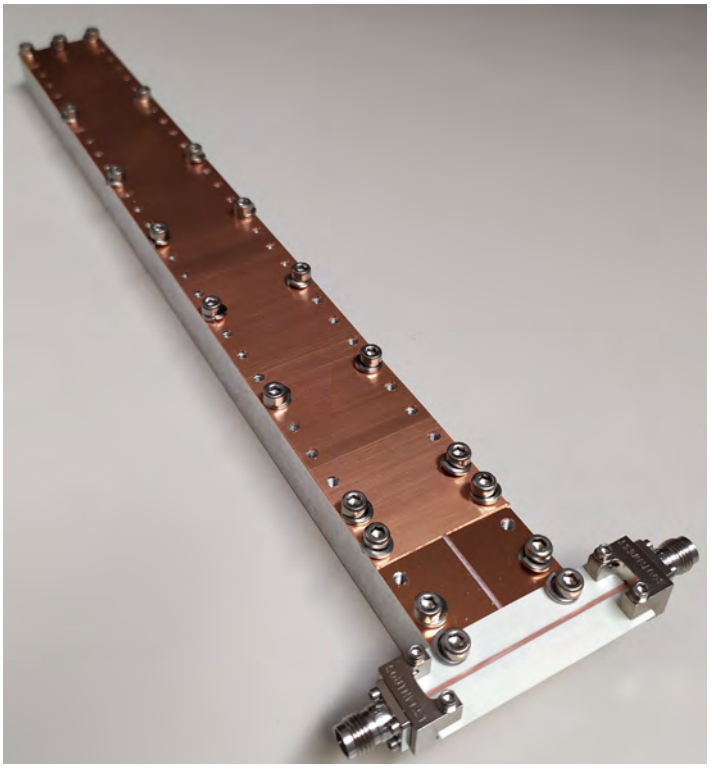

Figure 2.7: Fabricated structure with a effective slot length of 25 mm.

predict the values of the propagation constant when the mode is under cut-off since the reflection coefficient of every waveguide is the same and the cross-ratio of (2.7) results in an indetermination. The results are compared with the propagation constant of (2.1) when f_c is 2.1 GHz and ε_{reff} is $1.09 - j0.58/f(GHz)^2$. These values of the model parameters were obtained heuristically from the simulation results. Discrepancies in the attenuation constant between simulation, measurement, and model are expected because the measurements were not made in an anechoic chamber and part of the losses of the structure at higher frequencies is due to radiation. Furthermore, the original method, on which the proposed procedure is based, is less accurate for computing the attenuation constant. Since its value is very low, its determination is more sensitive to errors. Nevertheless, the agreement between simulations and measurements is excellent for the phase constant and very good for the attenuation constant up to 5 GHz. The agreement between the model and the simulation and measurements indicate that the frequency dependence of the extracted results behaves as expected.

An additional case is also provided there. The same waveguide was filled with Teflon instead, and the same measurements were performed. Three layers of Teflon were needed to completely fill the structure. Fig. 2.10 shows the propagation constant of the mode after applying the same technique to the measured and simulated results,

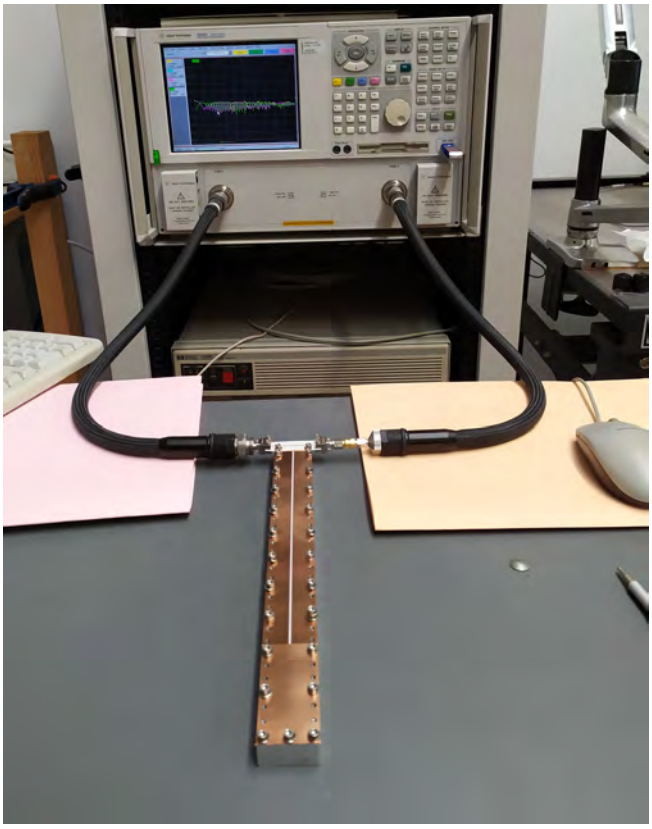

Figure 2.8: Fabricated structure with a shorter short-circuit layer to produce an effective slot length of 200.6 mm being measured.

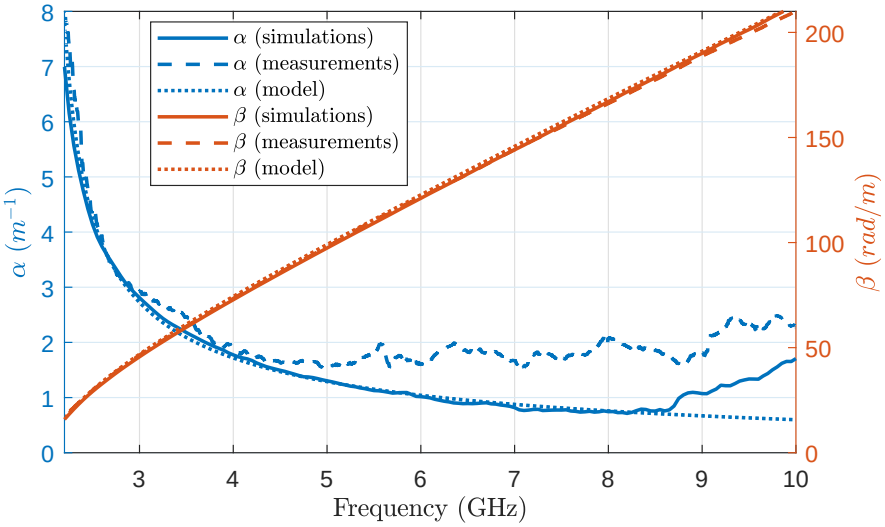

Figure 2.9: Value of the propagation constant after applying the proposed method to the simulated and measured data of 14 structures filled with Eccostock SH. The solid lines correspond to the method applied to simulation data, whereas the dashed lines represent the results from measurements. Additionally, the model of (2.1), adjusted from simulation data, is plotted as dotted lines.

compared again with the model of (2.1). The parameters model, in this case, are $f_c = 1.9$ GHz and $\varepsilon_{reff} = 1.43 - j0.39/f(GHz)^2$. A discrepancy between the simulated and measured phase constant is found. It is believed that it is due to using three layers of Teflon instead of a solid block, which can reduce the effective dielectric constant. Again, despite the determination of the losses being difficult, the propagation constant behaves as expected with frequency.

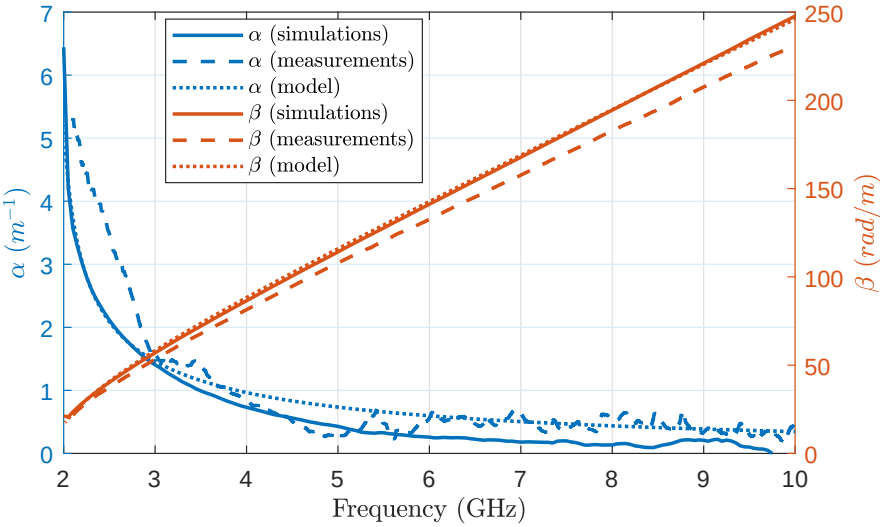

Figure 2.10: Value of the propagation constant after applying the proposed method to the simulated and measured data of 14 structures filled with Teflon. The solid lines correspond to the method applied to simulation data, whereas the dashed lines represent the results from measurements. Additionally, the model of (2.1), adjusted from simulation data, is plotted as dotted lines.

2.3 Conclusion

The slot mode of a rectangular waveguide was presented in this chapter. It was shown that the characterization of the mode through electromagnetic simulations is not straightforward: the waveports of HFSS do not work as expected for this mode and the use of lumped ports carry new problems. For this reasons, a broadband method to determine its propagation constant was proposed. Additionally, a physical implementation has been developed and fabricated in order to apply the technique to measurements. The experimental results have been corroborated with simulations. The method has been applied to simulated and measured data using two different filling materials, and have been compared with an approximate model. Excellent agreement has been obtained for the effective phase constant, and good results have been achieved for the attenuation constant, even when this value is considerably low. For the method

to work, however, the mode must not be under cut-off. It is believed that the method is especially suitable for the extraction of the propagation constants from measurement results since the excitation method and the termination of the waveguides are irrelevant. This can be very advantageous when the exact values of the substrate characteristics or the fabrication tolerances are unknown. A similar approach of the proposed technique could be used in other leaky-modes of any sort of waveguide, even those whose theoretical analysis is difficult.

Chapter 3

The Stripline-Fed Cavity-Backed Slot Radiating Element

In the last decades, the use of compact and high-performance wireless devices have spread significantly, and they are becoming essential in our everyday life. This has increased the need for wideband, low-profile, low-cost and low-loss antennas with suitable radiation characteristics. Slot-like antennas have been widely used, as they meet the aforementioned requirements and, thus, they have been extensively studied and analyzed in the past [21–24]. In order to help with the design and understanding of this radiating element, several Transmission-Line-based (TL-based) equivalent circuits for single-layer radiating slots have been proposed in the literature [25–28]. Very recently, an improved circuit model was introduced in [29], which provides both physical insight and accurate results. However, these radiating elements have bilateral radiation which limits the applicability of these elements in directive arrays. To solve this problem, traditionally, a shallow cavity is placed behind the slot, forming a CBS.

Recently, CBS antennas have increased in popularity, due to their unidirectional radiation pattern and the easy manufacturing of the cavity using SIW-like technology [5,30,31]. CBS radiating elements were extensively studied in the past. In [4], the admittance of a CBS antenna was analytically derived. This admittance was mathematically related to the one from a single-layer slot in [32]. Furthermore, a more general and accurate approach was presented in [33]. These studies, however, computed the input parameters of the structure, without providing a simple, understandable model for the CBS. Very recently, the TL modeling of a CBS antenna was tackled for the first time [34], but the proposed circuit lacked of enough parameters to provide accurate

results.

Strip-feeding is a common way to excite a CBS radiating element [35–41]. This type of feeding requires a more complex analysis than the previous case, but it was nonetheless performed in [42–44]. Again, these analyses did not find a model which provided physical insight about the structure. The modeling of strip-fed CBS radiating elements was first tackled in [45]. This model included the effect of the slot as a parallel RLC circuit which does not help with the understanding of its behavior and is narrowband. Besides, it includes the effect of the rectangular cavity as TE_{10} modes propagating in waveguides which are coupled to the rest of the circuit by transformers. This added unnecessary complexity to the model. A magnetic-coupling equivalent circuit was proposed in [46,47]. The slot is modelled as a lossy transmission line which accounts for all the radiation of the structure, neglecting the radiation of the slot end-effect and the dielectric and conductor losses. Furthermore, the previously proposed equivalent circuit is not truly wideband because the effect of the cut-off frequency of the mode propagating throughout the slot is not considered. This mode is, in fact, the slot mode of a rectangular waveguide, which was already studied in Chapter 2.

In this chapter, a wideband equivalent circuit is proposed for stripline-fed CBS radiating elements which are excited at the center of the slot. In order to provide both physical insight and accurate results along a wide frequency band, the slot behavior is modelled by a slot-mode TL element. To the authors' knowledge, it is the first time that this sort of TL is used to propose the equivalent circuit of a finite-slot. To complete the equivalent circuit, the well-known model of the slot end-effect and the strip-slot transition is included. The main radiation effect of the structure is modelled by the end-effect resistance of the slot, placed at the end of the TL. A novel capacitive effect is also added to the strip-slot transition which considers the shift of the resonance frequency of the slot when the distance between the strip and the slot is changed. A simple dependence with this distance of the element values of the transition is also found. All parameters of the equivalent circuit are extracted from the electromagnetic simulation of the structure. The working bandwidth of the model is limited by other resonant modes which have not been taken into account, like cavity-resonant modes. In any case, the proposed model is very useful for the design of series-fed arrays (like leaky-wave antennas) using CBSs in which the prior knowledge of the radiating element behavior is a powerful tool to avoid the heavy computation of the whole array simulation.

The problem of finding an equivalent circuit for the stripline-fed CBS is tackled by modeling three different parts of the structure in order. The first one is the character-

ization of the mode propagating along a CBS-line segment, which is shown in Section 3.1. The second consists in adding to the proposed TL the well-known end-effect of the slot, which is done in Section 3.2 The third part adds the effect of feeding the slot by a stripline, described in Section 3.3. Once the three effects are added to the equivalent circuit, it is applied to a more realistic case with measurements in Section 3.4. Conclusions are given in Section 3.5.

3.1 Equivalent Circuit of a CBS-Line Section

The CBS-line section, shown in Fig. 3.1, corresponds with the section of a slotted waveguide and, then, the mode propagating along this structure is the slot mode studied in Chapter 2. Thus, the proposed equivalent circuit of the slot section is a TL whose propagation constant, γ_{CBS}, and characteristic impedance, Z_0, are defined, respectively, by (2.1) and (2.2). The parameters of those equations will only depend on the dimensions of the transverse section of the structure and the medium inside the cavity. A CBS-line section has been simulated using the commercial software HFSS, in the lumped-port configuration presented in Section 2.1.1. The dimensions of the transverse section of the simulated structure are as follows: $h = 10$ mm, $w_{cavity} = 20$ mm and $w_{slot} = 1$ mm. The length of the line is $l = 80$ mm. The dielectric inside the cavity is considered lossless, with dielectric constant $\varepsilon_r = 2.2$ and zero-thickness PEC is used for the conductor parts. Using (2.4) and (2.5), the desired values of Z_0 and γ_{CBS} can be found. They are shown in Fig. 3.2. Significant ripples appear at frequencies around 2.3, 3.4 and 4.6 GHz (shadowed regions), due to resonances, as explained in the Section 2.1.1. The ripples are larger in this case because there are less losses.

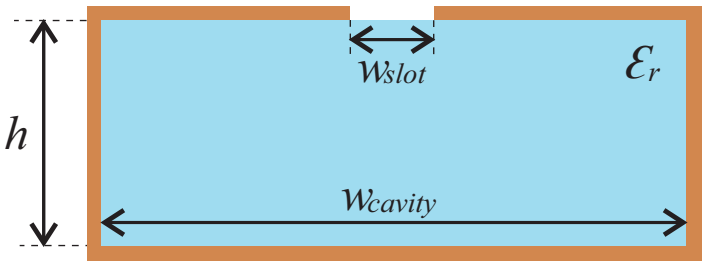

Figure 3.1: Transverse section of the CBS.

Using these simulation results, it is possible to find the values of the TL parameters. The cutoff frequency, f_c, in the cases of lossy modes, is defined as the frequency when $\alpha(f_c) = \beta(f_c)$, where α is the attenuation constant and β the phase constant [17]. Thus, it can be extracted directly from simulated results. After f_c is found, ε'_r can be

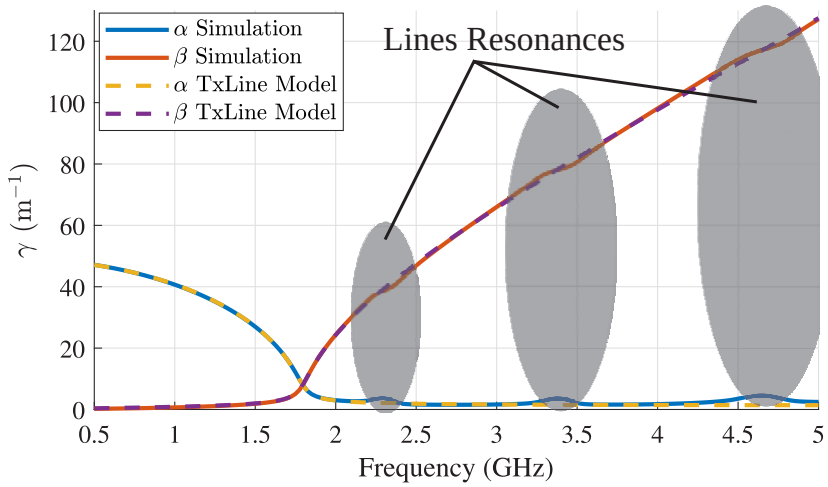

(a)

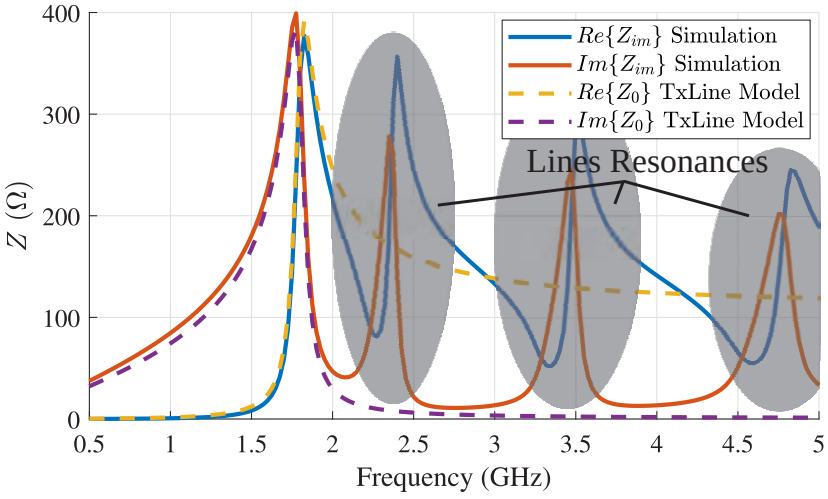

(b)

Figure 3.2: Comparison between image parameters of a simulated CBS section and the TL equivalent circuit. Simulated results in the shadowed region are inaccurate due to resonances in the simulated line. (a) Propagation constant. (b) Characteristic impedance.

adjusted so both the β obtained from simulation and the equivalent circuit have the same asymptotic behavior for higher frequencies. The value of ε_r'' can be chosen to be frequency-dependent or constant, depending on its suitability modeling the loss phenomenon. In this case, the only considered losses are due to radiation and it has been found, heuristically, that these losses can be associated with a constant conductivity:

$$\varepsilon_r'' = \frac{\sigma}{2\pi f \varepsilon_0}, \tag{3.1}$$

where ε_0 is the electric permittivity in vacuum, and σ is an equivalent conductivity.

The value of σ can be found so that the attenuation constant, α, of the simulation and the equivalent circuit, have the same level under the cutoff frequency. Lastly, the value of Z_m from (2.2) is obtained so $|Z_0| = |Z_{im}|$ at f_c.

Using the aforementioned procedure, the parameters of the model have been obtained: $f_c = 1.795$ GHz, $\varepsilon'_r = 1.7$, $\sigma = 0.009$ S/m and $Z_m = 148\ \Omega$. As expected, the value of ε'_r is very close to the $\varepsilon_{r_{eff}}$ of a slotline, which would be 1.6. As also shown in Fig. 3.2, the agreement between the simulation and the equivalent circuit is very good near the cutoff frequency and below. As expected, the inaccuracies of the simulated γ_{CBS} and Z_{im} around the resonance frequencies of the line make difficult to verify the model with the simulation at those frequencies. It can be seen, however, that the asymptotic behavior is similar.

3.2 End-Effect of the Slot

Once the slot segment has been modeled, an equivalent circuit for the short-circuit termination must be found. The short-end discontinuity of a slotline was studied in [48], and the proposed equivalent circuit was an inductor and a frequency-dependent resistance connected in series. The inductive effect makes the slotline appear electrically longer than it really is, while the resistance represents the effect of the radiation in the discontinuity. In the case of a CBS, the discontinuity has similar characteristics to the slotline and, thus, the same equivalent circuit is used here.

Up to this point, the proposed equivalent circuit of the CBS, assuming center-feeding, would be the parallel combination of two TLs ended in the series combination of R_{end} and L_{end}. The length of the TLs would be half the length of the slot, $l_{slot}/2$, and their propagation constant and characteristic impedance would be those from (2.1) and (2.2):

$$Z_{in} = \frac{1}{2} Z_0 \frac{R_{end} + j2\pi f L_{end} + Z_0 \tanh(\gamma_{CBS} l_{slot}/2)}{Z_0 + (R_{end} + j2\pi f L_{end}) \tanh(\gamma_{CBS} l_{slot}/2)}. \tag{3.2}$$

The values of this Z_{in} cannot be accurately computed using lumped ports in HFSS, as the length of a standard slot is too short and higher-order mode effects appear. It could be possible to compute it in the case of very long slots, but the value of R_{end} and L_{end} would not be the same as the ones of a standard-length slot. For this reason, the values of the end-effect parameters, R_{end} and L_{end}, will be extracted from the simulation results of stripline-fed CBS, in Section 3.3, using a wave port.

3.3 Stripline-Feed Effect

In this section, a stripline-fed CBS will be considered. The feeding strip is beneath the slot, at a certain distance from the bottom of the cavity, d, and feeds the slot across its center. Fig. 3.3 shows the geometry of this structure.

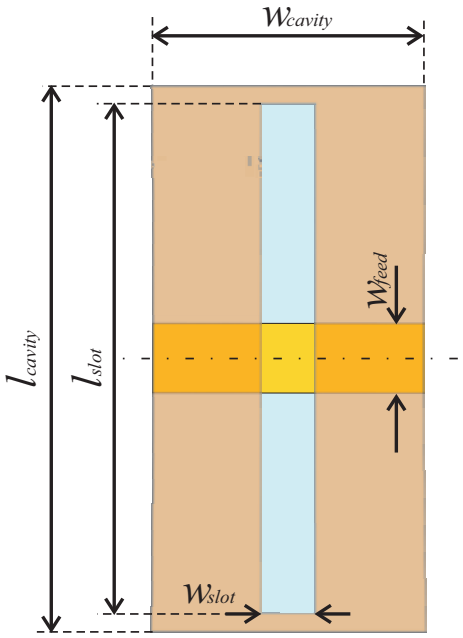

Figure 3.3: Top and side views of the stripline-fed CBS structure. (a) Top view. (b) Side view.

For the third and last part of the model, an equivalent circuit of the transition between the feeding stripline and the CBS is obtained. As found in the literature [16], this transition has been traditionally modeled by an ideal transformer. The turns ratio, n, of this transformer represents the amount of coupling between the stripline and the slot fields. When the distance between the slot and the stripline, $h - d$, is small, both are strongly coupled, and n is higher.

Taking into account the effect of the transformer, the total impedance of the slot,

according to the proposed equivalent circuit, is

$$Z_{slot} = \frac{n^2}{2} Z_0 \frac{R_{end} + j2\pi f L_{end} + Z_0 \tanh(\gamma_{CBS} l_{slot}/2)}{Z_0 + (R_{end} + j2\pi f L_{end}) \tanh(\gamma_{CBS} l_{slot}/2)}. \tag{3.3}$$

First, this impedance was computed using HFSS. In this simulation, however, the feeding striplines were excited by wave ports and the reference planes were placed coincidently at the center of the structure. The width of the stripline was $w_{feed} = 2$ mm, and its distance from the bottom of the cavity is $d = 9$ mm. The total length of the slot is $l_{slot} = 40$ mm and the length of the cavity is $l_{cavity} = 60$ mm. The transverse section of the CBS was not changed from that of Section 3.1. Then, the value of the simulated Z_{slot} is compared with the value of (3.3), where Z_0 and γ_{CBS} are those extracted in Section 3.1 from (2.1) and (2.2). Using least-squares fitting, the other parameters, n, R_{end} and L_{end}, are found. The results showed a value for R_{end} of 11.7 Ω, which was considered constant vs. frequency for the sake of simplicity, and a negligible L_{end}, which seem to be reasonable compared with the results of [48]. The value for the turns ratio, n, was found to be 0.96. Fig. 3.4 shows the comparison between simulation and the equivalent circuit.

As expected, since the slot and strip were close, the obtained value of n was high, close to 1. As the distance between them increases (i.e. as d decreases), the value of n is reduced. However, the resonance frequency of the slot also shifts. This effect is modeled using a capacitance, C, placed in parallel with the rest of the circuit and its value is higher as the distance between the strip and slot increases. Fig. 3.5 shows the proposed equivalent circuit for the complete structure. Fig. 3.6 shows four additional comparisons, where the distance of the strip from the bottom of the cavity has been gradually reduced. The obtained values of n and C are shown for these and several more cases in Fig. 3.7. The rest of parameters of the equivalent circuit were not changed. Since the values of n clearly increase linearly with d, the values were curve fitted using $n = 0.106d(\text{mm})$ and plotted altogether in Fig. 3.7. In the same manner, the values of C were curve fitted using $C(\text{pF}) = 40[d(\text{mm})]^{-3}$. These results show how simple the variation of the equivalent circuit parameters with the distance between the slot and the feeding strip is.

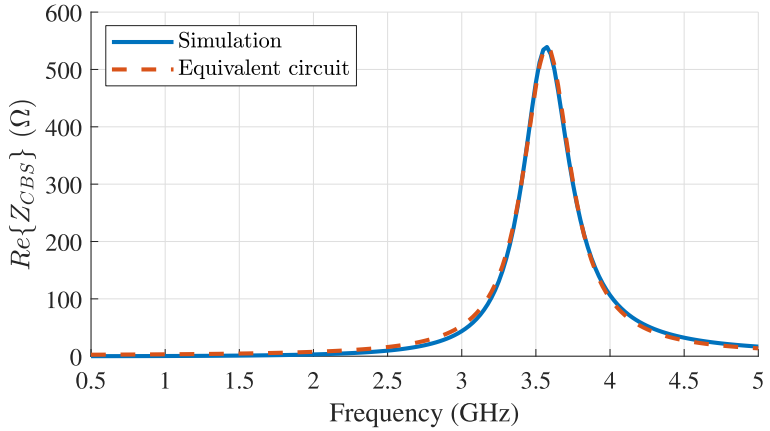

(a)

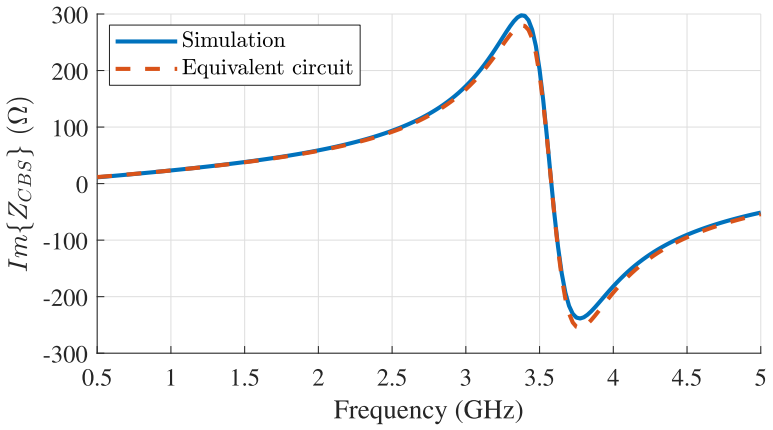

(b)

Figure 3.4: Impedance of the stripline-fed CBS, according to simulation and model when $d = 9$ mm. (a) Real part. (b) Imaginary part.

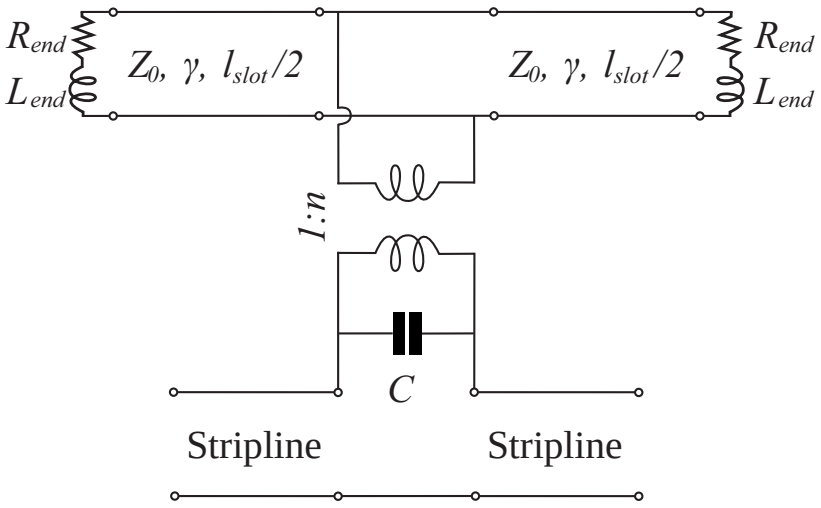

Figure 3.5: Proposed equivalent circuit for the stripline-fed CBS.

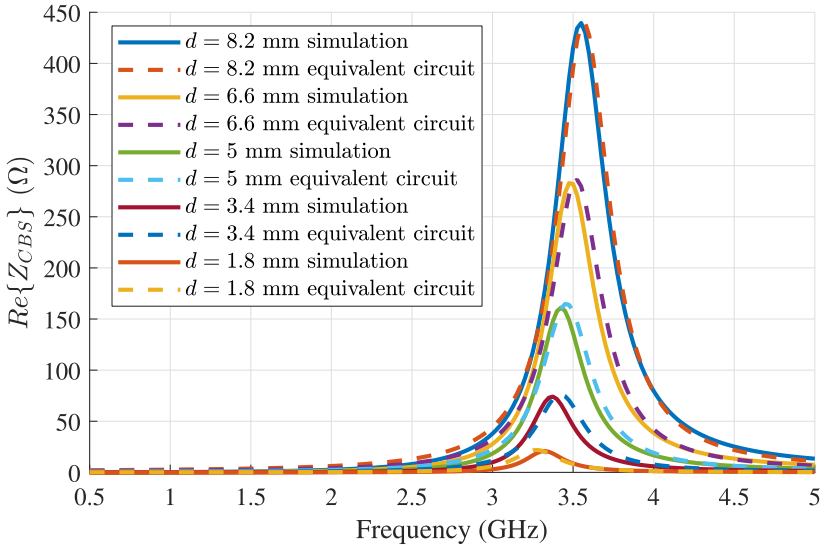

(a)

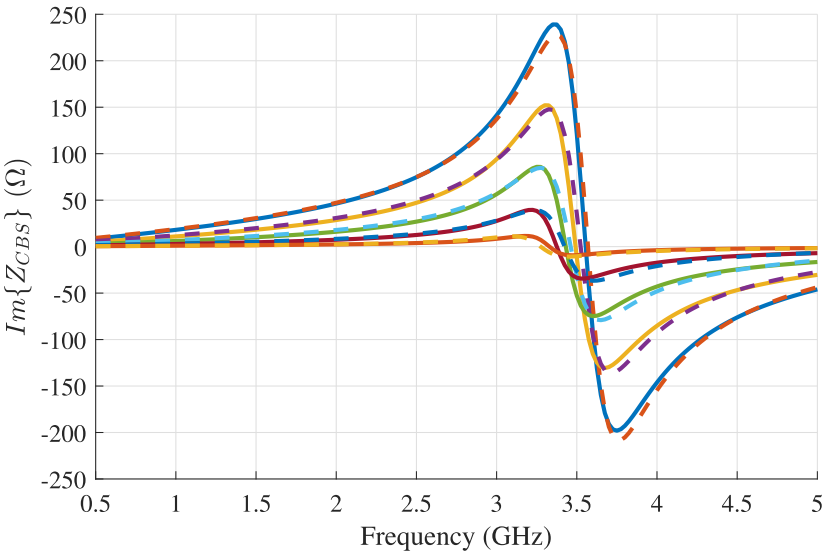

(b)

Figure 3.6: Impedance of the stripline-fed CBS, according to simulation and model for different values of d. (a) Real part. (b) Imaginary part.

3.4 Measurement results

In order to verify the proposed equivalent circuit with experimental results as well, it was applied to a different case with an available prototype, which is shown in Fig. 3.8. To make the fabrication easier, the measured prototype was fed by an enclosed microstrip and the cavity walls were made using screws. Rogers RO4350B with dielectric constant, ε_r, of 3.66 and thickness of 0.51 mm was used. The width of the microstrip line was 1.1 mm, the width of the cavity was 22.4 mm, its length of 32 mm, and

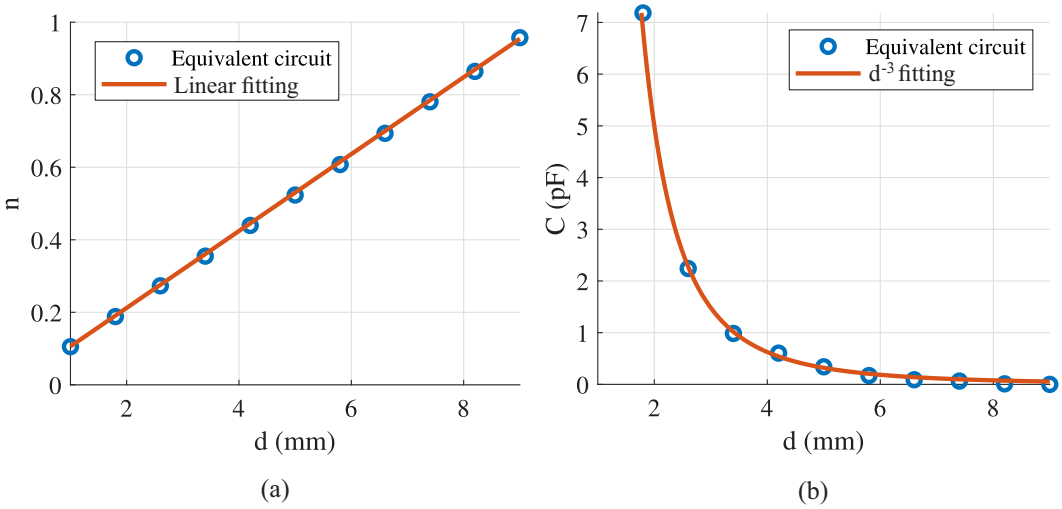

Figure 3.7: Values of the turns ratio and capacitance of the equivalent circuit for different values of d and curve fitted using simple equations. (a) Turns ratio n. (b) Parallel capacitance C.

its height of 3.71 mm. The length of the slot was 22 mm and its width of 0.3 mm. The screws had a diameter of 2 mm and were placed with a separation of 5.6 mm between them. A TRL calibration kit was fabricated in the same technology and used to place the reference planes at the center of the structure. More information about this prototype can be found in [49] and in Chapter 4.

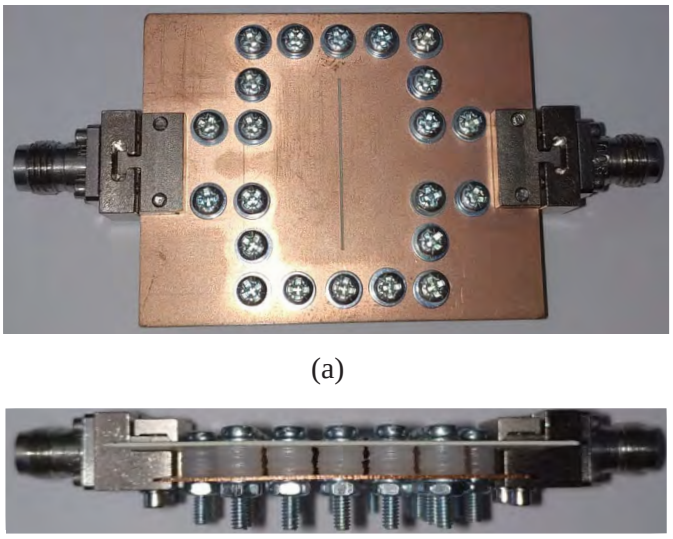

(a)

(b)

Figure 3.8: Picture of the available prototype used to experimentally verify the model. (a) Top view. (b) Side view.

Since the TL model proposed in Section 3.1 neglected dielectric losses in the line, those have been considered by changing the value of ε_r'', to the following:

$$\varepsilon_r'' = \varepsilon_r' tan\delta, \tag{3.4}$$

where $tan\delta$ is an equivalent loss tangent that accounts for the losses of the TL, and is, in this case, another parameter of the equivalent circuit. The conductor and radiation losses of the line have not been taken into account in this particular case since dielectric loss is the main loss factor at the frequencies of interest.

Fig. 3.9 shows the values of the impedance of the CBS structure from the measurement results and using the proposed equivalent circuit. The equivalent circuit parameters are: $f_c = 2.418$ GHz, $\varepsilon_r' = 1.75$, $tan\delta = 0.004$, $Z_m = 132\ \Omega$, $R_{end} = 4.3\ \Omega$, $L_{end} = 0$, $n = 0.86$ and $C = 0$. The agreement between measurement and the equivalent circuit is excellent up to 6.5 GHz. Between 6.5 GHz and 8 GHz, a small discrepancy is found. This is caused by the effect of the resonant mode TE_{101} [18] inside the cavity, which was not considered. The resonance frequency of this mode in this case is 7.5 GHz and its effect has been shown in [41, 49] and the following chapter.

3.5 Conclusion

We have introduced a wideband equivalent circuit for stripline-fed CBS radiating elements. The proposed model provides physical insight and accurate results while being simple. The equivalent circuit consists of a lossy TL with cutoff frequency ended in a resistor and inductor connected in series. The frequency dependence of the losses can be chosen depending on the dominant losses (dielectric, conductor or radiation). The TL is connected to the feeding stripline through an ideal transformer and a parallel capacitor and the relation of these parameters with the distance between the stripline and the slot is found. An almost direct extraction of the parameters of the model is also provided. Although the equivalent circuit has only been applied to two particular cases, it is expected that it will behave properly under a wide range of geometric and electric parameter values of the structure. The fact that all the parameters of the model except for the resistance of the end-effect of the slot are constant over the frequency band provides the equivalent circuit with a general character and confirms its validity. By separating each of the effects of the CBS, the equivalent circuit greatly helps with the understanding of its behavior, allowing to discern how each part of the

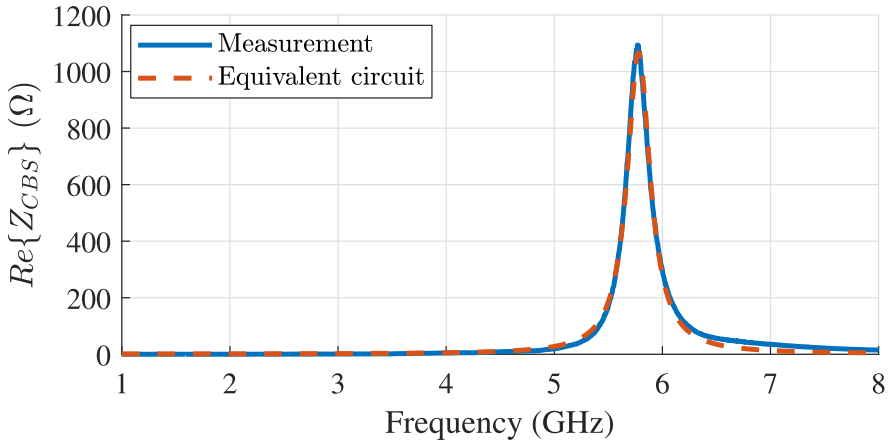

(a)

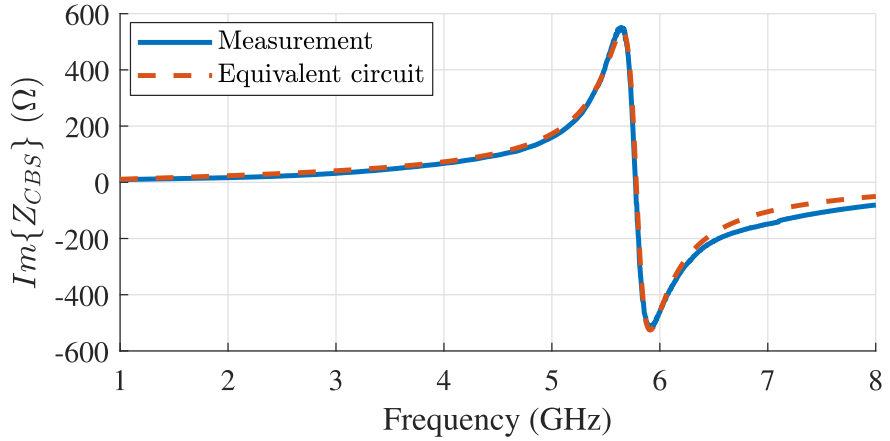

(b)

Figure 3.9: Impedance of the stripline-fed CBS, according to measurement and model. (a) Real part. (b) Imaginary part.

structure affects the response of the circuit. The model can be used as an approximated starting point for wideband stripline-fed CBS antennas or arrays where the CBS is the radiator, like in series-fed arrays or leaky-wave antennas. Besides, the characterization of the slot-mode propagation can be of use in leaky-wave antennas and the proposed transition for the strip-slot could also be of great help in the design of circuits and transitions.

Chapter 4

Broadly-Matched Strip-Fed Cavity-Backed Slot Radiating Element

Society's increasing needs for widebandwidth wireless communications demands broadband, directive and reconfigurable antennas to be easily integrated into small terminals. Slot-like antennas have been studied and used intensively in recent decades [50] due to their many advantages, which include low cost, low profile, durability, easy manufacture and integration in the casing of almost any device. Therefore they are strong candidates for building arrays that can comply with the aforementioned requirements.

Nevertheless, these antennas usually radiate towards the entire space, thus exhibiting bilateral radiation. This feature makes them poorly suited for their use in conventional directive arrays since the radiation pattern will always have at least two main lobes. In order to prevent radiation towards one of the half-spaces, a cavity made of a conductive material can be placed behind the slot, forming a so-called Cavity-Backed Slot (CBS). This structure was studied and used during the second half of the last century [51, 52] founding that the radiation properties are determined by the dimensions of the cavity. Later, these antennas were left out due to their bulkiness and complex manufacture using planar technology. The development of Substrate Integrated Waveguide (SIW) technology opened up a way for a compact and easy implementation of CBS antennas [53, 54] by using metallic via holes to build the cavity.

In addition to the aforementioned drawbacks, slot and CBS antennas have a narrow

impedance bandwidth due to the resonant nature of the element. A recent work [55] uses the SIW technique and a bow-tie slot antenna to increase its impedance bandwidth, but still only 9.4% is achieved. A solution to the narrow bandwidth which uses transmission configuration and offers an ultra broad bandwidth was proposed in [1] for the case of microstrip-fed slots. Very broad bandwidth is achieved by using a stub complementary to the slot that matches the impedance of the structure, resulting in an all-pass section. The two-port configuration of this radiating element enables the design of tunable series-fed arrays, as shown in [56]. However, the bilateral radiation problem still exists for the so-called *complementary strip-slot*. In an attempt to address this issue, a reflector was placed behind the array in [56] and [57] with the drawbacks of narrowing the working band of the antenna and considerably increasing its size.

A novel compact stripline-fed CBS radiating element using planar technology is studied in this chapter. In a similar way as in [1], its complementary stub is placed under the slot to enhance the impedance bandwidth. The two-port transmission configuration is also adopted here and the cavity is implemented using SIW technology. The present work can be seen as a transformation of the *complementary strip-slot* to obtain unidirectional radiation. This is achieved by replacing the microstrip line by a closed structure (stripline or enclosed microstrip), preventing the structure from radiating towards one half-space. These modifications in the geometry entail several challenges: the CBS behaves differently than that of a conventional slot, the additional ground plane makes it more difficult to obtain impedance matching, and controlling the modes supported by the structure becomes a fundamental part of the design.

Stripline-fed CBSs were also researched in the last century [58–60] and were proposed [59] as a candidate for series-fed arrays. More recently, the stripline-feeding approach has been used as an alternative to cavity feeding [61]. Furthermore, they have previously been used in conjunction with SIW technology [62]. The impedance bandwidth of the CBS antennas found in the literature is usually very narrow, less than 5%, for both one-port and two-port (transmission) configurations. The designs presented in this work shows a very broad fractional impedance bandwidth (48% or more). Thus, to the authors' knowledge, this new radiating element exhibits the highest impedance bandwidth from among the other unidirectional-radiating narrow slots cited in the bibliography. With these characteristics, the element can be used to make wideband series-fed antenna arrays as in [56], but featuring unidirectional radiation, as will be shown in Chapter 5.

The chapter is structured as follows: Section 4.1 describes the structure and its

design procedure, giving physical insight. Section 4.2 presents two different implementations of the element and their measurement results. Section 4.3 describes its use in series-fed arrays. Section 4.4 compares the proposed matching method to a classic one. Section 4.5 proposes two modifications to improve the bandwidth of the element. Finally, the conclusions are summarized in Section 4.6.

4.1 Analysis and Design

4.1.1 Structure and Supported Modes

The proposed structure consists of a CBS excited in transmission configuration by an asymmetric stripline where a stub, complementary to the slot, is placed beneath it. The slot is etched on the upper ground plane and the stub is aligned with it but placed on the stripline layer. Lateral metallic walls are used to keep the structure closed, building the cavity, which is filled with dielectric material. Fig. 4.1 shows the geometry of the proposed radiating element.

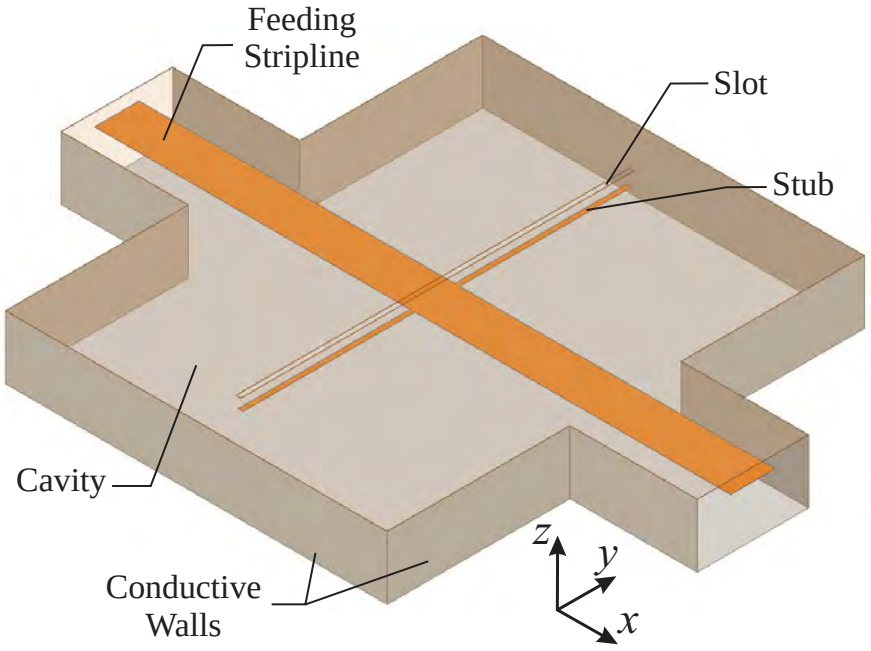

Figure 4.1: Geometry of the proposed structure.

The behavior of the structure is determined by the modes supported by the section of the structure (shown in Fig. 4.2) along the direction transverse to the feeding line (y-axis in Fig. 4.1). The fundamental mode of this structure is a quasi-TEM mode with no cut-off, supported by the two conductors in the structure (strip and cavity

walls), in a similar way to a classic stripline TEM mode. Due to the slot, the structure is not completely closed as is a classic stripline. However, the field leaked outside the structure by the slot is not significant and, thus, it is possible to assume that the fundamental mode is almost a TEM mode. Another mode supported by the structure is the slot mode of a rectangular waveguide, studied in detail in Chapters 2 and 3, which has a cut-off frequency. The presence of the strip does not change the characteristics of the slot mode. Furthermore, higher-order modes can also appear. The first higher order mode supported by this structure is the TE_{10} mode of the rectangular waveguide, which will disrupt the behavior of the structure at higher frequencies.

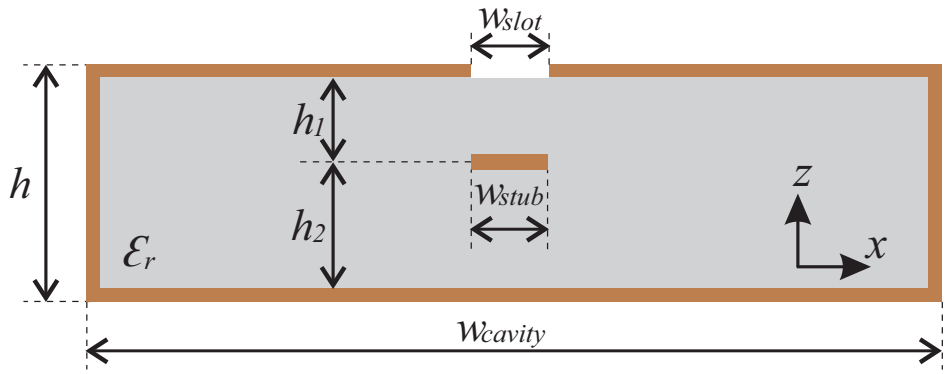

Figure 4.2: Cross-section of the slot-stub part of the structure.

As will be justified later, in order to cancel out the resonant behavior of the slot and achieve broad matching, it is necessary for both the slot and the quasi-TEM modes to be excited. If the dimensions of the cavity are chosen properly, the element can successfully operate in a wide frequency band. The structure's lowest working frequency is limited by the cut-off frequency of the slot mode of the CBS, because its propagation is necessary for the structure to radiate. The TE_{10} mode is unwanted and its appearance will limit the working frequency band at higher frequencies. The cut-off frequency of the unwanted TE_{10} mode could limit the highest working frequency. Thus, its cut-off frequency should be as high as possible. However, since the other modes inside the structure do not excite the TE_{10} mode, the presence of this mode will go unnoticed even above its cut-off frequency. However, since the transmission system is short-circuited at its ends (by the metallic walls that close the structure), a cavity is formed. The TE_{10} mode will resonate inside this cavity at the resonance frequency of the resonant mode TE_{101}. This resonant frequency can be computed as in [18]:

$$f_{101} = \frac{c}{2\sqrt{\mu_r \varepsilon_r}} \sqrt{\frac{1}{w_{cavity}^2} + \frac{1}{l_{cavity}^2}}, \tag{4.1}$$

where l_{cavity} is the total length of the cavity. The effect of this higher order mode will become noticeable at this resonant frequency. To increase the cut-off frequency of the TE_{10} mode and, thus, a wider working bandwidth, a narrow cavity, with a low w_{cavity}, is preferred. However, if the cavity width, w_{cavity}, is reduced, the cut-off frequency of the slot mode will increase. To broaden the operating frequency band, the cut-off frequency of the slot mode can be lowered by increasing the height of the stripline and thus the cavity, h. However, the radiating element will be thicker. The width of the slot, w_{slot}, also changes the cut-off frequency of its mode. Lower values of the width reduce the frequency and thus are desirable. However, very low values of w_{slot} could be difficult to implement accurately and could reduce the radiation of the element significantly. Another way of obtaining a high resonance frequency of the resonant mode TE_{101} is making the length of the cavity as short as possible, lowering l_{cavity}. However, the length of the cavity is limited by the length of the slot. In conclusion, the dimensions of the cavity must be chosen carefully due to the trade-off between the operating bandwidth of the element and its thickness.

4.1.2 Lattice-Network-Based Equivalent Circuit

In an analogous way as in [1], a lattice network ([63], Fig. 4.3) is proposed to model the element. The field distribution of a symmetric structure can be separated into two contributions: the field distribution of the even mode and the field distribution of the odd mode. Thus, if the reference planes are chosen appropriately (coincident at the symmetry plane, in this case), the lattice network separates the contribution of both the even and odd modes in each of the branches, allowing the creation a model of the structure from independent models of the even and odd modes. These two modes correspond to the quasi-TEM mode of the stub and the slot mode of the rectangular waveguide as described previously.

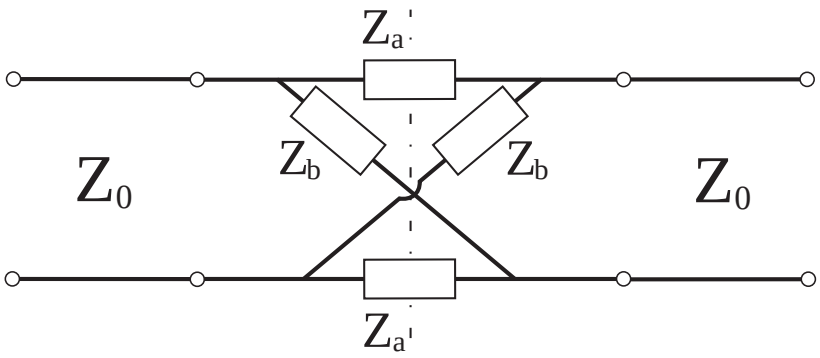

Figure 4.3: Equivalent lattice network of the complementary structure.

The circuit chosen to model the contribution of the quasi-TEM of the stub, Z_b, is a simple lossless transmission line ended in open-circuit, in the same way as in [1]. The modeling of the slot contribution, however, is more challenging, as shown in Chapter 3. To simplify the model and, thus, the design procedure, another lossless transmission line will be used as an approximation to model the slot. In this case, ended in short-circuit. Fig. 4.4 shows the circuit model of the impedances of each branch. To improve the accuracy of the model, the model for the slot proposed in Chapter 3 can be used if necessary.

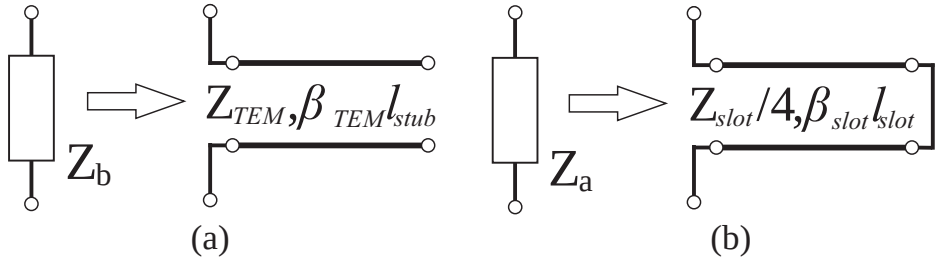

Figure 4.4: Circuit model of the lattice network impedances using transmission lines. (a) Z_b. (b) Z_a.

4.1.3 Design Procedure

Firstly, the dimensions of the cross-section of the cavity (w_{cavity}, h, ε_r, and w_{slot} in Fig. 4.2) must be chosen according to the following two criteria: first, obtaining a cut-off frequency of the slot mode lower than the design frequency and, second, achieving a resonance frequency of the TE_{101} as high as possible. The effect of these dimensions on these frequencies has already been discussed in Section 4.1.1.

Secondly, the length of the slot, l_{slot}, is chosen so that the resonance of the slot coincides with the design frequency. The slot resonance is modeled with a transmission line as shown in Fig. 4.4(b). As the propagation constant, β_{slot}, is already determined by the parameters chosen in the previous step, the length of the slot, l_{slot} will only modify the electrical length of the transmission line. This length will also determine the minimum length of the cavity, l_{cavity}, which sets the resonance of the resonant mode TE_{101}.

Lastly, the other parameters, w_{stub}, l_{stub} and h_1 must be chosen in order to obtain broad impedance matching. To do this, first, let us express the image impedance of the equivalent circuit of the complementary structure shown in Fig. 4.3 as a function

of Z_a and Z_b, as in [63]:

$$Z_{im}(\omega) = \sqrt{Z_a(\omega)Z_b(\omega)}. \tag{4.2}$$

The image impedance of the structure must be constant and with the same value as the characteristic impedance of the feeding line, Z_0, over a wide range of frequencies. As modeled in Fig. 4.4, the impedances Z_a and Z_b have poles and zeros at the corresponding resonance frequencies. For Z_{im} to be approximately constant, these poles and zeros must coincide in frequency so they properly cancel each other out and the impedance level does not change over frequency. For this to happen, the electrical length of the transmission lines modeling Z_a and Z_b must be the same. These conditions can be expressed as follows:

$$\frac{1}{2}\sqrt{Z_{TEM}Z_{slot}} = Z_0 \tag{4.3a}$$

$$\beta_{TEM}l_{stub} = \beta_{slot}l_{slot}. \tag{4.3b}$$

Although it is possible to modify Z_{TEM} using the width of the stub, w_{stub}, this may not be enough to fulfill condition (4.3a), since closed structures (i.e. stripline) have lower impedances than their microstrip counterpart. Increasing h allows a higher stub impedance, and thus, a higher Z_{TEM} to be achieved; however, increasing the distance between the strip and the slot reduces the impedance of the slot, Z_{slot}, as shown in the transformer of the equivalent circuit from the previous chapter (see Fig. 3.7(a)). In this case, an asymmetric stripline or enclosed microstrip can be used to increase Z_{slot}, as proposed in [64]. Decreasing the distance between the strip and the slot, h_1, while keeping constant h (increasing h_2) leads to higher values of Z_{slot}. Finally, condition (4.3b) can be fulfilled by adjusting the length of the strip. This length only modifies the electrical length of the transmission line in the model shown in Fig. 4.4(a), that is, the position of the zero of Z_b.

4.2 Implementations and Results

In this section, the fabrication results of two prototypes are illustrated. The first prototype is implemented using a suspended stripline configuration. To mitigate the shortcomings of this first configuration, the use of an enclosed microstrip was later

proposed. For the sake of completeness, the details of both fabrication configurations are included here.

4.2.1 Suspended Stripline Implementation

In order to make the overall size of the structure larger, easing the manufacturing requirements, a low permittivity substrate was chosen to implement a proof of concept structure. Thus, a suspended stripline configuration was first chosen, which also allows for a higher flexibility in the implementation of the heights h_1 and h_2. Three metallic layers have been printed on commercial substrates: lower ground plane, upper ground plane with the slot and the stripline layer. To suspend them in the air, nylon washers have been used around steel screws which pierce through the three layers as metallic posts to make the lateral walls of the cavity. Fig. 4.5 shows the geometry of the proof of concept structure.

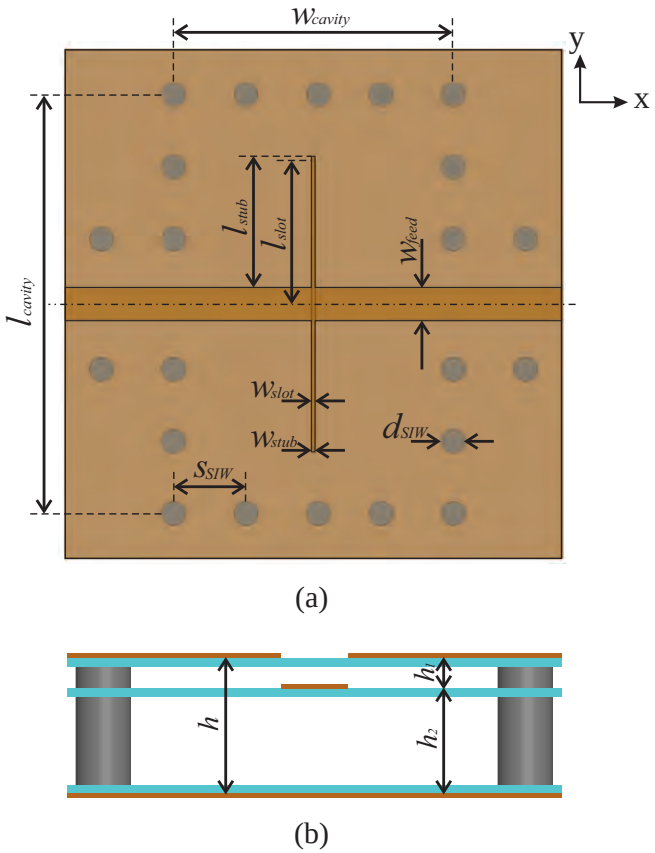

Figure 4.5: Simulated proof of concept structure. (a) Top view. (b) Section of the cavity. The stub and slot sections have been enlarged to improve the visibility of the elements.

The substrate used to manufacture the three metallic layers is Rogers RO4350B

with thickness of 0.25 mm and ε_r of 3.66. The width of the feeding stripline, w_{feed}, was chosen to have a characteristic impedance, Z_0, of 50 Ω. The width and height of the cavity, w_{cavity} and h, and the width of the slot, w_{slot}, were chosen to ensure that the slot mode propagates from 3.5 GHz and the cut-off of the TE_{10} mode is 6 GHz. The width of the stub, w_{stub}, together with the asymmetry of the stripline (h_1 and h_2) were selected to achieve condition (4.3a). With the current implementation possibilities, it would not have been possible to satisfy this condition using a higher effective dielectric constant. The lengths of the complementary elements, l_{slot} and l_{stub}, were designed to ensure complementarity, fulfilling condition (4.3b). The pole of Z_a and the zero of Z_b are placed at 5.2 GHz. The length of the cavity, l_{cavity} is chosen to be high enough not to affect the behavior of the strip and slot ends. The chosen value results in an approximate resonance of the TE_{101} resonant mode around 6.7 GHz. The analysis in the previous section did not take into account either the multiple layer structure or the presence of the metallic posts and nylon washers, so some tuning of the dimensions using HFSS was needed to obtain the final design. The prototype was manufactured and assembled. 50 Ω standard stripline connectors were used. Fig. 4.6 shows the result of the manufacturing process and its dimensions.

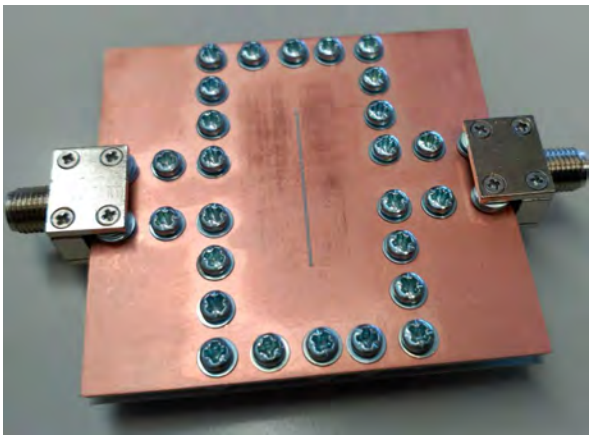

(a)

(b)

Figure 4.6: Manufactured prototype. (a) Top view (w_{feed} = 2.8 mm, w_{cavity} = 24 mm, l_{cavity} = 35 mm, w_{stub} = 0.3 mm, l_{stub} = 11.1 mm, w_{slot} = 0.3 mm, l_{slot} = 12.15 mm, h = 3.912 mm, h_1 = 0.787 mm, h_2 = 3.125 mm, d_{SIW} = 2 mm and s_{SIW} = 6.1 mm). (b) Lateral view.

In order to place the reference planes at the center of the element (coincident), a TRL calibration kit was designed. Fig. 4.7 shows the magnitude of the S_{11} and S_{21} parameters for both the simulated and measured cases. Using the criterion of -10 dB for the S_{11} to determine the impedance bandwidth, impedance matching of up to 6.7 GHz is found in the measurements, versus 6.8 GHz in the simulation. The CBS does not exhibit significant radiation below 4 GHz (radiated power of less than 5% of the input power), which limits the use of this radiating element at lower frequencies and, thus, a fractional bandwidth of about 48% is obtained (50% in the simulation). The spurious ripple at 6.8 GHz can be explained due to the appearance of the TE_{101} resonant mode, as was expected from the analysis of Section 4.1.1. It can be shown analytically that a small difference in either the lengths of the stubs or the effective dielectric constants can produce a kind of ripple at the frequency corresponding to the zero of Z_b. Therefore, the small ripple found in measurements around 5.3 GHz is attributed to a difference in the electrical length of both stubs, due to manufacturing errors.

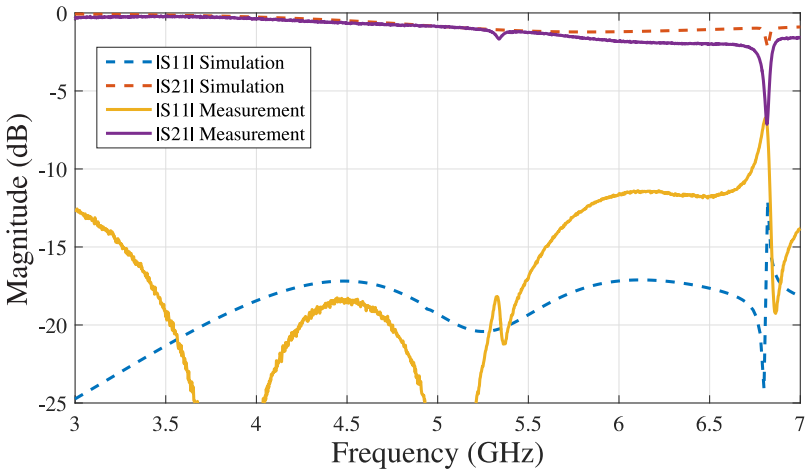

Figure 4.7: Magnitude of the S-parameters of the simulated and measured structure.

To explain the differences between the model, simulation and measurements in Fig. 4.7, the values of the impedances of the lattice network, Z_a and Z_b, are extracted from the S-parameters and compared with those of the transmission line model of Fig. 4.4. The results are shown in Fig. 4.8. Good agreement between the model and simulation is found, which proves the validity of the independent designs of the stub and CBS elements. It can be seen that the pole of Z_a and the zero of Z_b appear around the design frequency, 5.2 GHz, resulting in the complementarity of the structure. The frequency shift in the pole of Z_a in the measured case explains the difference between the simulation results and the measurements in Fig. 4.7. Due to limitations of the

manufacturing technology available, the thicknesses of the substrates are thinner than expected and they bend a little across their surfaces, especially on the slot, where there is almost no dielectric left. The absence of dielectric near the slot reduces the effective ε_r of the slot mode, leading to a frequency shift. In order to verify this effect, additional simulation results using the actual dimensions of the prototype have been included in Fig. 4.8 as *Simulation 2*. The missing dielectric in the center of the slot has been simulated with a length of 10 mm, and the thicknesses of the top, middle and bottom layers, instead of being the target 0.25 mm, are around 0.15 mm, 0.2 mm and 0.24 mm respectively. These changes explain the frequency shift. Given the sensitivity of the element to the thicknesses of the substrates and the uncertainties introduced by the manufacturing process, the discrepancies in the impedance level are reasonable. The effect of the bending and reduced thicknesses of the substrates is also present in the manufactured TRL calibration kit and may have introduced additional errors in the measurements.

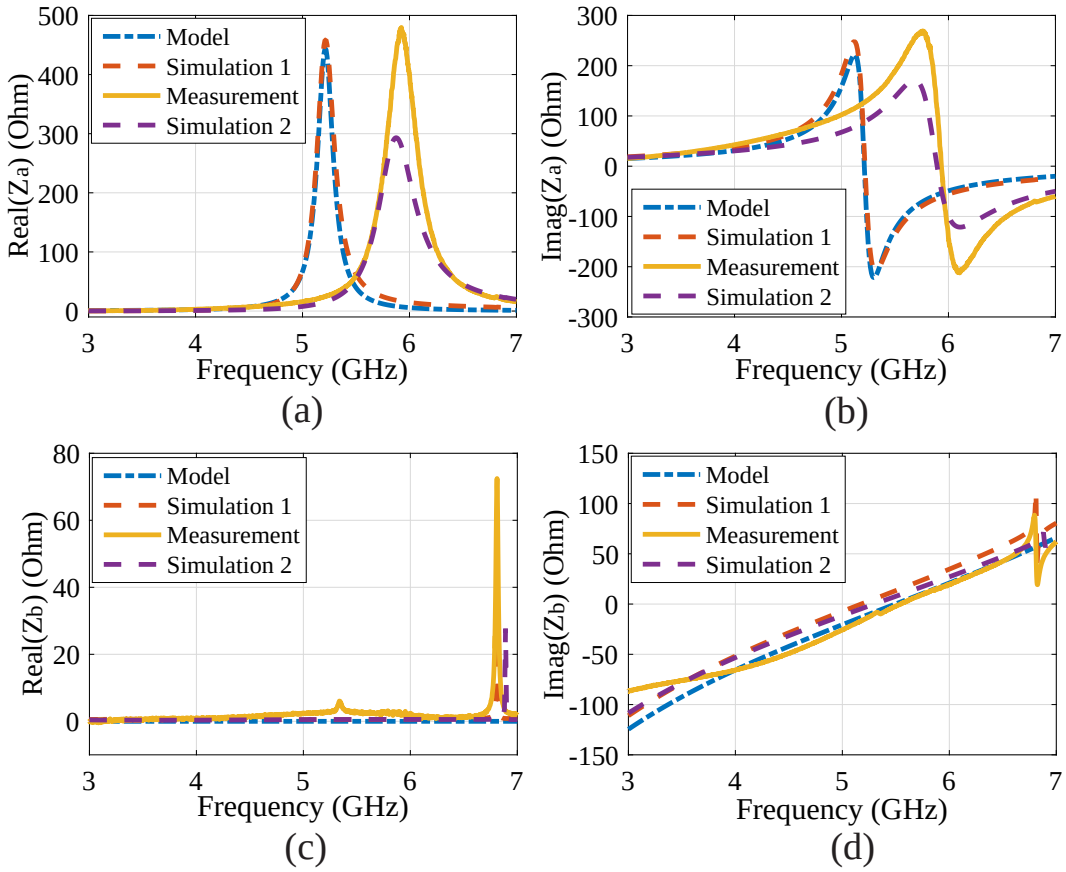

Figure 4.8: Lattice network impedances of the radiating element: model, design simulation (with nominal dimensions), prototype measurement and the prototype simulation (with actual manufactured prototype dimensions). (a) Real part of Z_a. (b) Imaginary part of Z_a. (c) Real part of Z_b. (d) Imaginary part of Z_b.

Finally, the radiation properties of the prototype have been measured, as shown in Fig. 4.9. Fig. 4.10 represents the gain over frequency for both the simulated cases, and the measurement in the broadside direction (+Z-axis in Fig. 4.9). Given the sensitivity of the manufacturing process, reasonable agreement is found between the measurements and the simulations, showing an increasing gain up to the frequency of 5.5 GHz, from which it slowly decreases. Some discrepancies were expected as there are significant differences between the simulated gains in the structure with the target design dimensions and the structure with the manufactured actual dimensions. The low values of gain are expected, since the power radiated by this two-port element is only about 20% or less of the input power throughout the working band. This is due to power leaking to the second port as desired, since the structure is proposed as a radiating element for series-fed arrays. Fig. 4.11 shows the radiation gain patterns of the simulation, using HFSS, and manufactured structure at 5.2 GHz and 6 GHz. It can be seen, as expected, that the structure exhibits broadside radiation in only one half-space. Measurement and simulation differences may be due to the presence of the connectors and the heads of the screws, not considered in the simulation. Nevertheless, good agreement between them is found. The polarization obtained is linear in the principal planes with very good cross-polarization discrimination. The cross-polarization simulation results were omitted since they were less than -50 dB.

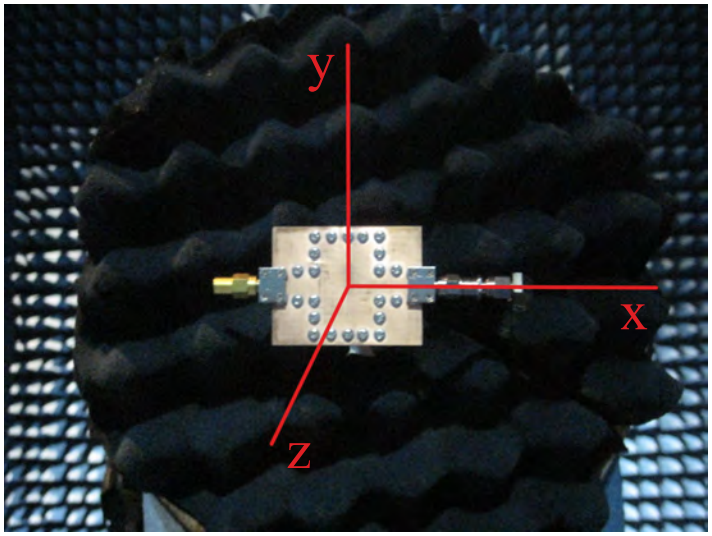

Figure 4.9: Proof of concept structure built and measured. Radiation measurements made in the anechoic chamber of the Laboratorio de Ensayos y Homologación de Antenas, Universidad Politécnica de Madrid, Madrid (Spain).

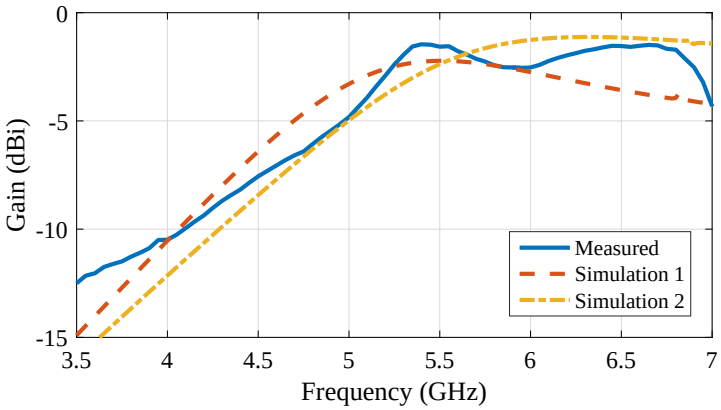

Figure 4.10: Measured and simulated gain of the radiating element sampled in broadside direction.

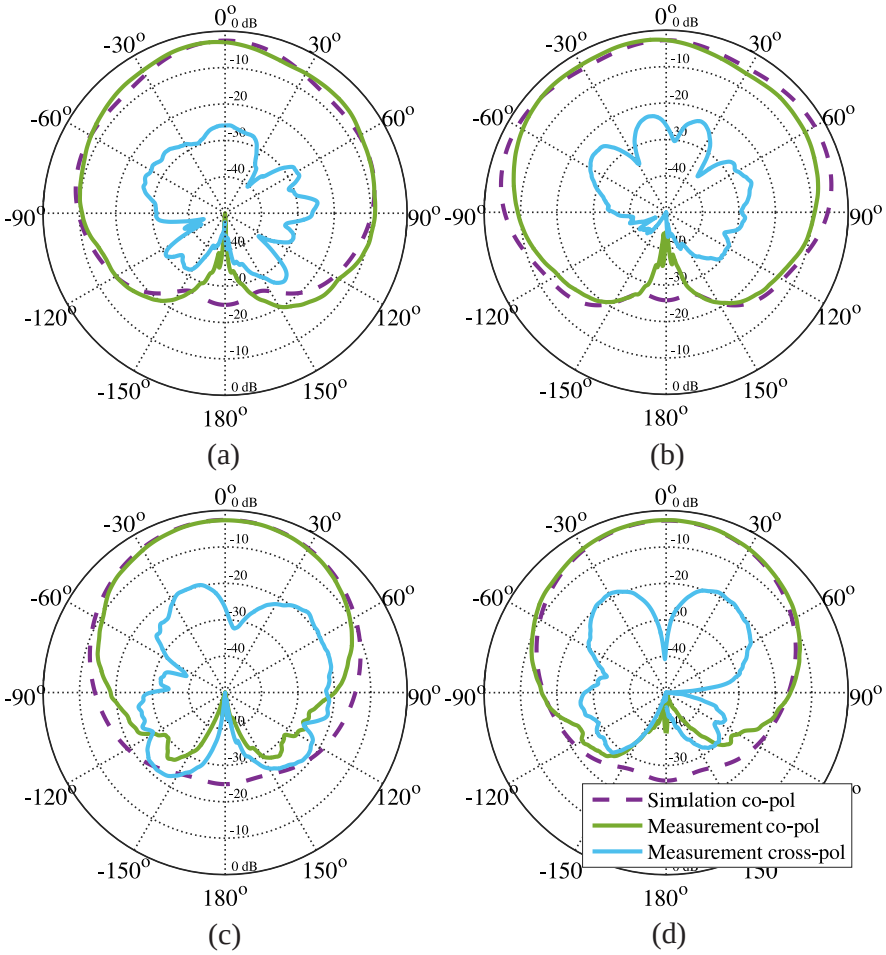

Figure 4.11: Radiation gain patterns of the simulated and measured structure. (a) 5.2 GHz, XZ plane. (b) 6 GHz, XZ plane. (c) 5.2 GHz, YZ plane. (d) 6 GHz, YZ plane.

4.2.2 Enclosed Microstrip Implementation

The suspended stripline prototype had several implementation issues: it required three layers of substrate, the fabrication process was somewhat sensitive and inaccurate, and

the employed symmetric stripline connectors did not match the structure properly. An alternative, simpler implementation for this structure is developed here, with a new prototype being fabricated.

Its structure is formed by three items: the first one, a microstrip substrate with both complementary elements printed, one on each side; the second one, a copper sheet which is placed beneath the microstrip line, leaving a gap of air between them; the last one, the metallic walls which are made by steel screws, connecting both ground planes. To keep a fixed distance between the substrate and the copper sheet, nylon washers have been placed around the screws. This way, microstrip connectors could be used and only one layer of substrate is needed, unlike the prototype of the previous subsection.

Using the design considerations described in Section 4.1.3, another design was carried out. The substrate employed was Rogers RO4350B with dielectric constant, ε_r, of 3.66 and thickness 0.51 mm. The height of the substrate was chosen small enough so the stripline feeds the slot properly but big enough so the slot mode is not altered by the strip. A 50 Ω microstrip line of 1.1 mm of width was chosen as the feeding line. The width of the cavity was set to 22.4 mm and, thus, the cut-off frequency of the TE_{10} mode is approximately 6.7 GHz. The distance from the substrate to the lower ground plane was fixed to 3.2 mm and the width of the slot to 0.3 mm in order for the slot mode to be propagated from the frequency of 3.4 GHz upwards. The width of the strip was also set to 0.3 mm to achieve an impedance level of 50 Ω. After, the lengths of the complementary elements were designed so that the first pole and zero are around the frequency of 5.2 GHz, resulting in a length for the slot of 22 mm and 18.6 mm for the strip. The length of the cavity is larger than the length of the slot, 32 mm. Finally, the screws had a diameter of 2 mm and were placed with a separation of 5.6 mm between them.

The result of the fabrication process led to a simpler and more robust prototype, as shown in Fig. 4.12. Furthermore, another TRL calibration kit was designed and fabricated in order to obtain measurements with coincident reference planes in the middle of the structure.

Fig. 4.13 shows the magnitude of its S-parameters compared to simulation results obtained using the software tool HFSS. Good agreement between them has been found. The working frequencies of the element are limited by its low radiation up to 4 GHz and by the resonance of the TE_{101} mode of the cavity at 7.5 GHz. The fractional impedance bandwidth of this prototype is 50%. The reflection coefficient is lower than

(a)

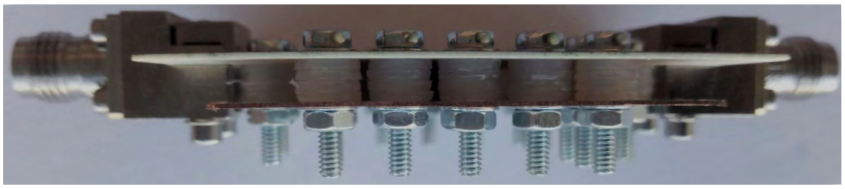

(b)

Figure 4.12: Fabricated prototype. (a) Top view. (b) Side view.

-12 dB in the working band.

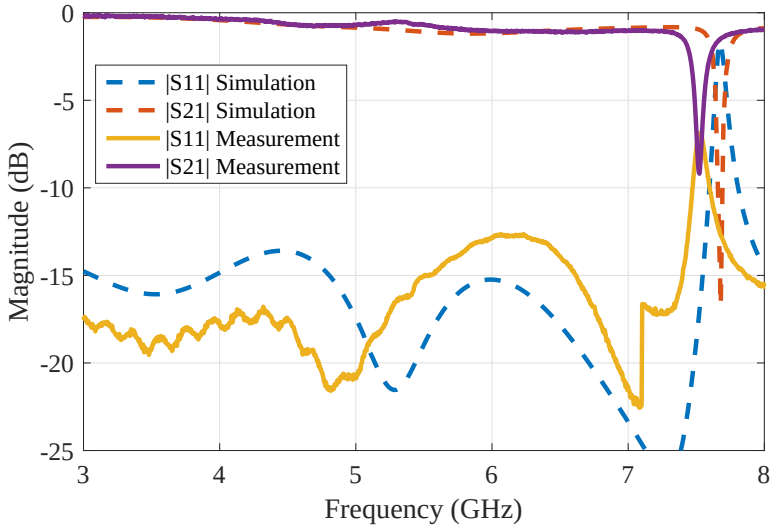

Figure 4.13: Magnitude of the S-parameters of the simulated and measured structure.

Fig. 4.14 shows the imaginary part of the impedances of the lattice network of the element extracted from simulation and measurements. As previously mentioned, it is possible to see that the pole and the zero are placed around the same frequency, which

explains the broad impedance bandwidth.

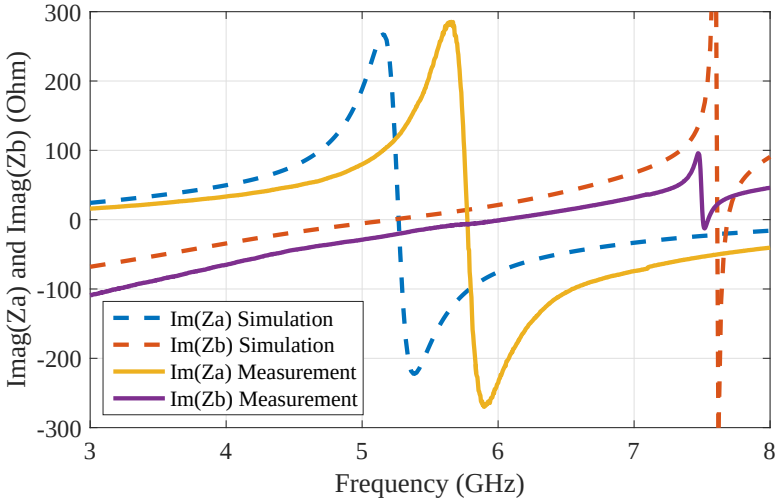

Figure 4.14: Simulation and measurement of the imaginary parts of the impedances of the lattice network of the radiating element.

Regarding its radiation properties, only simulation results are available. Fig. 4.15 shows the radiation efficiency. This radiation efficiency has been calculated as the radiated-accepted power ratio, as in the 'leakage factor'. As expected for radiating elements fed in transmission configuration, most power is carried to the second port and, in this case, around 15% is radiated. Fig. 4.16 shows radiation patterns of the simulated prototype at 5.2 GHz and 6.5 GHz. As expected, broadside radiation into only one half-space is obtained, and radiation patterns are similar at both frequencies. The obtained polarization is again linear, with a very high cross-polarization discrimination.

4.3 Use in Series-fed Arrays

The transmission configuration of this element makes it especially suitable for traveling-wave, series-fed arrays. Its broad impedance matching allows frequency reconfigurable arrays to be built without requiring the modification of the geometry of the element (as needed when resonant elements are used), simplifying the design, as done in [56]. In these arrays, the control of the power radiated by the elements is very important. The power radiated by the proposed element can be controlled by changing the width of the slot. However, as stated in Section 4.1.1, an increase in the width of the slot leads to a higher cut-off frequency in the slot mode. To solve this problem, increasing the height of the cavity can help to maintain a wide, working bandwidth. In return,

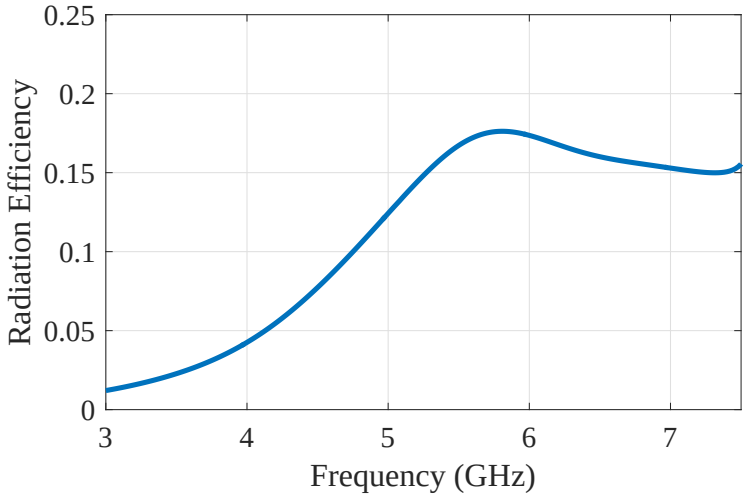

Figure 4.15: Simulated radiation efficiency of the proposed element.

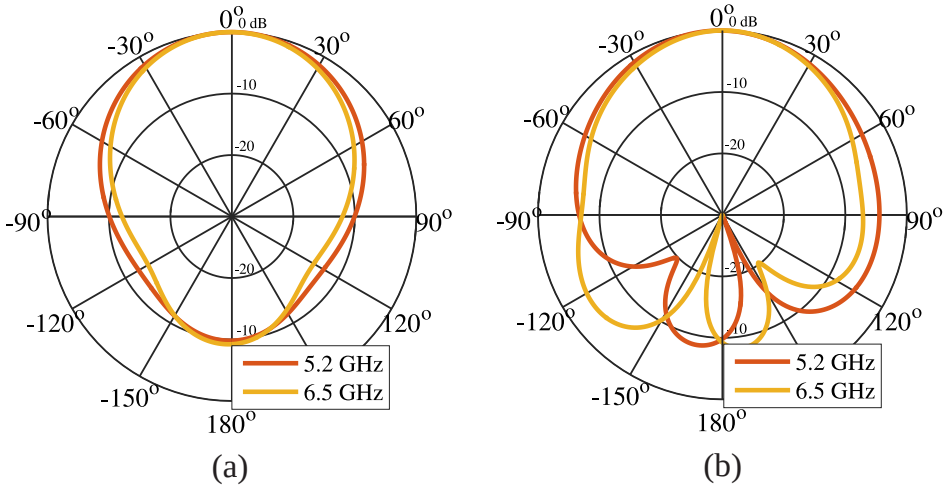

Figure 4.16: Simulated co-polar radiation patterns of the element at 5.2 and 6.5 GHz. (a) H-plane. (b) E-plane.

the impedance of the slot mode will change and, in order to satisfy condition (4.3a), the width of the stub should be readjusted.

To illustrate the control of the radiation properties by changing the width of the slot, another design has been simulated. The design is based on the suspended stripline from Fig. 4.5. In this case, the width (w_{slot}) and length (l_{slot}) of the slot are set to 1.5 mm and 13.2 mm respectively. The width (w_{stub}) and length (l_{stub}) of the stub are 0.8 mm and 10.7 mm respectively. The distance between the strip and the bottom ground plane, h_2, has been increased to 5.5 mm. The other parameters have not been modified. Fig. 4.17 shows the simulated fraction of the input power that is radiated by this element compared to that of the original design of Fig. 4.6. A significant increase

in the percentage of the radiation power can be observed throughout the working bandwidth. This means that a series-fed array with 8 elements radiating each 25% of their input power would radiate around 90% of the input power of the array, ignoring losses. This way, by controlling the radiated power of the radiating element, it is possible to choose the size of the array and, thus, the directivity.

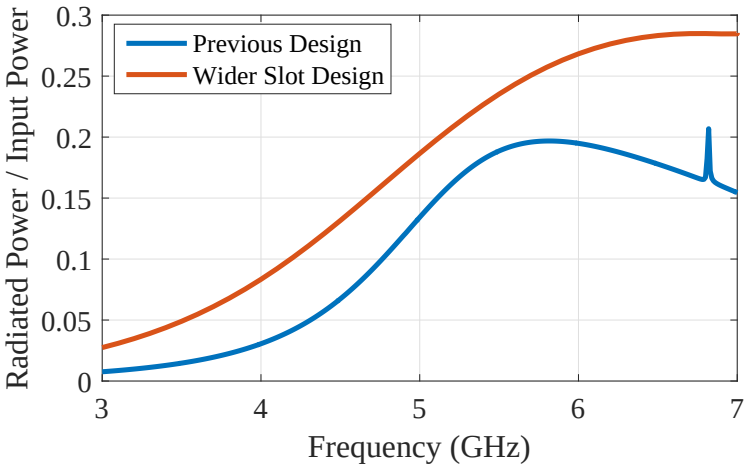

Figure 4.17: Simulation results of fraction of radiated power of input power of the suspended stripline design and a design featuring a wider slot.

The spacing between the elements of the array is also another important parameter to take into account. The minimum distance between elements is limited by the width of the cavity, w_{cavity}, since the same row of metallic posts can be used to make the vertical walls of the cavity of two adjacent elements. This space should be enough for most arrays but, if this were not the case, a material with a higher ε_r could be used if the implementation technology allows it.

4.4 Comparison of the Matching Technique

The novelty of the radiating element proposed in this chapter can be seen as a method of matching a CBS. Generally, the impedance of a slot fed by a transversal strip (centered) is high, about hundreds of ohms. Previously, the distance between the feeding stripline and the center of the slot was adjusted in order to obtain impedance matching in CBS radiating elements [59, 65], as shown in Fig. 4.18(a). This matching method has been also used in more recent works [40], and consists in reducing the impedance level of the slot. When doing this, however, either the matching condition is obtained only in a narrow band or the power radiated by the slot is significantly lowered. On the other hand, in the technique used in this chapter, the impedance matching is obtained

using a stub in the strip, just beneath the slot, as shown in Fig. 4.18(b). The stub cancels the resonant effect of the slot, nullifying its reactance, resulting in a very broad impedance bandwidth. Using a single branch of the stub instead of using two as in previous designs have proven to lessen its impedance requirements without providing additional effects. The impedance of the stub is higher and, thus, must be wider and easier to fabricate this way. The aim of this section is to compare these two ways of designing CBS radiating elements using simulation examples.

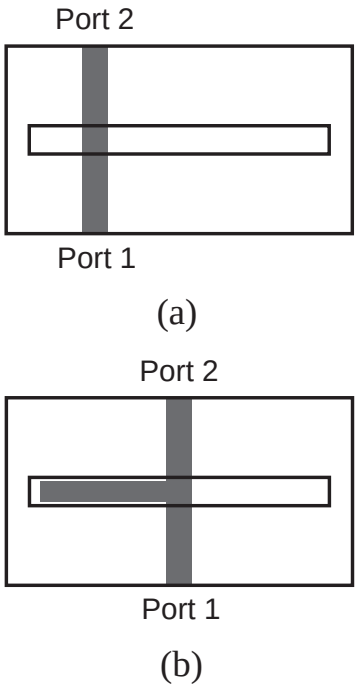

Figure 4.18: CBS matching techniques. (a) Increasing the off-set feeding distance. (b) Using a matching stub.

4.4.1 Decentering of the feeding line

In order to match a strip to a coupled slot, one of the most used techniques consists in increasing the off-set feeding distance of the stripline, as in Fig. 4.18. As shown in [23], the impedance of a center-fed slot can be seen as two slotlines in parallel ended in short-circuit, whose lengths would be half the slot length. However, when the slot is decentered, the lengths of these lines change, and one of the slotlines would be longer than the other, as depicted in Fig. 4.19. The higher the off-set feeding distance is, the lower the total impedance of the slot results.

As the usually high impedance of the slot is reduced, the impedance bandwidth of the element is increased. The impedance bandwidth of the element can reach very

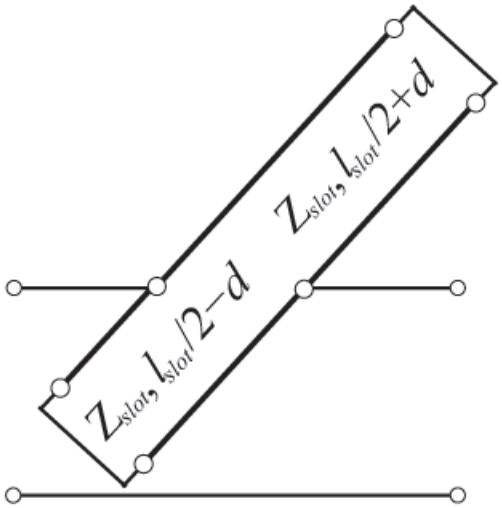

Figure 4.19: Model of the decentering of the feeding line technique.

high values using this technique; however, the radiated power in the working band is adversely affected. This technique can be used either in microstrip-fed slots or in stripline-fed slots.

4.4.2 Comparison Results

In order to compare these two techniques, a CBS has been matched using both methods and simulated using the commercial electromagnetic simulator HFSS. The dimensions of the cavity, l_{cavity}, w_{cavity} and h, are, respectively, 90 mm, 40 mm and 10 mm. The length of the slot, l_{slot}, is 78 mm and its width, w_{slot}, is 2.22 mm. The cavity is filled with a dielectric whose ε_r is 2.2 and its loss tangent is 0.0012. In both cases, the slot is fed by a strip placed 0.762 mm (h_1) beneath it, and whose length, w_{feed}, is 2.22 mm. These dimensions are shown in Fig. 4.20.

The impedance bandwidth of the CBS for different off-set feeding distances (d in Fig. 4.20(a)) has been evaluated. As shown in Fig. 4.21, it is possible to control the matching when d is modified. The impedance bandwidth is only about 200 MHz around 2.1 GHz when $d = 30$ mm, but it is very broad when $d = 36$ mm, $d = 38$ mm or when the matching stub is used. The dimensions of the stub, l_{stub} and w_{stub}, are 26 mm and 1.8 mm, as shown in Fig. 4.20(b). It is worth noting that, while the S-parameters of the matching-stub case are quite insensitive to small modifications of its dimensions, the off-set feeding technique is very sensitive to the distance d.

As illustrated in Section 4.3, the amount of power radiated by a single element is key

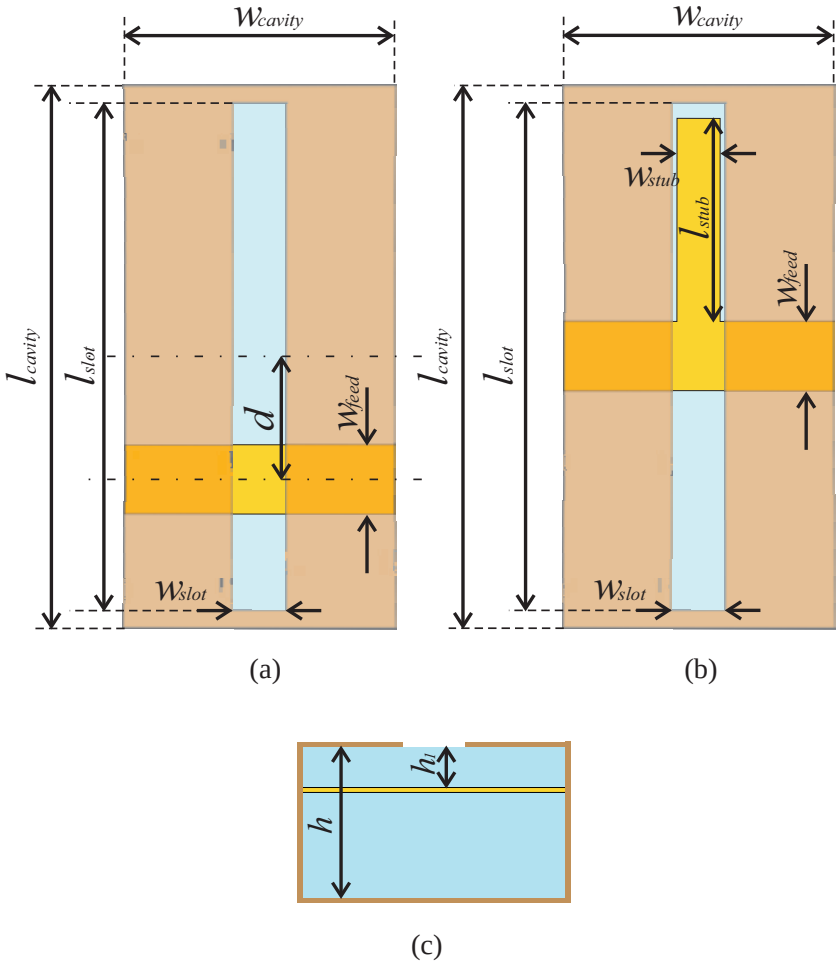

Figure 4.20: Top and side views of the simulated structures. (a) Top view of the decentered case ($w_{feed} = 2.22$ mm, $w_{cavity} = 40$ mm, $l_{cavity} = 90$ mm, $w_{slot} = 2.22$ mm, $l_{slot} = 78$ mm, $d =$ mm). (b) Top view of the matching stub case ($w_{feed} = 2.22$ mm, $w_{cavity} = 40$ mm, $l_{cavity} = 90$ mm, $w_{slot} = 2.22$ mm, $l_{slot} = 78$ mm, $w_{stub} = 1.8$ mm, $l_{stub} = 26$ mm) (c) Side view ($h = 10$ mm, $h_1 = 0.762$ mm).

when building series-fed arrays. Although it is possible to obtain a similar bandwidth using both techniques, the radiated power may be very different. Fig. 4.22 shows the ratio between the radiated power and the incident power for the studied cases. It can be seen that the radiated power has a more constant response in the working frequency band when using the matching stub. In addition, the maximum radiated power is reduced when the off-set feeding distance is increased, and the amount of radiated power can be very low in the broadly matched case, limiting the bandwidth in which the structure radiates effectively. In order to increase the power that is radiated by the structure, impedance bandwidth can be traded in for radiation power, e.g. when $d = 30$ mm.

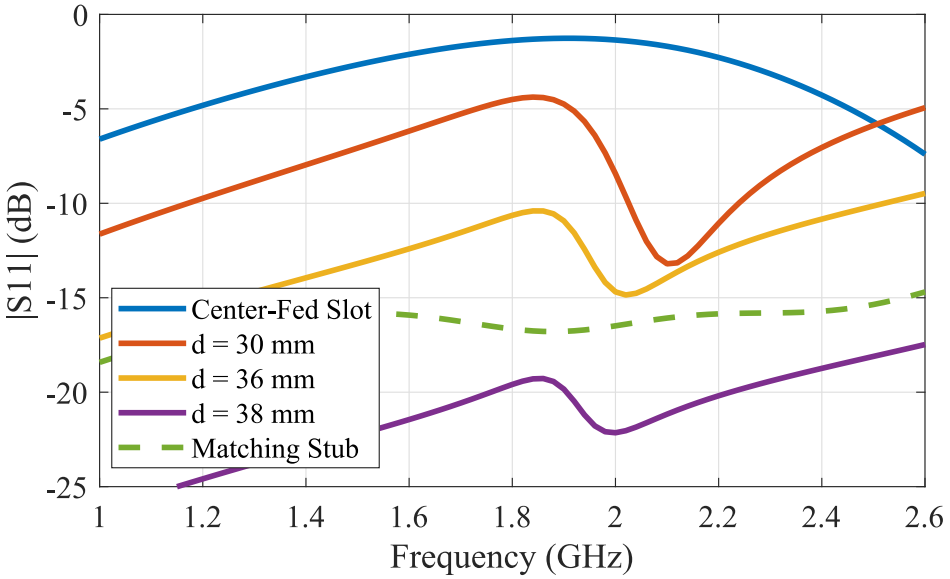

Figure 4.21: Magnitude of the S11 parameters of the CBS fed by a stripline for different off-set feeding distances and using the matching stub technique.

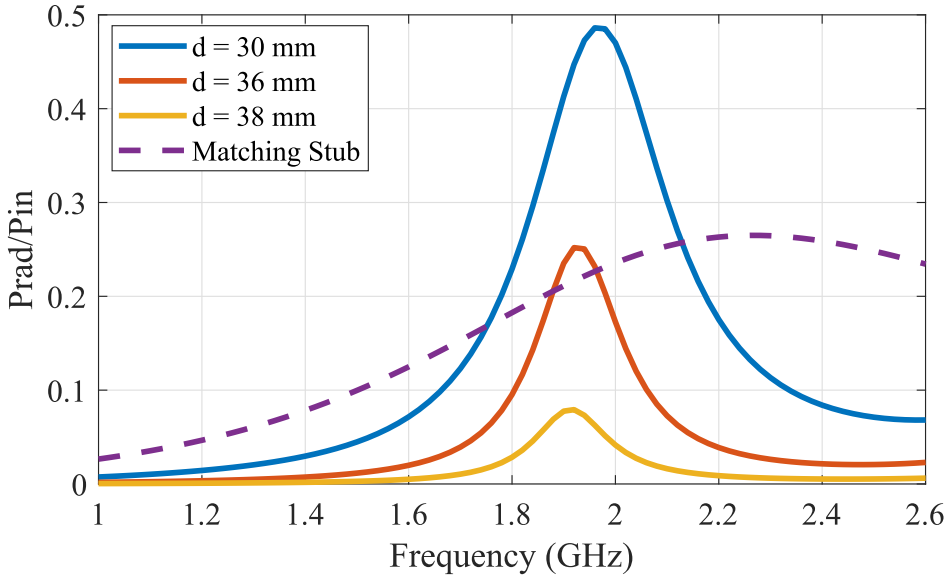

Figure 4.22: Radiated power incident power ratio for different off-set feeding distances and using the matching stub technique.

In conclusion, both methods can be used to design radiating elements with a very broad impedance bandwidth, but only when using the matching stub the element radiates effectively along the broad bandwidth. On the one hand, increasing the off-set feeding distance is a very simple solution that can be used in any kind of strip. On the other hand, when using an asymmetric feeding stripline or enclosed microstrip, the use of a matching stub results in a higher bandwidth and in a more robust behavior.

4.5 Bandwidth Improvements

The prototypes shown in this chapter have around a 50% of fractional bandwidth. However, the original "complementary strip-slot" (microstrip, bilateral radiation) had a wider impedance bandwidth and a more constant radiated power. This is due to the cavity behind the slot, which resonates at its resonance frequency, preventing the element from working properly at that frequency. In this section, two ways of improving the bandwidth for this radiating element are illustrated, and the results of using them shown.

A way of increasing the bandwidth of the element is increasing the resonance frequency of the cavity. However, the behavior of the slot is strongly affected by the dimensions of the cavity, and when reducing these, the frequency at which the slot starts radiating considerably will also increase. Therefore, narrowing the cavity will increase the upper working frequency but will also increase the lower working frequency. Thus, in that case, a higher-frequency design will be obtained instead of one with a higher bandwidth.

So, instead of reducing the width of the cavity to increase the resonance frequency of the TE_{101} mode, the approach followed in this section consists in reducing the length of the cavity, as it also increases this resonance frequency, as shown in (4.1). The minimum length of the cavity, however, is limited by the length of the slot and, thus, different techniques to reduce its longitudinal size are used.

4.5.1 Double-T Slot

The first technique used to increase the bandwidth of the element consist in increasing the length of the slot without it reaching the edge of the cavity. More precisely, bending the edges of the slot, lengthening it in a orthogonal direction. This way, the slot will start radiating at lower frequencies. Fig. 4.23 shows the proposed modification. The slot was lengthened in two directions to keep the symmetry so the lattice-network equivalent circuit from Section 4.1.2 is still valid and, thus, use the same design considerations. Of course, since the resonance frequency of the slot is now lower, the length of the stub had to be also increased to obtain broadband matching.

To compare the result of introducing the proposed modification, the HFSS-simulation results of two different designs are presented. The first design is the one from Section 4.2.2 but with solid metallic walls instead of screws. The second design has the mod-

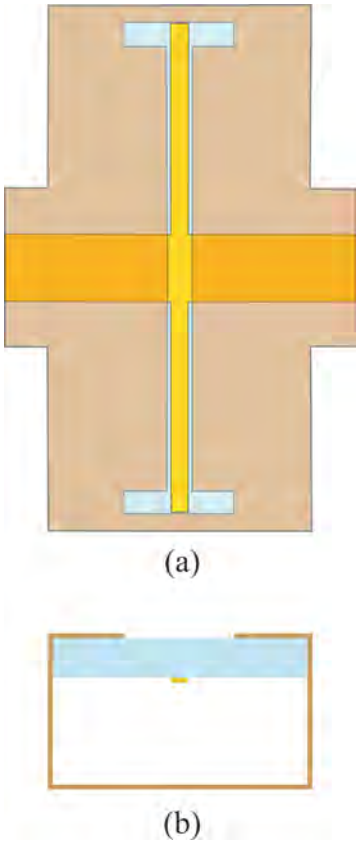

Figure 4.23: Topology of the modified structure. (a) Top view. (b) Front view.

ified slot, with an horizontal branch of 5.5 mm long and a slightly longer stub of 22 mm. These are the only differences between both designs.

Fig. 4.24 shows the S parameters of both structures, where it can be seen that both of them have a wide impedance bandwidth, up to the resonance frequency of the cavity at 8 GHz. Note that this resonance frequency is higher that the one shown in Fig. 4.13 because of the effect of using a solid metallic wall instead of metallic posts/screws, which changes the effective width of the cavity. Fig. 4.25 shows the imaginary part of the impedance of the slot in each case. It can be observed that the resonance frequency of the slot have been reduced from 5.4 GHz to 4.3 GHz when bending the slot with the double-T configuration. The impedance level of the new slot is lower because, when splitting the edge in two, the resulting impedance is the parallel of both slot segments. The aim of this section is to compare objectively the use of this slot and, thus, no more modifications were added to the structure. However, the effect of the reduced impedance can be easily compensated with a tune of the widths of the stub/slot to obtain an even lower S11 parameter.

Regarding the radiation, Fig. 4.26 shows the radiated power to input power ratio

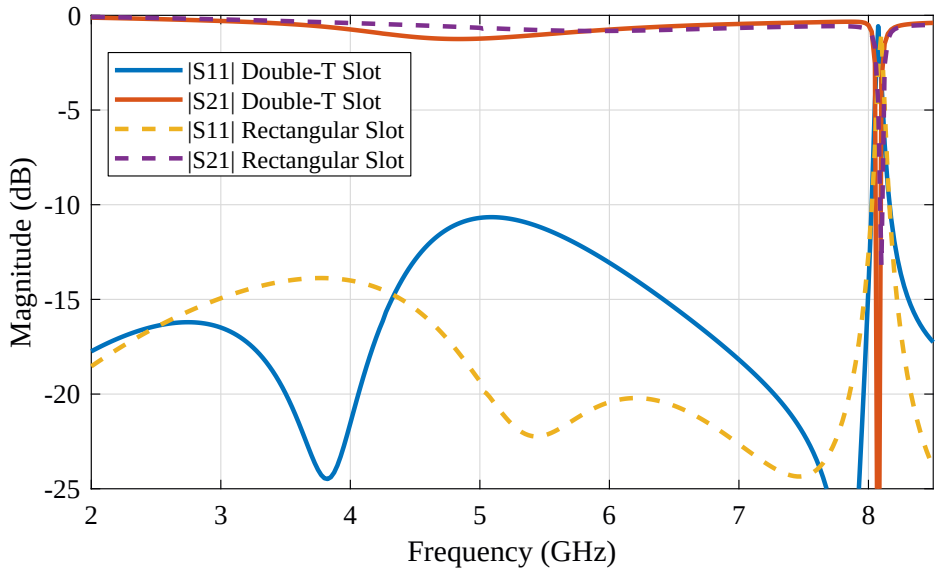

Figure 4.24: Magnitude of the S parameters of the double-T slot and the rectangular slot.

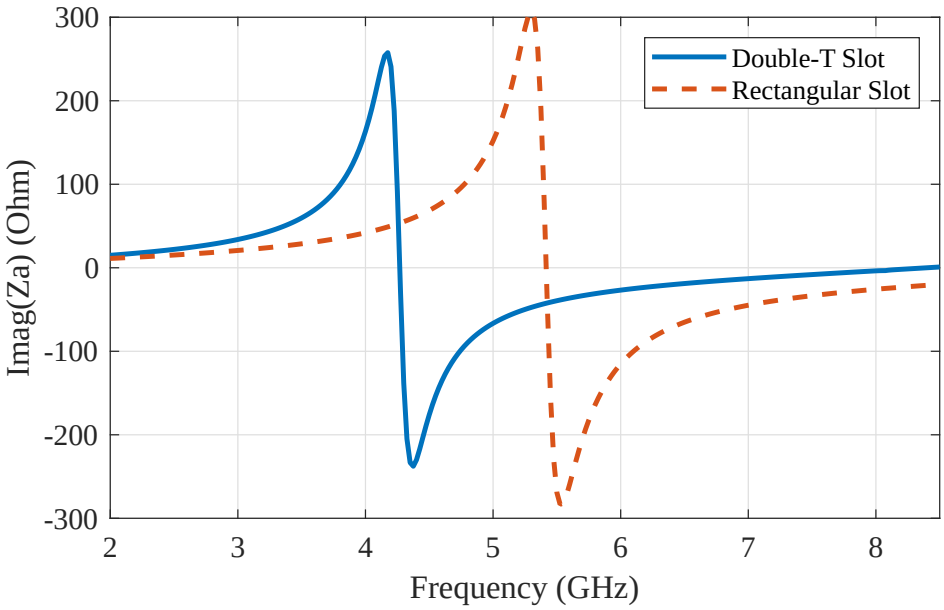

Figure 4.25: Imaginary part of the impedance of the double-T slot and the rectangular slot.

in both cases. It can be seen that when the modification is used, the element start radiating at lower frequencies. This is the effect that achieves a wider useful bandwidth of the radiating element. When using the double-T slot, it starts radiating considerably at 1 GHz less than when using the original slot. The fractional bandwidth has increased approximately from a 66% to a 90%. Fig. 4.27 shows the radiation pattern of both designs. The use of the double-T slot do not change the radiation pattern. Thus,

the radiation characteristics are the same as in the original case: the polarization is linear with a very high cross-polarization discrimination and a stable shape along the bandwidth.

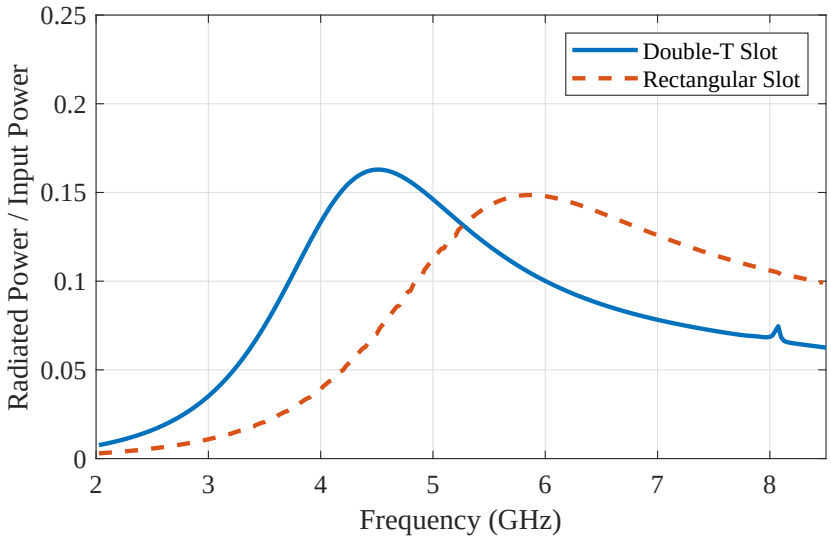

Figure 4.26: Radiated power to input power ratio of the simulated double-T slot and rectangular slot.

In conclusion, the use of a double-T-shaped slot makes possible the reduction of the frequency from which the slot starts radiating and, this way, the working bandwidth of the element can be increased. The results are quite satisfying since no additional drawbacks were added with the modification.

4.5.2 Bow-Tie Slot

In this subsection, another modification of the radiating element is proposed to improve the stability of the radiated power along the bandwidth. Changing the shape of the slot into a bow-tie keeps the radiated power constant in a significantly wider bandwidth. In addition, and in a similar way to the double-T shaped slot, the length of the bow-tie slot is shorter than the length of the rectangular slot, making the cavity shorter and its resonance frequency higher.

Another novelty of the design in this section is the use of the element in the millimeter-wave band. The increasing number of applications in the millimeter-wave band have brought attention to antenna systems at these frequencies. For these applications, reconfigurable and high-gain antennas are typically desired. Traveling-wave antennas, especially of the leaky-wave type, are good candidates to solve the problem of the phase shifters in mm-wave antenna arrays [66]. This is due to their simple-

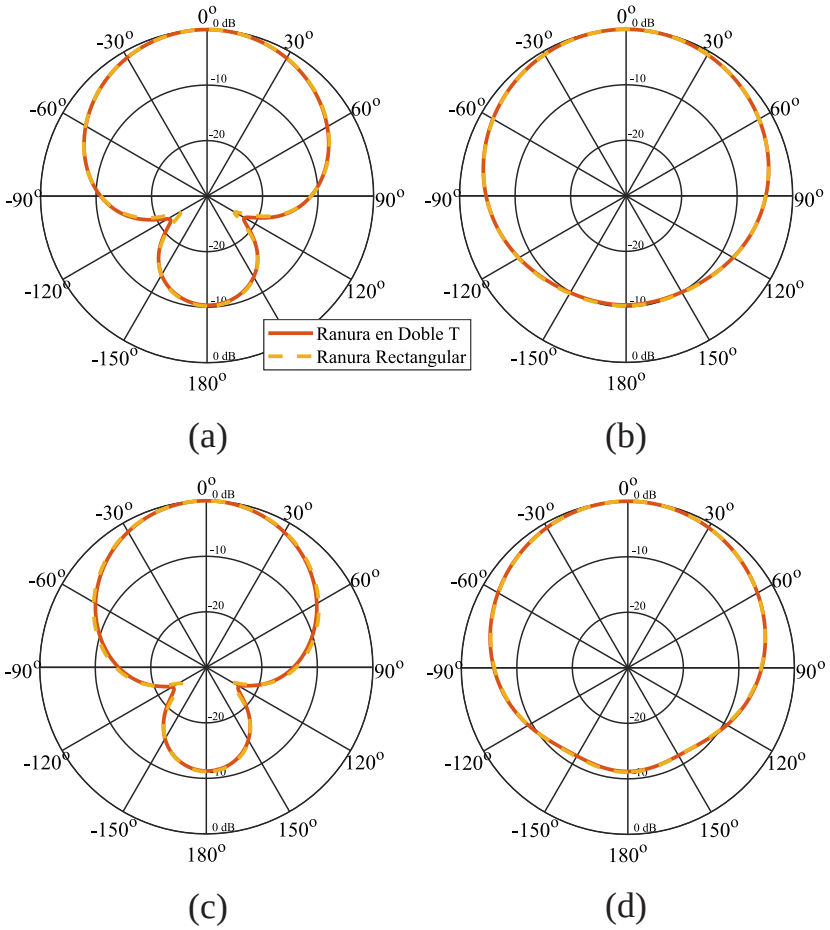

Figure 4.27: Simulated radiation pattern of the double-T slot and the rectangular slot. (a) H-plane, 4 GHz. (b) E-plane, 4 GHz. (c) H-plane, 6 GHz. (d) E-plane, 6 GHz.

feeding and frequency-scanning capabilities. Thus, the radiating element proposed in this chapter can be especially useful in this frequency band. The analysis of the element done in Section 4.1 is still valid for higher frequencies. A disadvantage of the CBS radiating element is that, in some cases, its total thickness can be too large. As it is expected, increasing the working frequency of the element reduces its overall size, making it more compact and suitable for integration. For these reasons, the radiating element presented here is a very good candidate to build reconfigurable arrays for millimeter-wave frequencies.

The geometry of the modificated structure is very similar to the ones already shown in the chapter. The main difference is the shape of the slot and cavity which, instead of being rectangular, are now bow-tie-shaped. The proposed geometry is shown in Fig. 4.28. The new shape of the slot makes its radiation more uniform in the working frequency band, while it also produces the effect of the double-T slot that increases the bandwidth. The shape of the cavity has also been modified to keep the slot to metal

ratio of the section. The feeding structure in this case is an asymmetric stripline with a homogeneous dielectric.

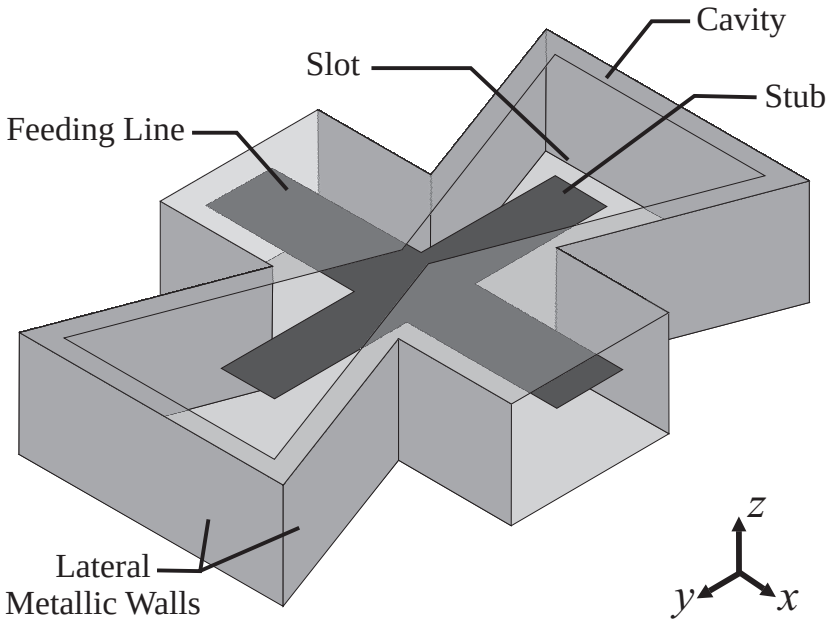

Figure 4.28: Geometry of the proposed structure.

The slot length, l_{slot}, has been designed to have its resonance around 70 GHz. This resonance is also dependent on the size of the cavity, which must be previously designed to allow the propagation of the slot mode, as explained in 4.1.1. The maximum width of the slot, w_{slot}, is chosen to ensure that the angle between the bow-tie is 130 degrees, which is a standard value for bow-tie shaped slots. The shape of the cavity is the same as the slot, but its dimensions are larger enough to contain the slot. Once the slot is designed, the stub dimensions, l_{stub} and w_{stub}, must be adjusted to obtain a broad impedance bandwidth. The impedance of the feeding stripline is 50 Ω. Metallic lateral walls are used in this design but they could be implemented using metallic posts in the same way as in 4.2.2 and [67]. All the dimensions of the proposed structure are shown in Fig. 4.29.

The structure has been simulated using the HFSS commercial electromagnetic simulator. Fig. 4.30 shows the magnitude of the S_{11} and S_{21} parameters. As expected, a very broad impedance bandwidth is achieved. The existence of the cavity resonance is clearly seen at 103 GHz in Fig. 4.30, increasing the losses at that frequency. Fig. 4.31 shows the simulated values of the radiated power to input power ratio. The structure starts radiating significantly around 30 GHz, thus the working bandwidth of the element spans from 30 GHz up to about 100 GHz (more than 100% fractional bandwidth). Compared to previous results (i.e. Section 4.2.1, 48%), the fractional bandwidth has

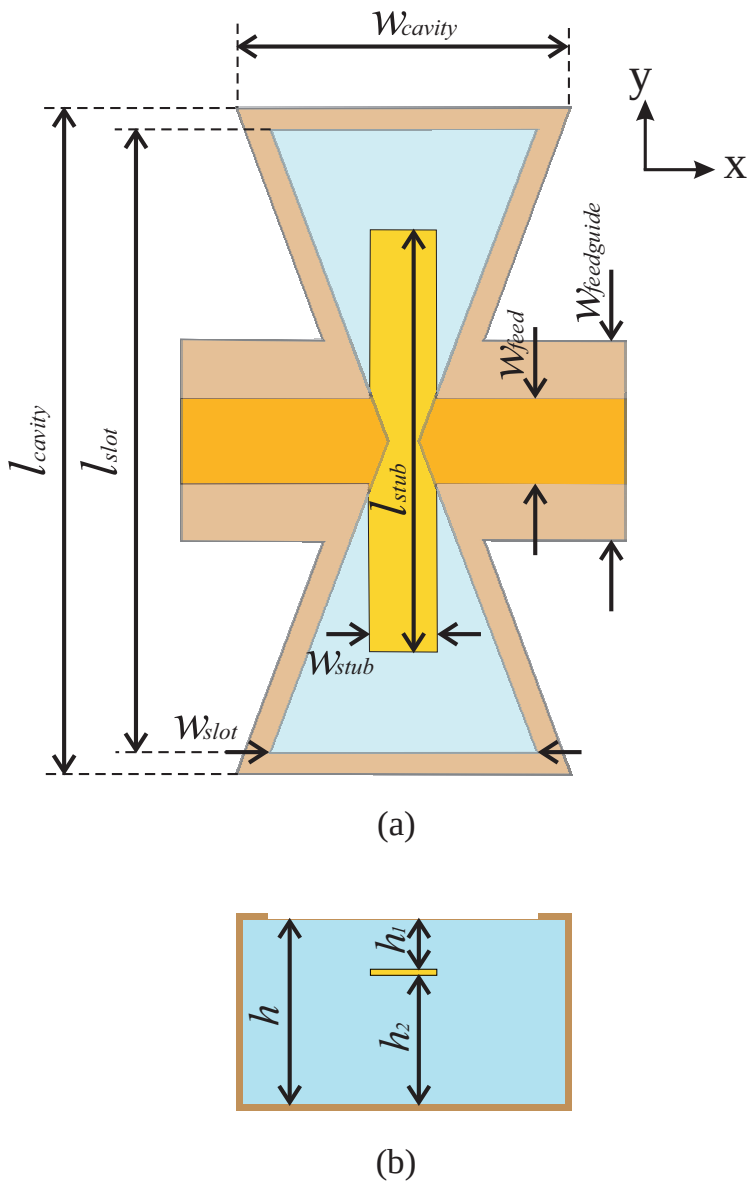

Figure 4.29: Top and side views of the bow-tie shaped structure with dimensions. (a) Top view (w_{feed} = 0.38 mm, $w_{feedguide}$ = 0.9 mm, w_{cavity} = 1.5 mm, l_{cavity} = 3 mm, w_{stub} = 0.3 mm, l_{stub} = 1.9 mm, w_{slot} = 1.2 mm, l_{slot} = 2.8 mm). (b) Side view (h = 0.6 mm, h_1 = 0.15 mm, h_2 = 0.45 mm).

been increased noticeably. It is worth noting that, from 70 GHz up to over 100 GHz, the radiated power to input power ratio is almost constant. The amount of radiated power is considerably higher that in other designs due to the increased width of the slot. Finally, the simulated radiation pattern is shown in Fig. 4.32. The results show a very stable radiation pattern along the working bandwidth.

With this design, it is illustrated that a further modification of the shape of the slot allows not only a wider bandwidth but also a more stable radiation level. Furthermore,

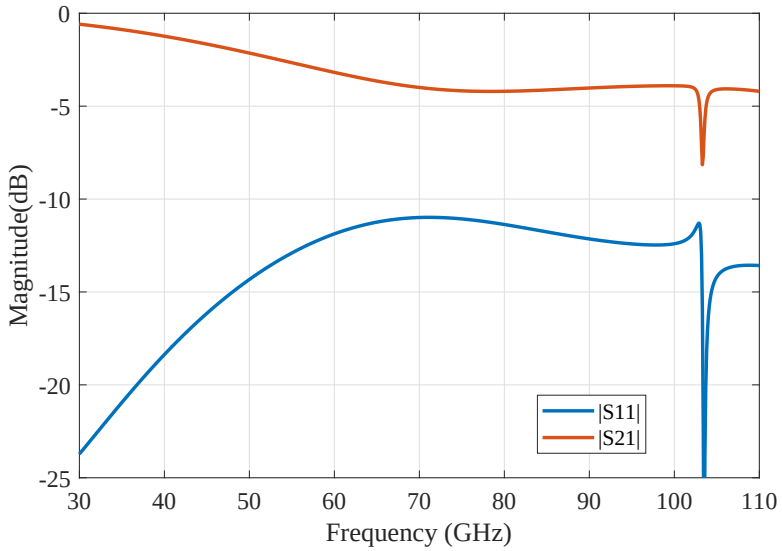

Figure 4.30: Magnitude of the S-parameters of the simulated bow-tie shaped slot structure.

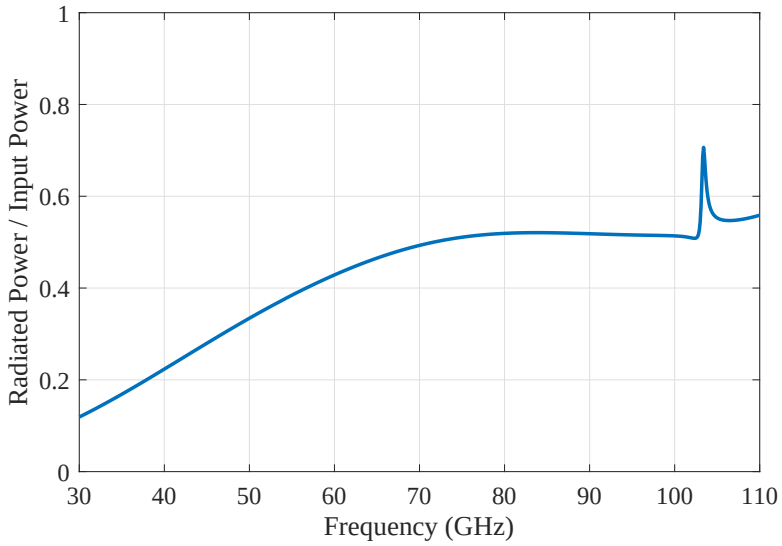

Figure 4.31: Radiated power to input power ratio of the simulated bow-tie shaped slot structure.

this is the first time that this element is proposed at millimeter-wave frequencies.

4.6 Conclusion

A broadband CBS radiating element fed by a strip with a transmission configuration was proposed in this chapter. Its main novelty is the enhanced impedance bandwidth obtained when a complementary stub is placed beneath the slot. The modes

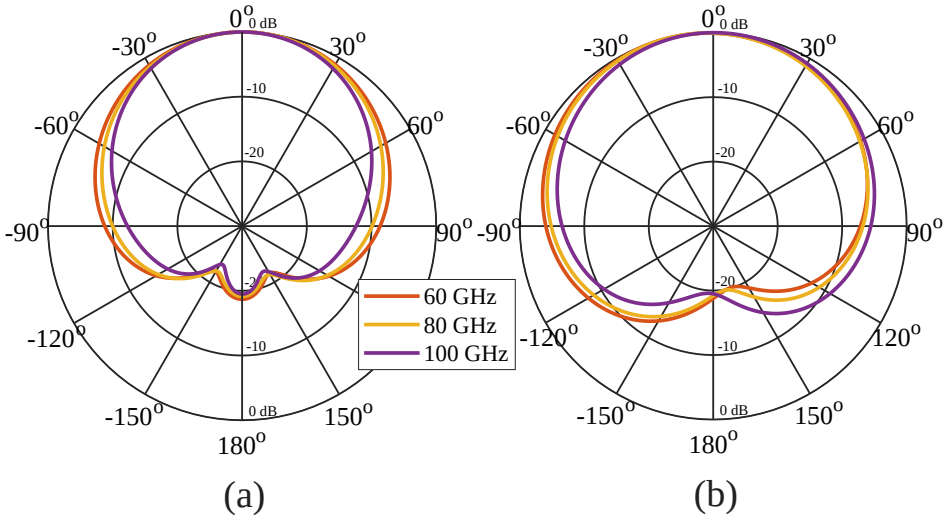

Figure 4.32: Normalized-gain radiation patterns the simulated bow-tie shaped slot structure. (a) YZ plane. (b) XZ plane.

propagating through the cavity play a fundamental role in its behavior. In order to understand the performance of the structure and simplify its design, a lattice network-based transmission line model was proposed. This methodology greatly avoids the use of a parametric analysis.

Several structures based on this concept were designed and measured. Their results show a wide impedance matching and unidirectional radiation with a very pure linear polarization. The structure was firstly fabricated using a suspended stripline technology which was later improved to an enclosed microstrip, achieving a more simple implementation.

Adjusting the width of the slot it is possible to control the amount of power that is radiated. This was illustrated with a design example. This control can be essential when building traveling-wave arrays.

A comparison between the proposed way of matching a CBS and the standard way (changing the feeding point of the slot) was also shown. The use of a matching stub seemed a clearly superior technique for wider-band designs.

Also, even though the resonance of the cavity limits the bandwidth of the radiating element, two different ways of overcoming this drawback were developed. Both ways are based on reducing the length of the slot to make the cavity smaller. The use of these modifications did not alter the performance of the element.

The proposed structure is very suitable to build wideband series-fed arrays to be used in bandwidth-intensive wireless communications systems. Additionally, it can also

be used in the millimeter-wave band for applications such as new-generation communications and radars.

Chapter 5

Broadband-CBS-Based Linear Series-Fed Arrays

The immediate application of the radiating element proposed in Chapter 4 is to build series-fed arrays. Series feeding is advantageous over corporate feeding in several situations, e.g. when the size, losses, or complexity of the feeding lines are important, or when frequency beam-steering is desired. As opposed to the element proposed in [1], the unidirectional radiation of the CBS-based radiating element allows the design of single-beam arrays without needing a reflector plane, which increases the size and reduces the bandwidth of the antenna. Thus, this chapter aims to build arrays similar to the ones proposed in [56] and [3] but with unidirectional radiation using the new element.

The implementation of linear series-fed arrays in microstrip technology was straightforward, loading the line with several strip-slot elements. However, the presence of a cavity in the new radiating element can be detrimental not only in the design of the array but also in its fabrication. For this reason, new design techniques and different implementations will be required to fix these problems.

The chapter is divided into two main sections, one for each prototype whose fabrication has been carried out. First, Section 5.1 will describe the design, fabrication, and results of a Traveling-Wave Array (TWA) antenna. Then, Section 5.2 will do the same with a log-periodic array.

5.1 Traveling-Wave Array

In TWAs, a wave travels across the antenna and the power is radiated gradually, either continuously or discretely. Thus, an array of series-fed CBSs can be regarded as a TWA or, more specifically, as a Leaky-Wave Antenna (LWA) since the radiating mechanism is a fast-wave. An LWA radiates as a fan beam, making it possible to scan the beam by controlling the phase progression between the elements (in this case, the frequency). Thus, they are a very simple way of fabricating frequency-scanning antennas.

Usually, linear arrays made of series-fed slots are built to have a single-frequency-shaped beam. This is due to the resonant nature of the slot, which greatly limits the bandwidth of the radiating element. Since the matching method explained in Chapter 4 overcomes this drawback, the excellent radiating properties of a slot can now be also used in scanning-beam LWAs. This was already done in [56], but using microstrip-fed slots which had bilateral radiation. Thus, the antenna always had at least two beams, a feature not very useful in directive antennas. When using a CBS, however, only one beam is obtained.

Fig. 5.1 shows a series-fed array made of several broadband CBSs. When the first radiating element is fed, the power that is not radiated or reflected goes to the second element and, thus, each element radiates a small amount of power. As explained in Section 4.3, it is important to adjust the power radiated by each element according to the total number of elements in the array. As in phased arrays, the phase difference between the radiating elements plays a fundamental role in the shape of the diagram of the array factor. In the case of LWAs, this phase difference is controlled by the frequency and the distance between the elements. In order to design an array that scans with frequency, it is also very important to adjust the distance between the elements so the array scans in the desired frequency range.

5.1.1 Implementation Considerations

To make the implementation of the array possible using the available fabrication technology, some considerations were made. First, the width of the cavity of the radiating element must be moderately small to have a margin to adjust the distance between the elements later. To do this without compromising the performance of the radiating element, the height of the structure must be increased, making it less planar.

Secondly, to reduce the number of screws and washers used, a cavity made of

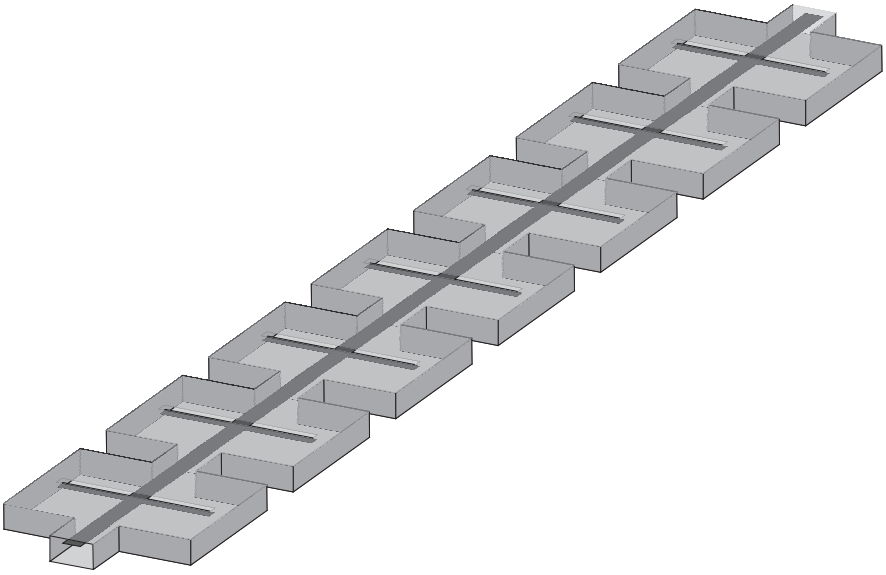

Figure 5.1: Geometry of the proposed array.

aluminum was used instead. Since the arrays can have a large number of elements, using the holes and screws approach was too tedious. This way, the aluminum cavity allows more control in the dimensions of the cavity, reduces its complexity, and let us have a more robust structure. Fig. 5.2 shows the fabricated cavity. It was mechanized from a solid block of aluminum using milling cutters.

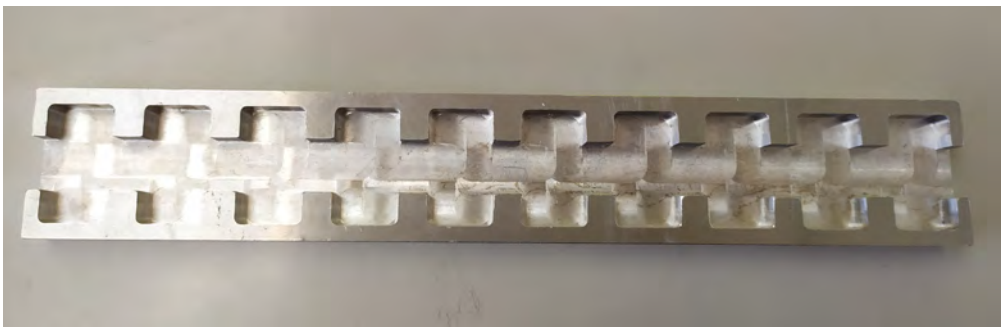

Figure 5.2: Aluminum cavity mechanized to fabricate the array.

Thirdly, a 3D-printed dielectric fill was placed inside the cavity to support the microstrip substrate where the strip and slot are printed. The dielectric material is HIPS [68] and was printed to fit the aluminum cavity. According to in-house measurements of the HIPS, its relative electric permittivity, ε_r, is around 2.42 and its dielectric loss tangent is 0.005 in the 1-5 GHz frequency range. The use of this technology in an array proves that 3D printing can also be useful in the fabrication of antennas. Fig. 5.3 shows the aluminum cavity filled with the 3D-printed material.

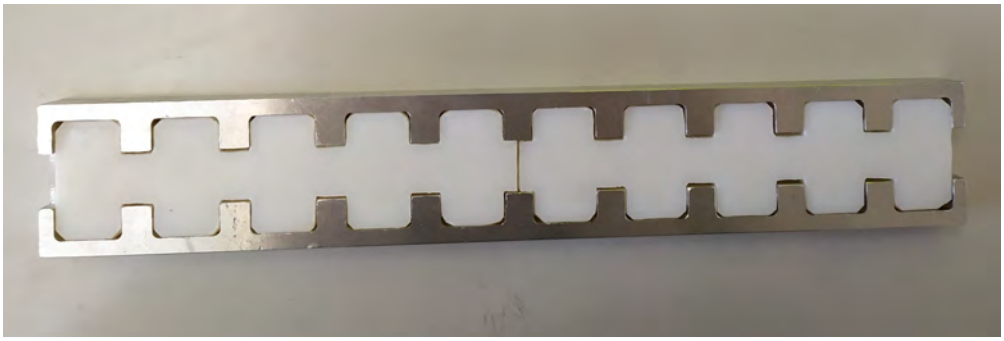

Figure 5.3: Aluminum cavity filled with the 3D-printed dielectric to assemble the array.

5.1.2 Design

Using the design procedure of Section 4.1.3 and the implementation considerations of Section 5.1.1, another realization of the radiating element was simulated using HFSS. As in Section 4.4, only a single branch of the stub is used to obtain a wider stub, which is easier to fabricate. To keep the array simple, the bandwidths improvements of Section 4.5 have not been used. The cavity is, in this case, made of aluminum and filled with HIPS, resulting in an enclosed-microstrip configuration with HIPS instead of air. The substrate where the stub, slot, and feeding line are etched is Rogers RO4350B with dielectric constant, ε_r, of 3.66 and thickness 0.51 mm. A 50 Ω microstrip line of 1.05 mm of width was chosen as the feeding line. The width and height of the cavity were set to 20 mm and 8 mm, respectively. The slot width was increased to 2 mm in order for the element to radiate more power. The width of the strip was set to 2.1 mm to achieve an impedance level of 50 Ω. After, the lengths of the strip and slot were designed so that their pole and zero are around the frequency of 3.9 GHz, resulting in a length for the slot of 30 mm and 11.7 mm for the strip. The length of the cavity is larger than the length of the slot, 36 mm. The S-parameters of the simulated structure are shown in Fig. 5.4. A broad impedance bandwidth up to the resonance of the TE_{101} at 4.6 GHz is demonstrated. Fig. 5.5 shows its radiated to input power ratio, which increases with frequency along with the bandwidth, reaching the maximum value of 0.2. The ripple around 4.6 GHz at both figures is due to the resonance of the cavity and so, the array will be designed to work up to that frequency.

The next step in the array design is to determine the distance between radiating elements. To do this, the theory of periodic leaky-wave antennas was used [69]. The wave that propagates through the feeding line is a slow wave ($\beta > k_0$, where k_0 is the free space wavenumber and β the phase constant of the feeding structure). However,

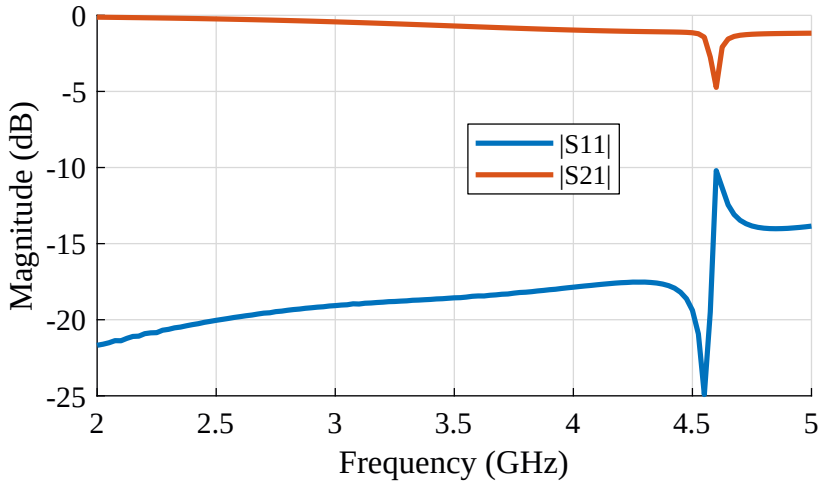

Figure 5.4: Magnitude of the S parameters of the simulated unit cell of the array.

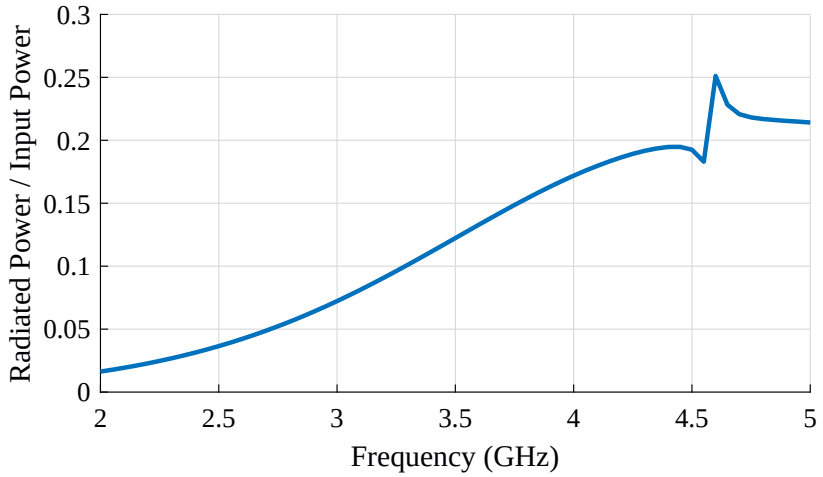

Figure 5.5: Radiated power to input power ratio of the simulated unit cell of the array.

only fast waves ($\beta < k_0$) will escape the structure and radiate. When the discontinuities (the slots in this case) are added, the periodicity introduces an infinite number of space harmonics, each characterized by a phase constant β_m, and related to each other by

$$\beta_m = \beta_0 + \frac{2\pi}{d}m, \quad \text{with} \quad m \in \mathbb{Z} \tag{5.1}$$

where d is the distance between the periodic discontinuities and β_0 the fundamental space harmonic, which is the phase constant β somewhat modified by the presence of the discontinuities. β_m can take on a large variety of values, but, usually, only when $m < 0$ the mode will be a fast wave and, thus, radiate. For this reason, the value of d must be designed so only one mode radiates in the desired bandwidth (usually, the space harmonic number $m = -1$), implying that only one beam will appear. Furthermore,

if there is radiation, the value of β_m will determine the angle of the main beam, θ measured from broadside following

$$\theta \approx \arcsin(\beta_m/k_0), \tag{5.2}$$

considering a small leakage factor and isotropic radiating elements. Thus, if the structure has frequency dispersion (β_m is a nonlinear function of frequency), the pointing angle will change with frequency and frequency-scanning will be possible.

Using these considerations, the size of the cell unit, d, has been designed for the CBS presented previously in this subsection. Fig. 5.6 shows the radiation cone when $d = 29$ mm, this is, the the phase constants of the different space harmonics, β_m, multiplied by d, with the air lines ($k_0 d$). This figure is an alternative representation of (5.1) and, thus, we can foresee from it that an array of this CBS with $d = 29$ mm (around $\lambda/3$ at the center of the band) will scan with a single beam approximately from 2.75 GHz to 4.5 GHz. Additionally, according to (5.2) the broadside will take place at the frequency when $\beta_m = 0$, which is at 3.5 GHz. Furthermore, the number of elements, N, must also be chosen. Since each radiating element radiates up to 20 % of the power (depending on the frequency), a number of elements big enough to radiate a significant part of the input power must be chosen without compromising the size of the antenna. The amount of power that will not reach the end of the array (being, thus, radiated or dissipated) without taking reflections into account is

$$P_{\text{lost}} = 1 - |S_{21}|^{2N}. \tag{5.3}$$

In order to use around 90 % of the input power at the higher frequencies and keep the length of the array reasonable, a number of elements, N, of 10 was chosen ($3.4\lambda_0$ at broadside frequency). Another aspect that must be chosen is the termination of the array. Usually, a periodic LWA is ended either in an open circuit or in a matched load. The open-circuit allows to radiate more power and increase the radiation efficiency of the antenna at the cost of more reflection. The matched load has a better VSWR and a more predictable radiation pattern but the power dissipated at the load is lost. The matched load case will be addressed in this work.

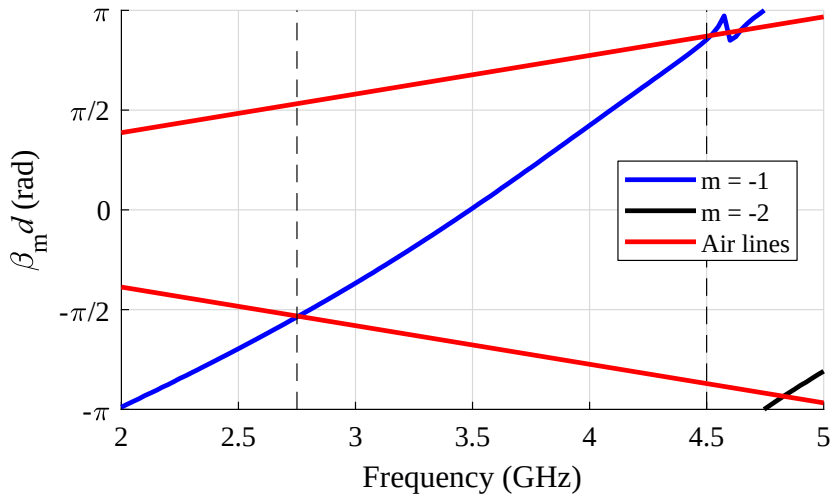

Figure 5.6: Phase constants of the space harmonics of the simulated unit cell multiplied by d. Air lines in red.

5.1.3 Open-Stopband Mitigation

A special problem that periodic LWAs have is the well-known open-stopband effect. At broadside, this is, when $\beta d = 2\pi$, all the reflections from the radiating discontinuities add in phase. In that case, a significant portion of the input power is being reflected to the source instead of being radiated and, as a consequence, a high reflection coefficient of the antenna will be found in a narrow region around the broadside frequency. This limitation has restricted the use of wide-angle scan periodic LWAs. However, some techniques permit these arrays to scan through broadside.

Specifically, this problem was solved for the complementary strip-slot radiating element by introducing a misalignment between the strip and slot elements [2]. The degree of freedom of this asymmetry allows obtaining a lower level of the $|S_{11}|$ parameter of a single element, at the cost of increasing the $|S_{22}|$ parameter. This way, even if the reflections are added in phase, there will be less reflected power at the source because each element is better matched. However, the lattice-network analysis of the radiating element is only valid for symmetric structures. In order to extend and verify the analysis in the case of misaligned structures, an equivalent circuit for asymmetric two-ports that also separates into even and odd eigenmodes is presented in Appendix B. Applying this equivalent circuit it was observed that the misalignment did not modify the positions of the pole and zero of the slot and stub elements and, thus, the same matching principle is taking effect.

The same solution for the broadside issue is used in the proposed CBS radiating

element. The stub has been displaced from the slot until a minimum of the $|S_{11}|$ is found. In this case, the value was already low but moving the stub 0.04 mm forward gave the best results. It is important to note that this introduced distance is very small and, thus, it is very sensitive to fabrication inaccuracies or errors. Fig. 5.7 shows the $|S_{11}|$ parameter for the symmetric single element and when the misalignment is introduced. Even though the difference between the $|S_{11}|$ parameter at the broadside frequency, 3.5 GHz, is only of 2 dB, it makes a significant impact when all the reflections are added in phase. In Fig. 5.8 the reflection coefficient of the designed array with and without the misalignment to show the mitigation of the open-stopband effect. The antenna is well matched between 2.15 GHz and 4.5 GHz, although it is expected to radiate properly from 2.75 GHz onward. It can be seen that the matching has improved 4 dB in the broadside frequency. In this case, the matching of a single element was already very good (under -20 dB) and, thus, the antenna was matched even without the misalignment. However, when the prototype is fabricated, a worse matching can be expected due to the pole and zero not being coincident and, thus, the misalignment will probably be necessary. Lastly, Fig. 5.9 shows the radiation efficiency of the simulated antenna. It can be seen that it increases with frequency, as the slots radiate more at higher frequencies. The value can be increased at lower frequencies by increasing the number of elements, at the cost of a more unstable gain over the band. Another way of improving this figure at the cost of a worse VSWR and radiation pattern is ending the array in a open circuit, as discussed previously. Also, it can be seen that the antenna starts radiating significantly at around 2.75 GHz, as expected.

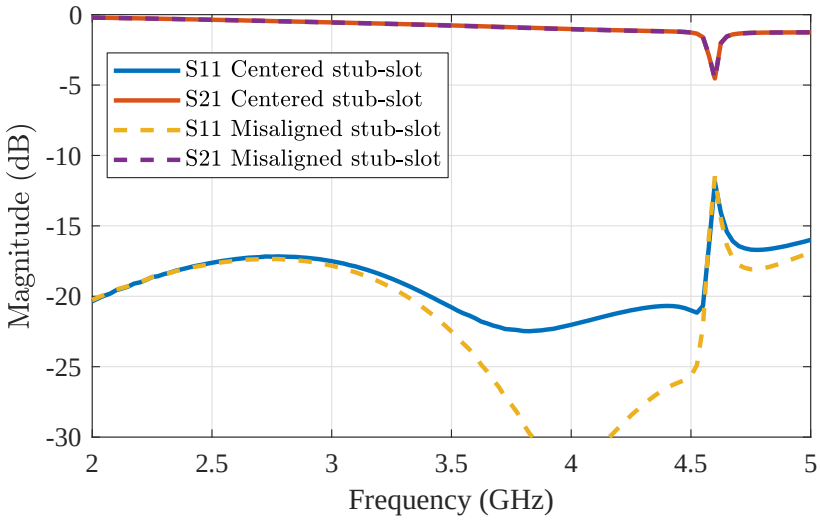

Figure 5.7: Simulated S parameters of the designed array unit cell with and without misaligment.

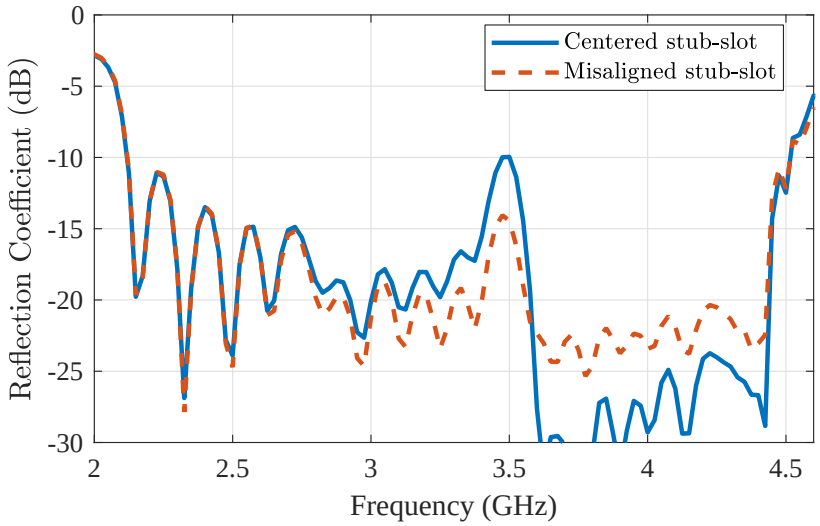

Figure 5.8: Simulated reflection coefficient of the designed LWA array with and without misaligment.

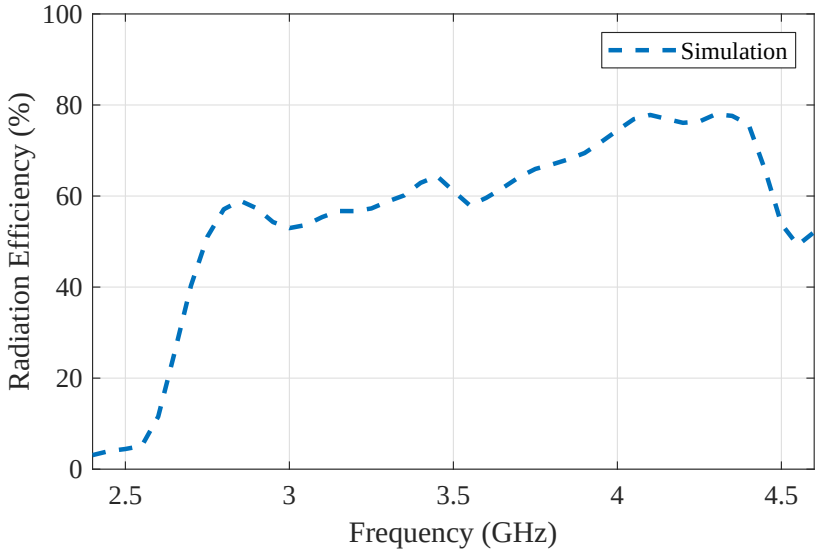

Figure 5.9: Simulated radiation efficiency of the designed LWA array.

5.1.4 Results

Taking into account the considerations of the Subsections 5.1.1, 5.1.2, and 5.1.3, an array has been fabricated and measured. A picture of the prototype is shown in Fig. 5.10a. Note that copper tape was used to ensure electric contact between the slot layer and the aluminum cavity, as in Fig. 5.10b. The measured S parameters of the measured structure are shown in Fig. 5.11 together with those from HFSS simulation. A shift up in the frequency response of the array around 150 MHz can be observed. It is believed that the reason for this shift is an inaccuracy of the slot pole due to fabrication errors,

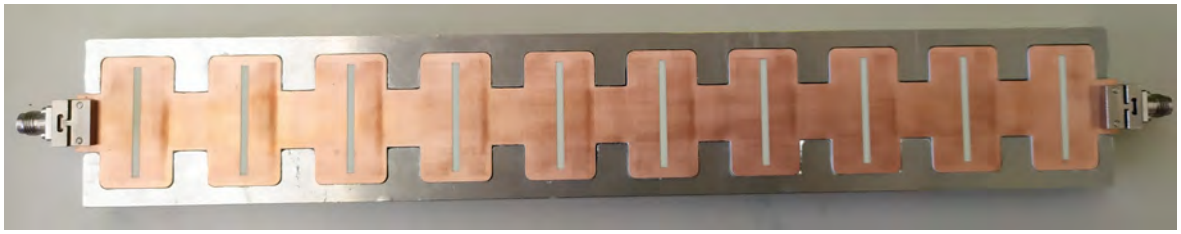

(a) Without copper tape.

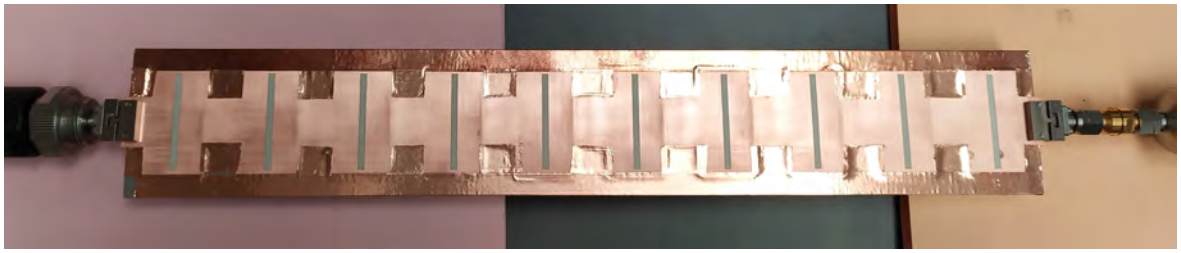

(b) With copper tape.

Figure 5.10: Pictures of the manufactured LWA array.

in a similar way as in Section 4.2. The matching at broadside has worsened due to the structure sensitivity to the misalignment and the inaccuracies of the fabrication procedure. However, still, good matching is obtained, with a maximum VSWR of 1.8 (return losses of more than 10 dB).

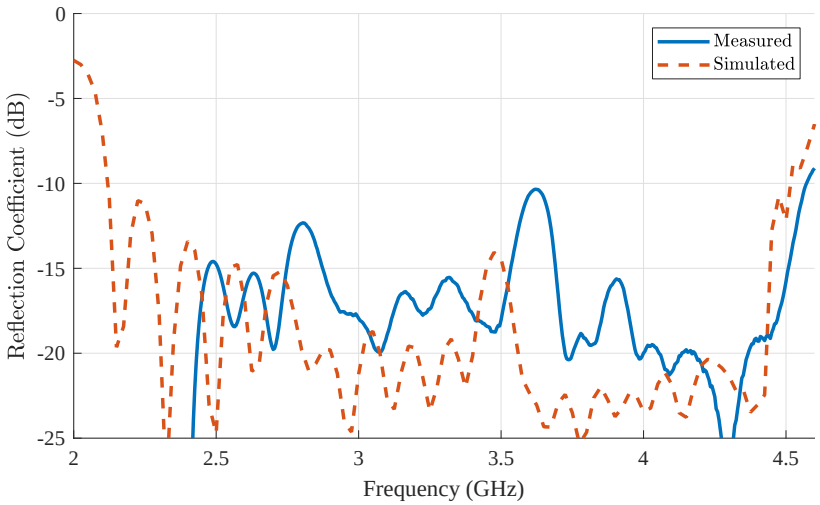

Figure 5.11: Measured and simulated S parameters of the fabricated LWA array.

To verify if the array is able to scan in frequency, the measurement of the radiation pattern was carried out in the anechoic chamber of the Laboratorio de Ensayos y Homologación de Antenas, Universidad Politécnica de Madrid, Madrid (Spain). Fig. 5.12 shows the radiation patterns in the plane longitudinal to the feeding strip (xz-plane) obtained for the array at several frequencies in the radiation band. It also shows the

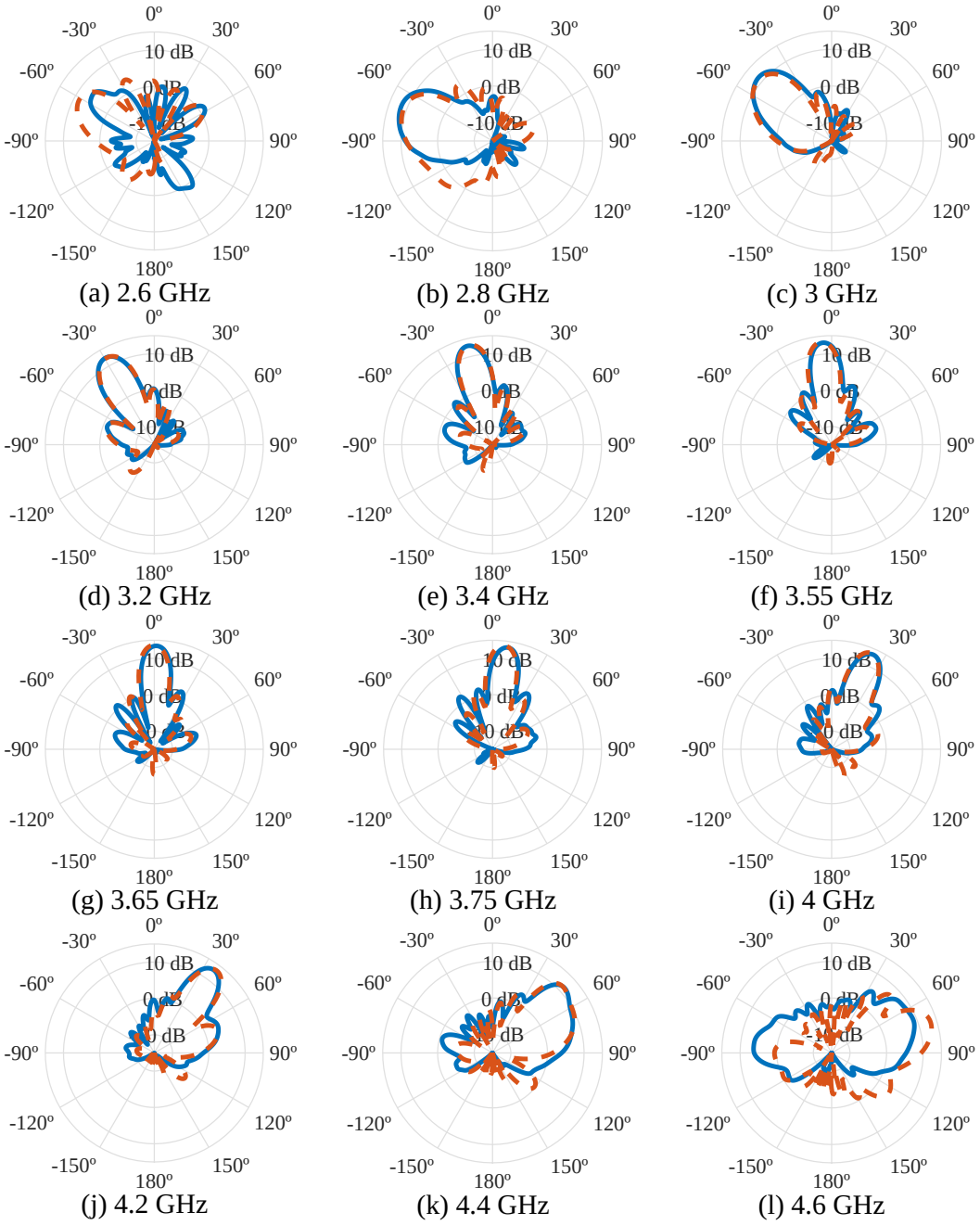

Figure 5.12: Measured (solid line) and simulated (dashed line) radiation patterns of the fabricated LWA array at different frequencies.

simulated radiation patterns shifted 150 MHz to match the difference between the simulation and measurement. The agreement between simulation and measurement is excellent and, as expected, they demonstrate its scanning behavior. The broadside direction is found to be 3.65 GHz (3.5 GHz in simulation, as expected by Fig. 5.6). No beam degradation is found at broadside as in [2], unlike most LWAs. The radiation pattern is, as expected, unidirectional, with a backward-to-forward ratio at broadside

frequency of over 20 dB. The antenna can scan its beam from -70° to 50° approximately. Fig. 5.13 shows the measured gain versus the simulated gain over frequency. The obtained maximum gain is reasonable given the size of the array, and is stable in frequency, changing only around 3 dB over the whole working band.

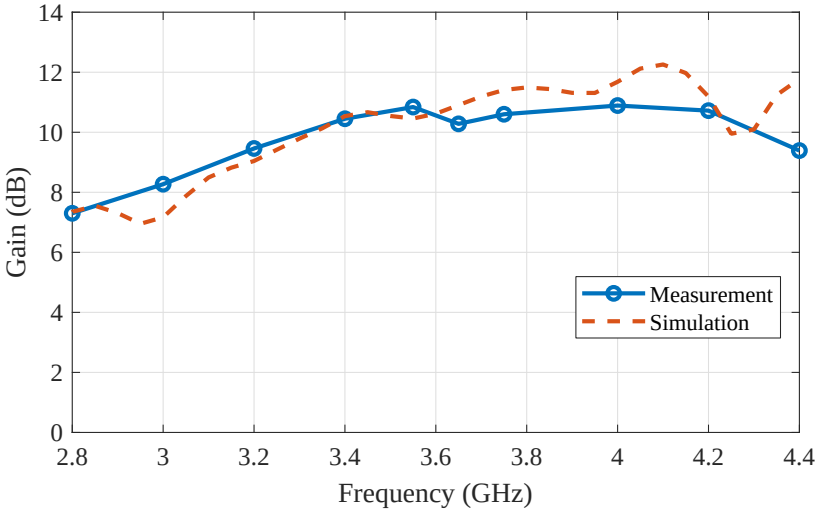

Figure 5.13: Measured and simulated gain of the fabricated LWA array versus frequency.

In conclusion, it has been proved that it is possible to design and fabricate a periodic LWA using the radiating element proposed in Chapter 4. It was implemented using an aluminum group of cavities and a 3D-printed filling. This sort of array can scan its beam with frequency and, thus, the wide impedance bandwidth of the element made the design of the array simple. The problem at broadside suffered by periodic LWA is solved here by misaligning the matching stub and radiating slot. Despite the design being simple, the fabricated array has a very solid performance in scan angle and gain, and a very good matching given its wide bandwidth (47% of fractional bandwidth).

5.2 Log-Periodic Array

LWAs like the one from Section 5.1 have a very broad bandwidth but the beam direction changes in the band. This is useful in some applications but, if that is not the case, a configuration where the beam is stable is desired. In this context, the log-periodic array is another linear array worth studying. Log-periodic arrays have a very wide bandwidth while keeping their radiation characteristics almost constant in the band. This comes at the cost of gain since not every element of the array is radiating at each frequency.

The broadband single layer slot of [1] was already used to build log-periodic arrays in [3] with significant success. The broadband nature of the radiating element allowed for a very simple yet effective design. However, it had a major drawback: the bilateral radiation. The final array had two main beams. It was possible to suppress one beam by using a reflector plane but this solution did not only increase the size of the antenna considerably, but also did not perform that well.

In this section, the radiating element proposed in Chapter 4 is used to design a log-periodic array which overcomes the drawback of bilateral radiation of [3]. The characteristics of this radiating element allowed using the array-design technique of [3], but at the same time other limitations due to the cavity and fabrication procedure arose. Additionally, the problem of mutual coupling between the elements was addressed, which improved the reflection coefficient of the array. Compared to other log-periodic antennas in the recent literature [3, 70–73], the proposed antenna has a lower VSWR in the band and is quite short, while keeping a good radiation performance.

5.2.1 Brief Review of Classic Log-Periodic Arrays

A log-periodic antenna is a multi-element, directional antenna designed to operate over a wide frequency bandwidth. It is composed of a transmission structure loaded with log-periodically scaled radiating elements at log-periodic spaces. This scaling will allow the radiating elements to perform in the same way at different frequencies. Fig. 5.14 shows the schematic of a general log-periodic array made of linear elements, where the parameters τ, σ, and α define its geometry:

$$\tau = \frac{l_{n-1}}{l_n} = \frac{d_{n-1}}{d_n} \tag{5.4}$$

$$\sigma = \frac{d_n}{2l_n} \tag{5.5}$$

$$\alpha = \tan^{-1}\left(\frac{1-\tau}{4\sigma}\right). \tag{5.6}$$

The idea behind the log-periodic scaling is that a group of radiating elements covers the radiation in a band, while other groups of radiating elements will radiate similarly at other bands. This way, the active region of a log-periodic array is defined as the elements that will radiate at a given frequency and will constitute a sub-array of sorts.

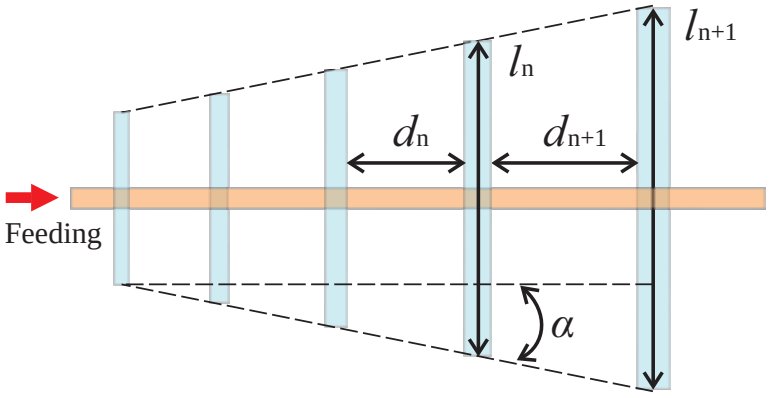

Figure 5.14: Schematic diagram of a log-periodic array.

These active regions will have the same radiation properties at different frequencies, so a very stable radiation pattern over frequency can be obtained. The region of non-radiating elements is called the transmission region since they will be part of the feeding network of the active region without affecting radiation. The main characteristic of a log-periodic array is that its total bandwidth is determined by the lengths of the shortest and longest radiating elements. At the lowest frequencies, the largest elements will be the ones radiating, whilst the power will go through the smaller elements. As frequency increases, the active region will shift towards the apex, and all the power will be completely radiated before reaching the longest elements. One of the advantages of this type of array is that its bandwidth can be increased by adding more elements. On the flip side, the directivity of the array will not increase when its size is increased since it is determined by the number of elements radiating in the active region.

One of the design parameters of a log-periodic array is the value of τ, which determines the number of radiating elements in the active region. If it is very close to 1, the variation between elements will be small and an array of a higher number of elements and, thus, size will be needed to cover certain bandwidth. The advantage of using a τ very close to 1 is that the active region will have enough elements to guarantee that all the power will be radiated by the elements and, thus, the radiation efficiency will be high. On the other hand, when τ is lower, it is possible to obtain arrays with a smaller size, but the radiation efficiency may be compromised.

The active region of the log-periodic array will perform in a similar way to the LWAs described in Section 5.1. This way, the antenna directivity will be determined by the number of elements that are radiating at a given frequency, which depend on τ and the amount of power radiated by each element (the radiated power to input power ratio). To obtain a more stable radiation pattern over the frequency band backfire

radiation is desired. To do this, the elements must be placed close to each other, i.e. σ being small, which also reduces the size of the array. However, if the elements are placed too close, the mutual coupling effect may interfere with the proper behavior of the array, as already noted in [3].

5.2.2 Design

The use of a broadly matched radiating element with a high-pass radiation efficiency adds some particularities to the design of the log-periodic array. Most of them were already covered in [3]. For instance, when the radiating elements have a narrow impedance bandwidth, it is indispensable to cause destructive interference in the transmission region by adding a frequency-constant 180° phase shift between adjacent elements. This problem is solved here by using a broadly matched element. Furthermore, in this case, τ can take lower values than classic log-periodic arrays since the radiation efficiency is not resonant, allowing a larger active region. However, if the active region has too many elements and they are very different between them (both τ and radiated power small) the distance between the elements will be too different from an element to another, and non-stable array factor over frequency or ripples will be obtained.

However, when using a CBS instead of a microstrip-fed slot, the challenge of dealing with the cavity appears. As in Section 5.1.2, it is desired to have a narrow cavity to have flexibility in the spacing between elements. In the case of a log-periodic array, an even narrower cavity is needed because the radiating elements must be closer together to obtain backfire radiation, as explained in Section 5.2.1. For this reason, a higher than wider cavity has been chosen. The cut-off frequency of the slot mode is more heavily determined by the largest dimension between the height and the width of the cavity. Thus, once the height is larger than the width, the cavity can be significantly narrower without increasing the cut-off frequency of the slot mode that much. Of course, this sort of configuration makes the antenna bulkier and less planar.

Taking into account the aforementioned considerations, a unit cell for a log-periodic array has been designed. The implementation was similar to that from Section 5.1, using an aluminum cavity with a substrate on top. However, to avoid the use of filler material, a small step of 0.5 mm tall and 0.5 mm long has been made into the aluminum to suspend the substrate, so the cavity is filled with air instead. As the widths of the cavities are smaller than their heights, thick drills must be used to fabricate the aluminum cavity. For this reason, the edges of the cavity are circular shaped. Actually,

the height to width ratio of the cavity was limited by the size of the drills used. The substrate where the stub, slot, and feeding line are etched is, again, Rogers RO4350B with dielectric constant, ε_r, of 3.66 and thickness 0.51 mm. The feeding microstrip line of 50 Ω has a width of 1.05 mm. As a trade-off between size and radiation efficiency, a τ of 0.95 was chosen. In order to cover an acceptable bandwidth, while keeping the total size of the array manageable, the chosen number of elements for the array is 15. The total size of the aluminum base is 197 mm long, 112.5 mm wide, and 29.7 mm tall ($2.1\lambda_0$ x $1.2\lambda_0$ x $0.3\lambda_0$). Fig. 5.15 shows the geometry of the array and the dimensions of each element are shown in Table 5.1. While most of the parameters scale with τ as expected, the lengths of the stub were chosen to improve the (already good) matching after optimizing using the electromagnetic simulator. Since the dimensions of the stub only affect the matching, the optimization process could be done as the last design step.

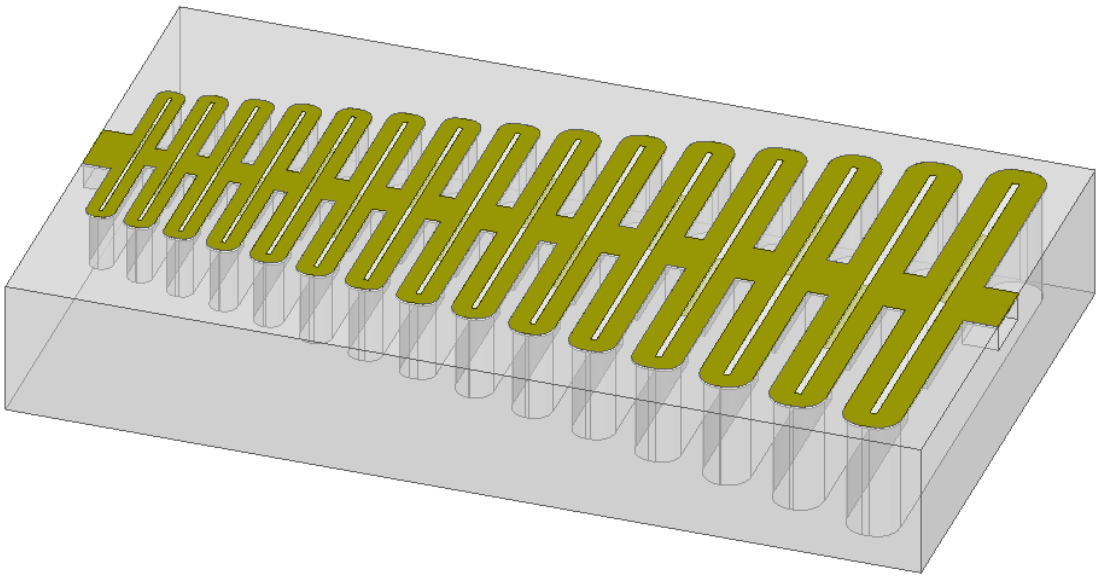

Figure 5.15: Geometry of the proposed log-periodic array.

In [3], the minimum value of σ was limited by the mutual coupling of the radiating elements. In the case of CBS, this effect can be also present. However, a way to considerably reduce the mutual coupling was found. Apparently, the coupling was produced inside the cavity. Thus, by narrowing the waveguide that crosses from one element to another, this is, reducing $w_{feedguide}$, it is possible to reduce the gap through which the coupling was being produced. This way, the problem of using a smaller σ was almost removed. The distance between elements was limited in this case by the fabrication procedure, since the aluminum walls between the smallest cavities had to be at least of 2.5 mm of thickness to be robust, leading to a σ of 0.092.

Element	l_{slot}	w_{slot}	l_{stub}	w_{stub}
1	45	0.75	12.8	0.7
2	47.4	0.789	13.1	0.736
3	49.9	0.831	14.1	0.776
4	52.5	0.875	14.7	0.816
5	55.2	0.921	15.6	0.859
6	58.2	0.969	16.5	0.905
7	61.2	1.02	17.3	0.952
8	64.4	1.07	18.1	1
9	67.8	1.13	19.1	1.06
10	71.4	1.19	20.2	1.11
11	75.2	1.25	21.2	1.17
12	79.1	1.32	22.3	1.23
13	83.3	1.39	23.5	1.29
14	87.7	1.46	24.7	1.36
15	92.2	1.54	26.3	1.44

(a) Dimensions of the slots and stubs of the array.

Element	d_n	l_{cavity}	w_{cavity}	h_{cavity}	$w_{feedguide}$
1	12.3	50	6.1	13	6.5
2	8.72	52.6	6.42	13.7	6.84
3	9.18	55.4	6.76	14.4	7.2
4	9.67	58.3	7.11	15.2	7.58
5	10.2	61.4	7.49	16	7.98
6	10.7	64.6	7.88	16.8	8.4
7	11.3	68	8.3	17.7	8.84
8	11.9	71.6	8.73	18.6	9.31
9	12.5	75.4	9.19	19.6	9.8
10	13.1	79.3	9.68	20.6	10.3
11	13.8	83.5	10.2	21.7	10.9
12	14.6	87.9	10.7	22.9	11.4
13	15.3	92.5	11.3	24.1	12
14	16.1	97.4	11.9	25.3	12.7
15	17	103	12.5	26.7	13.3

(b) Dimensions of the cavities and feeding waveguide.

Table 5.1: Dimensions of the proposed 15-element log-periodic array. All units in mm.

5.2.3 Results

The designed array was simulated and manufactured. The resulting structure can be seen in Fig. 5.16. A broadband 50 Ω load is placed at the second port. Fig. 5.17 shows the reflection coefficient of the antenna. The agreement between simulation and measurement is good. From 2.1 to 4.3 GHz, the matching is very good, below -12 dB (VSWR of 1.7 or lower), an uncommon figure for such a wide bandwidth antenna (over

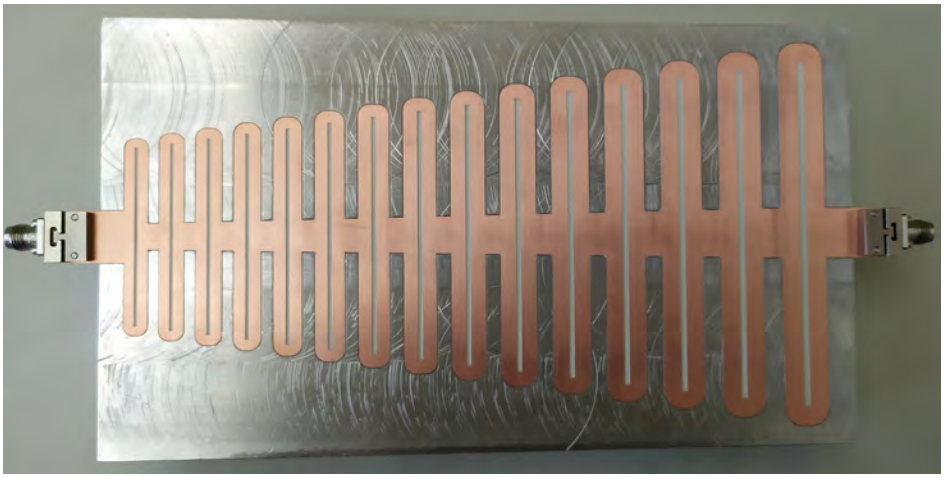

Figure 5.16: Fabricated log-periodic array.

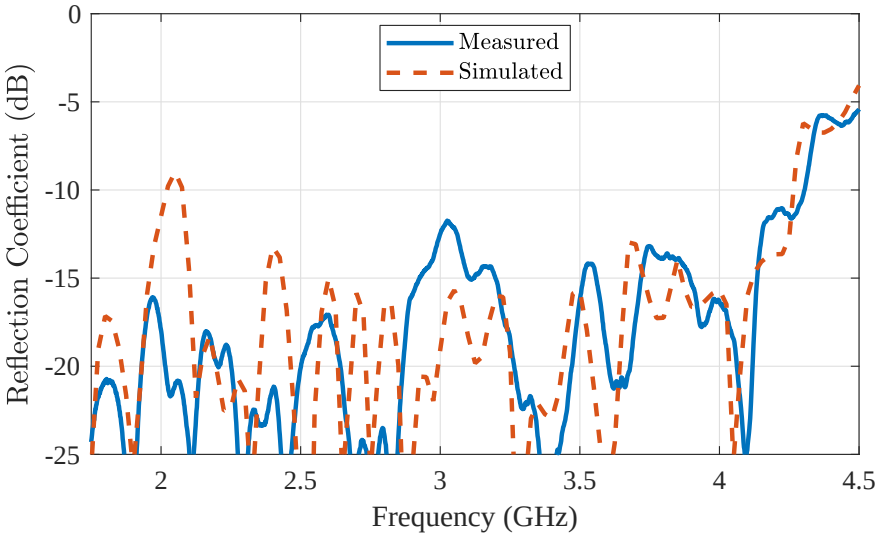

Figure 5.17: Measured and simulated reflection coefficient of the fabricated Log-periodic array.

60% of fractional bandwidth). Note that the bandwidth can be further increased by adding more radiating elements to the array, at the cost of antenna size.

Fig. 5.18 shows the measured and simulated radiation patterns at different frequencies. These measurements were taken in the anechoic chamber of the Laboratorio de Ensayos y Homologación de Antenas, Universidad Politécnica de Madrid, Madrid (Spain). The main direction of the beam is around -50° since the array factor has the maximum in the backfire direction and the radiating element has a null in the apex and the maximum at broadside. This combination leads to backward angle radiation. As expected, the shape and direction of the radiation pattern are mostly maintained over frequency. At some frequencies, though, the beam direction changes. This effect is not

uncommon in log-periodic arrays because the beam stability is only guaranteed at the log-periodic frequencies. Furthermore, at the start and end of the band, the truncation effects modify the patterns, lowering the gain at lower frequencies and moving the beam towards broadside at higher frequencies. As pursued, unidirectional radiation is obtained without any sort of reflector plane.

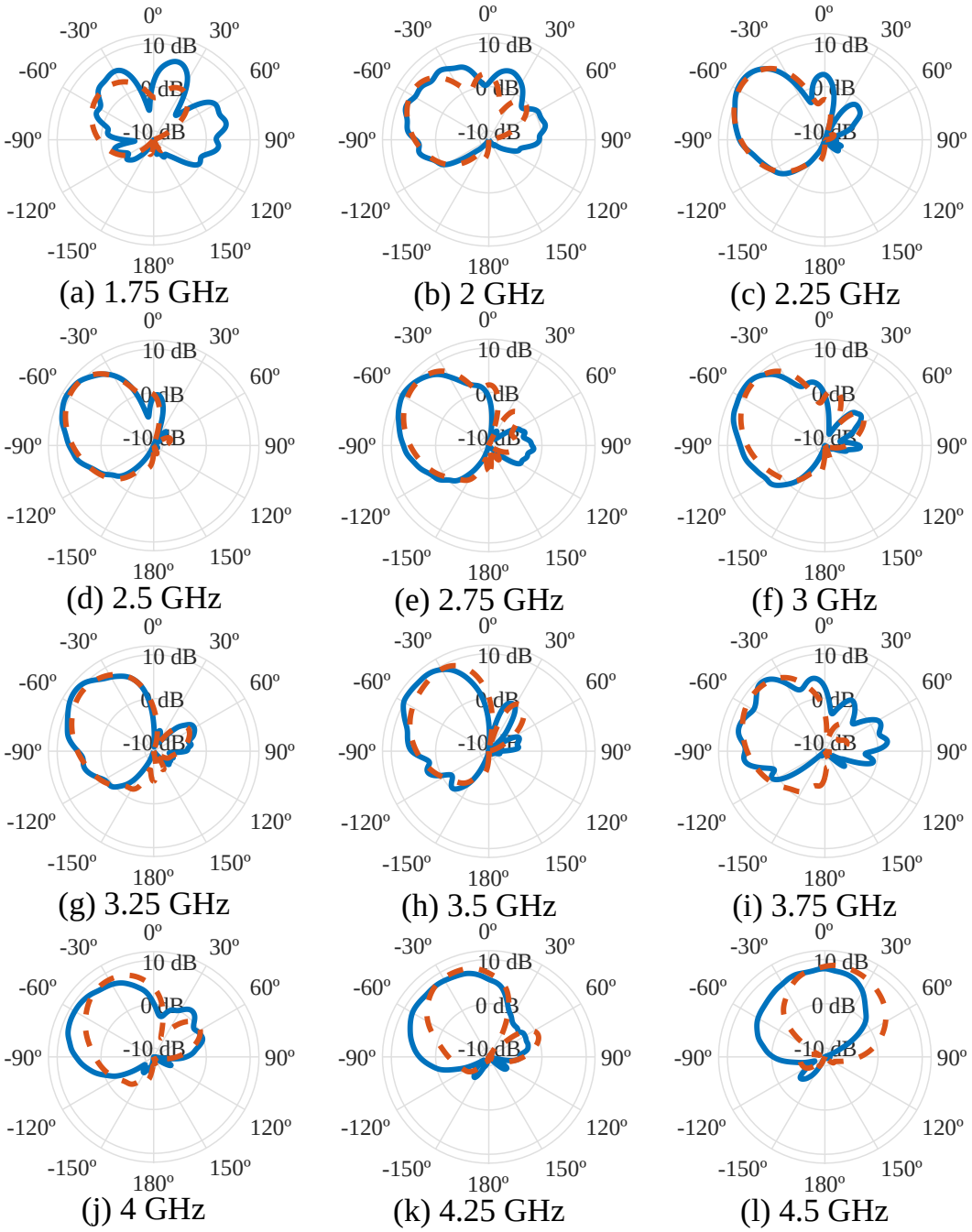

Figure 5.18: Measured (solid line) and simulated (dashed line) radiation patterns of the fabricated log-periodic array at different frequencies.

Fig. 5.19 shows the simulated maximum gain over frequency. It can be seen that

a maximum gain of around 9.5 dB is obtained and that the antenna starts radiating significantly at around 2.2 GHz. Again, it is possible to see that the values of the gain oscillate due to the effect of the periodicity. However, they are kept in the 9.5-6.5 dB range. Fig. 5.20 shows the simulated radiation efficiency of the array. Again, the radiation efficiency increases with frequency, up to 90 %, from 70 % at the lower frequencies.

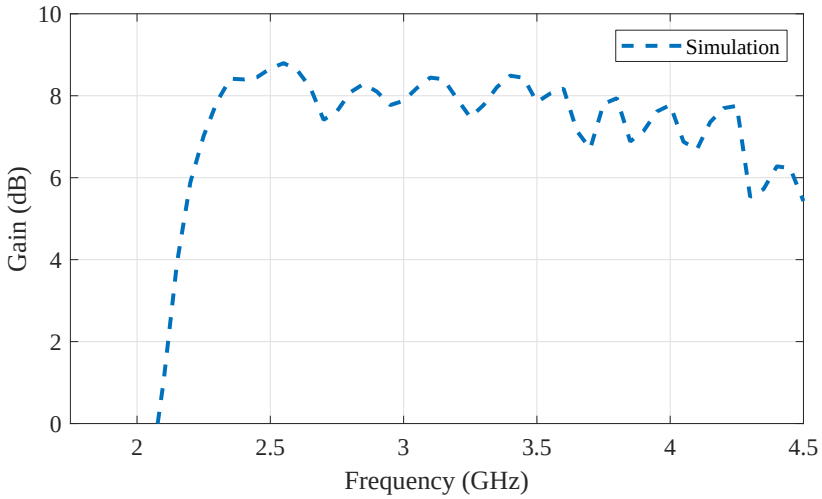

Figure 5.19: Simulated gain of the fabricated log-periodic array versus frequency.

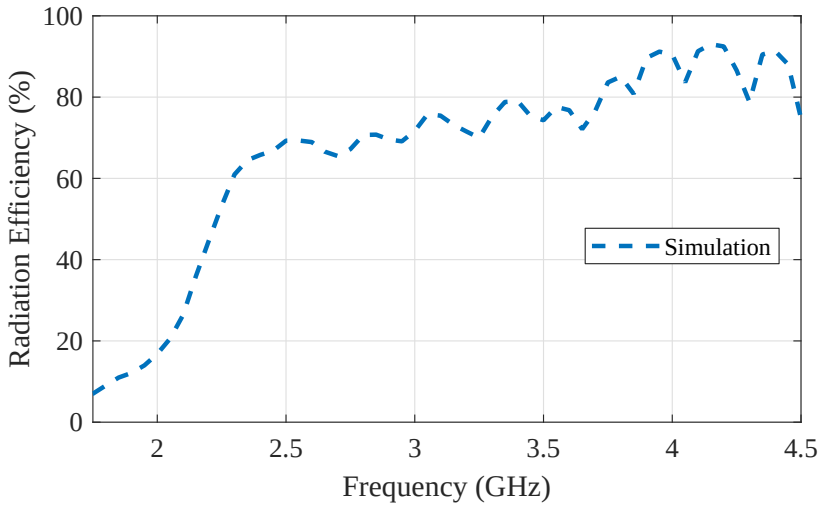

Figure 5.20: Simulated radiation efficiency of the designed log-periodic array.

In conclusion, the proposed log-periodic array allows a very simple and flexible design while obtaining good performance. There is no need to introduce a phase shift between the radiating elements due to their wide bandwidth, as opposed to other log-periodic arrays. The bandwidth of the antenna can be controlled by the number of radiating elements. Its gain and radiation efficiency, however, can be controlled by

the amount of power radiated by each element at the cost of pattern stability. The limitation of the coupling between the elements has been suppressed significantly by reducing the distance between the lateral walls of the feeding guide, which supposed a big limitation to the reflection coefficient of the array.

Chapter 6

Conclusions and Outlook

This final chapter summarizes the research work developed in this thesis and stresses the most remarkable contributions. Lastly, it points out different perspectives of future work to carry on with this research.

6.1 Summary and Conclusions

A wideband radiating structure based on the CBS has been studied in this Ph.D. thesis. It consists of a rectangular waveguide with a longitudinal slot on its top and short-circuited at its ends. The slot is fed by a transversal strip and, thus, it is especially suited for building series-fed arrays.

To completely understand the radiation mechanism of CBSs and to be able to develop a TL equivalent circuit, the slot mode of a rectangular waveguide has been studied and characterized. By using a commercial electromagnetic simulator, the characteristic impedance of the mode and its propagation constant have been obtained over a very wide frequency, albeit approximately. A very robust and precise method to obtain the propagation constant of the slot mode has been proposed. The method consists of simulating or measuring waveguides of different lengths to obtain ultra-wideband results. A specific structure to apply the method to this mode has been proposed, fabricated, and measured. The proposed structure allows measuring different slot lengths while using only a single waveguide. The results showed the propagation constant of the slot mode of the rectangular waveguide over a very wide bandwidth (an octave) with great accuracy. The precision of the results can be controlled by adjusting the number of

measurements.

By using the propagation constant of the slot mode of a rectangular waveguide, a comprehensive yet simple equivalent circuit for a strip-fed CBS has been proposed. The main component of the equivalent circuit is a TL with its propagation constant and characteristic impedance the ones of this mode. This TL models the propagation throughout the slot, and it is ended in a short-circuit that takes into account the end-effect of the slot. The equivalent circuit also models the coupling between the slot and the strip simply and effectively. The accuracy of the equivalent circuit was verified by simulation and measurement results with success.

Once the behavior of the CBS was fully understood, a bandwidth-enhancing method was studied. The method is a direct application of the complementary strip-slot to a strip-fed CBS. The resonant impedance of the CBS is canceled by a stub placed underneath the slot, in the feeding strip. A theoretical study of the structure in terms of even and odd modes and a straightforward TL equivalent circuit based on the lattice network have been provided. These provide the required analytical tools for the design methodology. However, the resonance of the cavity can prevent the radiator from working at some frequencies and must be carefully taken into account. Two prototypes have been fabricated and measured, the first one in suspended stripline configuration and an improved one in enclosed microstrip. Experimental and measured results confirmed that the presence of the strip does not hinder the good radiation characteristics of the CBS. The main advantage over the classic complementary strip-slot is that the radiation is unidirectional. This matching technique has been compared with a well-known method which consists of changing the off-set feeding distance between the center of the slot and the strip, and it has been proved the benefits of using the matching stub. Two other designs have been simulated to find modifications that increase the bandwidth of the radiating element. The modifications consist of reducing the physical length of the slot to make the cavity shorter and, that way, increase its resonance frequency. These designs are the double-T slot and the bow-tie slot. The bow-tie slot was designed for the millimeter-wave band with promising results for arrays at 60 GHz or more.

Finally, once the radiating element was analyzed and its design procedure clear, two arrays architectures have been used. Due to the series feeding of the element through a strip, series-fed arrays have been designed. The first one has been a linear traveling-wave array built by loading the strip with several equal broadband CBS radiating elements. By using this simple array architecture, frequency scanning from backward to forward direction has been achieved. In contrast with arrays made with the

complementary strip-slot radiating element, a single-beam antenna has been obtained. Measurement of a fabricated prototype verified the prediction of the LWA-design theory. The second array architecture that has been used is the log-periodic array. The superior impedance bandwidth allowed a simple design that did not require adding a phase shift of 180° between elements. Mutual coupling was reduced by alternating the direction of the stubs. This straightforward design was able to obtain a very low reflection coefficient (below -12 dB) in a wide bandwidth (over 60% of fractional bandwidth). The single-beam direction was around 50° backward due to the combination of the array factor and radiation pattern of the radiating element. The results were again verified by measurements.

Since a way of designing a broadband CBS has been found and antennas with appealing features have been designed, manufactured, and measured, it can be said that the work has met all the initial objectives. Apart from that, the work has been able to shed some light on how CBSs work by means of an equivalent circuit and a method to characterize the propagation constant of the mode that propagates inside the structure.

6.2 Original Contributions

The main contribution of this thesis is the use of a matching stub to design broadband strip-fed CBS radiating elements, the theoretical analysis to explain its operation, and a design methodology. These were achieved through a lattice-network equivalent circuit, which is another significant contribution that provided an excellent physical insight into the behavior of the radiating element.

The work related to the measurement of the propagation constants is also noteworthy. The application of a solid, established method to extract the even- and odd-mode propagation constants separately has allowed proposing a way of measuring the propagation constants of both modes in coupled lines. Applying this to a closely-related topic of this work has allowed obtaining a novel method to extract the propagation constant of the slot mode in a rectangular waveguide.

Another significant contribution of this thesis is a different point of view in the analysis of a strip-fed CBS. Considering the slot mode of a rectangular waveguide as the propagating mode inside the structure was not found before in the literature. Viewing the slot as a TL of this mode ended in short-circuit allowed understanding

the radiating element in a simple yet effective way. Based on this principle, a novel equivalent circuit was also proposed. It provided significantly more physical insight than previous analyses.

In relation to the array applications of the proposed broadband CBS, although the topologies are classic, the presence of the cavity limited the minimum distance between elements, and ways to reduce its size had to be considered. Furthermore, in the LWA design, a 3D-printed filling was used, proving that it could be an interesting idea to, for example, reduce the size of cavities of antennas or increase its robustness in a very flexible way. A significant contribution of the log-periodic array design is the way of reducing mutual coupling. It has been found out that the mutual coupling was caused mainly by the matching stubs and, thus, alternating their position significantly improved the reflection coefficient of the array.

6.3 Future Work

Some brief ideas and guidelines are presented below as future work that can carry on from this dissertation:

- **Characterizing the slot-mode impedance**

  Although a very precise method to obtain the propagation constant of the slot mode was proposed, the way of obtaining its impedance is still very inaccurate at some frequencies. It may be interesting to increase the precision of the equivalent circuit to find another way to obtain this impedance accurately in a wide bandwidth.

- **Include all the dimensions of the structure in the equivalent circuit**

  The equivalent circuit of the CBS must be found for a previously simulated slotted waveguide section. Furthermore, the equivalent circuit must be done a posteriori, and the values of all their parameters cannot be predicted from the dimensions of the structure. Obviously, this is not ideal. Future work could be done in order to find how the parameters change with the dimensions of the cavity, slot width, and dielectric filling. It would be especially interesting to find how the radiation losses change since they are essential in the design of arrays.

- **Implement the radiating element with other transmission systems**

The complementary strip-slot was applied to closed structures such as stripline and enclosed microstrip to obtain unidirectional radiation. However, it could be interesting to apply the same concept in other closed transmission systems such as rectangular waveguide or ridge gap waveguide. This would allow the use of a more standardized process in its fabrication, avoiding the use of any dielectric and reducing implementation errors.

- **Reduce the size of the cavity**

  Some limitations of the designed array were due to the size of the cavity. The solution adopted here was to make the cavity taller, which worsens the planar profile of the antenna. Cavity-reduction techniques could be employed to make the array easier to design or implement. Increasing the electric permittivity could be an option, but how this can change the radiation properties of the slot must be explored.

- **Implementation of other array topologies**

  Two array concepts have been analyzed in this work. However, the proposed CBS radiating element can be used in other array topologies. Any series-fed array configuration can be, in principle, built using the proposed radiator. Furthermore, the simulation of the bow-tie slot showed promising results in the millimeter-wave band and, thus, an array for the 60-GHz band would be very interesting and could have a huge impact on the state-of-the-art antennas.

Appendix A

Determination of the Even- and Odd-Mode Propagation Constants of Coupled Microstrip Lines

Accurate characterization of coupled transmission lines directly applies to the correct modeling of GaAs-based [74] and high-speed [75] integrated circuits, and even to the complex permittivity measurements of dielectric samples [76]. One main focus in the characterization of coupled and multiconductor transmission lines is the theoretical obtainment of the propagation constants of their normal modes, and the experimental measurement of these constants. A suitable measurement technique must provide accurate enough results for both the phase and the attenuation constants of each propagating mode.

A number of different measurement techniques has been proposed in the literature with this aim. The resonant, discrete-frequency techniques, [77, 78], report values at a few resonant frequencies of terminated transmission line sections, and can provide, in principle, more accurate results and some unsusceptibility to launcher and transition effects. As opposed to resonant methods, the broadband approaches, [6, 20, 79–84], do not make use of resonances, but rely on the propagation of the line modes, which allows to sweep a stimulus frequency continuously over the band.

In broadband methods, the propagation constant is derived from the eigenvalues of the multiport parameter matrices of some multiconductor line sections. In some cases, these are line sections to be measured when terminated both in short and open

circuit [84]. In other cases, as in the multimode Thru-Reflect-Line method [83], they are simple transmission lines of different lengths. The measurement of these multiport devices is time-consuming. In the simplest case of three-conductor transmission lines, an expensive, and not always available, four-port vector network analyzer (VNA) is required. If a two-port VNA is used, some of the ports have to be connected to external loads, and more elaborated calibration procedures have to be employed [85], which contribute to additional systematic and random measurement errors. A further difficulty relates to the fact that the attenuation constant can only be easily obtained when it is large enough (as in [79]). When losses are low, the attenuation constant can be hidden by noise and errors.

In this appendix, a measurement procedure of the propagation constants of symmetric coupled lines is shown. It requires only two-port measurements, and thus the use of a two-port VNA with no need for calibration. The method resorts to the measurement of a number of transmission lines of different lengths that can be terminated in the most convenient way. The measurement of lines with different lengths increases the measurement burden, but provides some reduction of, and control over, the error levels, and the ability to determine moderately low attenuation constants. The measurement technique is described in Section A.1, where the statistical improvement obtained by the measurement of a series of line lengths is detailed. This technique is used in the first chapter of the thesis as well. Section A.2 details the application of the method to symmetrical coupled lines, shows some full-wave simulated results, and includes the experimental results obtained for the even and odd modes of a coupled microstrip transmission line, along with a discussion of the sources of inaccuracies. A conclusion is provided in Section A.3.

A.1 Measurement Technique

Among the methods for the measurement of the propagation constants of transmission lines or waveguides, the one proposed in [6] shows some remarkable advantages. It is based on the measurement of the reflection coefficient at the input of four equally-terminated transmission lines of different lengths L_i ($i = 1, 2, 3, 4$). As explained in [6], the method takes advantage of the invariance of the cross-ratio of complex numbers under a bilinear transformation. This mathematical property makes the results of the method independent of, and insensitive to, the line impedance, the line termination used, the launcher characteristics (i.e., the likely unknown parameters of the two-port

between the network analyzer and the transmission line to be measured), and even insensitive to the network analyzer one-port calibration errors (if the usual three-term correction is assumed). The simplicity of one-port measurements becomes another one of the aforementioned advantages.

Using the four measured reflection coefficients, Γ_i $(i = 1, 2, 3, 4)$, the cross-ratio Γ_{1234} can be defined as:

$$\Gamma_{1234} = \frac{(\Gamma_1 - \Gamma_2)(\Gamma_3 - \Gamma_4)}{(\Gamma_1 - \Gamma_3)(\Gamma_2 - \Gamma_4)} \tag{A.1}$$

and the following equation can be written [6]:

$$\Gamma_{1234} = \frac{\left(1 - e^{-2\gamma\delta_{21}}\right)\left(e^{-2\gamma\delta_{31}} - e^{-2\gamma\delta_{41}}\right)}{\left(1 - e^{-2\gamma\delta_{31}}\right)\left(e^{-2\gamma\delta_{21}} - e^{-2\gamma\delta_{41}}\right)} \tag{A.2}$$

where γ is the unknown propagation constant of the transmission line, and $\delta_{ij} = L_i - L_j$.

The numerical solution of the nonlinear equation (A.2) provides the sought propagation constant γ. However, the method has also some drawbacks: four lines must be measured, and the result shows important errors when the differential lengths δ_{ij} are resonant or near resonance. This is because the cross-ratio Γ_{1234} requires four different complex numbers, and when two of them coincide, the cross-ratio has no sense. This is the case when $e^{-2\gamma L_i} \approx e^{-2\gamma L_j}$ which implies that $\gamma\delta_{ij} \approx jk\pi$ with integer k. In a wideband measurement of a low-loss transmission line, to find frequencies at which these coincidences (resonances) occur becomes unavoidable.

A.1.1 Statistical improvement

The original method can be significantly improved by increasing the measurement effort. If a larger number of terminated lines are measured, $N > 4$, a much larger number of sets of four lengths (let us call them 'quadruples') can be defined. In fact, there are $M = \binom{N}{4}$ quadruples (the binomial coefficient). Then, the following M equations can be obtained:

$$\Gamma_{mnpq} = \frac{\left(1 - e^{-2\gamma\delta_{nm}}\right)\left(e^{-2\gamma\delta_{pm}} - e^{-2\gamma\delta_{qm}}\right)}{\left(1 - e^{-2\gamma\delta_{pm}}\right)\left(e^{-2\gamma\delta_{nm}} - e^{-2\gamma\delta_{qm}}\right)} \tag{A.3}$$

with $m, n, p, q = 1, \ldots, N$, and the four indexes m, n, p and q different from each other. It is worth pointing out how quickly the number of quadruples grows with the number of measurements. For instance, with $N = 8$ there are $M = \binom{8}{4} = 70$ quadruples, whereas

with $N = 10$ there are $M = 210$, and with $N = 12$ the number of quadruples rises to 495. As the result of solving (A.3), each quadruple leads to an estimation of the propagation constant, γ_{mnpq}. At a given frequency, some of the estimations can have a noticeable error when for any of the involved δ_{ij} the condition $\gamma\delta_{ij} \approx jk\pi$ is fulfilled with some integer k. But many of the other estimations will be free of this resonance problem.

The proposed method is to make a statistical analysis of the M obtained values to calculate average values as well as standard deviations for both the real and the imaginary parts of γ_{mnpq}, assuming for both a normal distribution. All those values that are farther than three times the standard deviations from the average are rejected (i.e., those results are considered outliers), since they are likely the result of one of the aforementioned resonances. The averages and standard deviations are recalculated, and the new outliers rejected. The process is repeated until no outliers are detected, or there are less than the 80% of the initial M estimations.

Therefore, this procedure is capable of dealing with the accidental errors derived from resonant lengths. And these resonances are unavoidable if a wideband measurement is to be carried out. The proposed statistical method not only provides a way to circumvent that problem but also provides a measurement of the uncertainty of the result, by means of the standard deviation of the outlier-free data, available after the last iteration.

Two aspects of the implementation of this procedure are worth detailing: the selection of the N lengths L_i ($i = 1, \ldots, N$), and the use of an initial guess for solving (A.3).

There appears to be no optimal strategy for the selection of the N lengths, even after essaying some different procedures: a logarithmic distribution, a random selection, and procedures that try to reduce the quadruples with resonances in the whole measurement band. A procedure within this third group has been preferred.

Once the frequency sweep (f_k, $k = 1, \ldots, K$) and an initial set $\{L_i\}$ of N lengths have been selected, the distances between the complex values $e^{-2\hat{\gamma}_k L_i}$ and $e^{-2\hat{\gamma}_k L_j}$ are calculated as

$$d_{ij}(f_k) = \left| e^{-2\hat{\gamma}_k L_i} - e^{-2\hat{\gamma}_k L_j} \right| \tag{A.4}$$

by using a coarse estimation $\hat{\gamma}_k$ for the propagation constant at f_k, $\hat{\gamma}_k = \widehat{\gamma(f_k)}$, for which any well-known dispersion model can be used [16].

Each one of the M available quadruples is assigned the lower of the distances between its components:

$$D_{mnpq}(f_k) = \min_{ij\in\{m,n,p,q\}} \{d_{ij}(f_k)\}. \tag{A.5}$$

The higher this value is, the better the quadruple can be considered. Since some of the cuadruples are resonant, or near resonance, a certain fraction of them should be discarded. A 20% has proved to be a good rule of thumb. Thus, each frequency is assigned a weighted sum of the values $D_{mnpq}(f_k)$. The best 80% of the quadruples is assigned an almost unitary weight, whereas the worst 20% is added with an almost negligible weight. For this purpose the values $D_{mnpq}(f_k)$ are ranked, and multiplied by a sigmoid function:

$$D_k = \sum_{\mu=1}^{M} D_\mu(f_k) \frac{e^{0.8M-\mu}}{1+e^{0.8M-\mu}} \tag{A.6}$$

where $D_\mu(f_k)$ is the μ-th best $D_{mnpq}(f_k)$. Then, the whole length set is assigned the sum of the squared D_k values at all the K frequencies. The minimization of this sum leads to the final selected length set $\{L_i\}^*$:

$$\{L_i\}^* = \arg\left\{\min_{\{L_i\}} \sum_{k=1}^{K} D_k^2\right\} \tag{A.7}$$

The second aspect to be dealt with comes from the fact that equation (A.3) is solved by the Muller's method [86], which requires an initial guess. The same coarse estimation for γ which is used for the selection of the length set can be used for this purpose. However, since the results have proved to be slightly sensitive to the used guess, an iterative procedure is proposed. Initially, the coarse estimation is used and the results, in the form of effective permittivity and attenuation constant, are modeled. For the effective permittivity, a low-order polynomial is used, whereas for the attenuation a model of the form $Af + B\sqrt{f}$ is preferred. In the following steps, the predictions of both models are used as guesses. The process is iterated until the results are reproduced from one iteration to the following. In the cases analyzed no more than two, or occasionally three, iterations are needed.

A.2 Application to coupled lines measurement

A.2.1 Determination of the even- and odd-modes propagation constants

The original method in [6] was restricted to transmission media where only one fundamental mode was present. But its scope has been herein extended to the measurement of the propagation constants of the even and odd modes of symmetrical coupled lines.

Fig. A.1a shows a symmetric coupled-line section terminated in a symmetric two-port and excited by means of a symmetric four-port launcher. The S-parameters relating ports 1 and 2 can be measured in this setup for a number of different line lengths. For the i-th length:

$$[S_i^m] = \begin{bmatrix} s_{i11}^m & s_{i12}^m \\ s_{i21}^m & s_{i22}^m \end{bmatrix} \tag{A.8}$$

where $s_{i11}^m \approx s_{i22}^m$ is expected from symmetry, and $s_{i12}^m \approx s_{i21}^m$ from reciprocity.

From these measurements the even-mode reflection coefficient Γ_i^e of the half-problem with perfect magnetic conductor of Fig. A.1b, and the odd-mode reflection coefficient Γ_i^o of the half-problem with perfect electric conductor of the same figure, can be obtained as:

$$\begin{aligned} \Gamma_i^e &= (s_{i11}^m + s_{i22}^m)/2 + (s_{i12}^m + s_{i21}^m)/2 \\ \Gamma_i^o &= (s_{i11}^m + s_{i22}^m)/2 - (s_{i12}^m + s_{i21}^m)/2 \end{aligned} \tag{A.9}$$

where the averages of reflection and transmission parameters have been used to enforce symmetry and reciprocity.

Now, the two half-problems of Fig. A.1b, along with the measured reflection coefficients Γ_i^e and Γ_i^o of (A.9), constitute two measurement sets to be processed by the method detailed in the previous section.

A.2.2 Simulated Results

As a first check of the proposed measurement technique, eleven coupled microstrip line lengths—eleven lengths means $M = 330$ quadruples—have been simulated from 2 to 20 GHz (a decade) using the commercial full-wave finite-element electromagnetic simulator ANSYS HFSS. These coupled lines are fed by microstrip lines, which are excited in the simulation using wave-ports, and terminated to constitute a C-section,

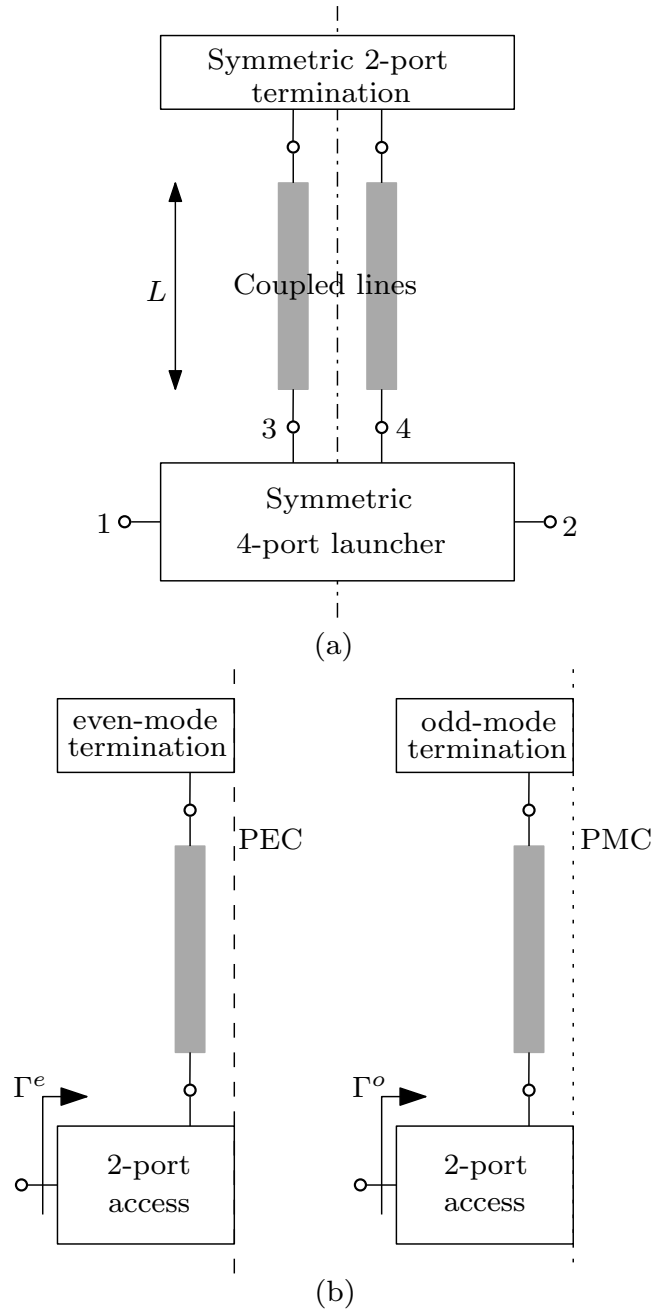

Figure A.1: Coupled line accessed and terminated with a symmetrical 2-port. (a) Whole symmetrical circuit. (b) Even-mode half-problem with perfect electric conductor (PEC) and odd-mode half-problem with perfect magnetic conductor (PMC).

as shown in Fig. A.2. From the resulting S-parameters of this simulation, the reflection coefficients Γ^e and Γ^o have been obtained in the same way as in (9) and, using the method proposed in Section A.1, the propagation constants of the even and odd modes are obtained.

The substrate used in the simulation of these structures is Rogers RO4350B with

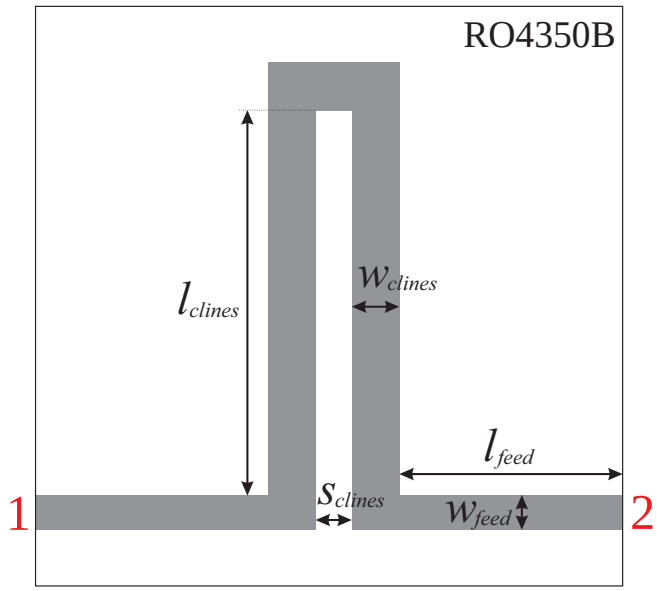

Figure A.2: Simulated structure. $w_{feed} = 1$ mm, $l_{feed} = 25$ mm, $w_{clines} = 1.3$ mm, $s_{clines} = 0.4$ mm, $l_{clines} = 25$, 31.1, 37.6, 44.7, 51.8, 58.9, 59.5, 67.7, 75, 91 and 125 mm (11 cases).

30 mil thickness, $\varepsilon_r = 3.66$, $\tan\delta = 0.004$ and 17.5 μm-thick copper metallization. The line dimensions can be found at Fig. A.2 caption. These lengths have been chosen by simultaneously using the algorithm described in Section A.1.1 with the estimations of the even- and the odd-mode propagation constants. The characteristic impedance of the feeding microstrip lines and the even-mode impedance of the coupled lines are both 66 Ω, and the odd-mode impedance is 44 Ω at 10 GHz. It is worth remembering that the mismatch between the feeding line and the coupled lines is irrelevant to this method.

Fig. A.3 shows the effective dielectric constants, $\varepsilon^e_{r_{eff}}$ and $\varepsilon^o_{r_{eff}}$, and the attenuation constant of each mode, obtained by using the proposed technique with this set of 11 lines. They are compared with the values obtained by using a dispersion model from [16]. Fig. A.3a shows a relative error of $\varepsilon_{r_{eff}}$ of about ±1% or lower for the even and odd modes. Fig. A.3b shows good agreement between the simulation results and the theory, especially in the 2 to 10 GHz frequency range.

A.2.3 Experimental Results

Once the method has been proved to work with simulated results, the 11 circuits were manufactured. The dimensions of the lines and the substrate are those presented in Section A.2.2. Fig. A.4 shows ten of the eleven lines that were manufactured (the

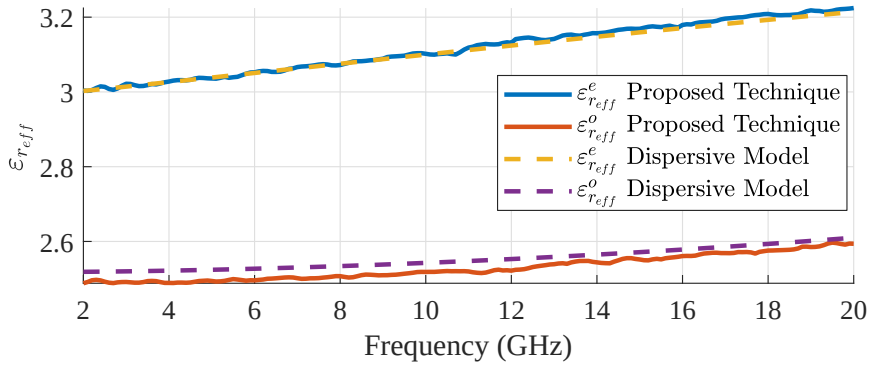

(a)

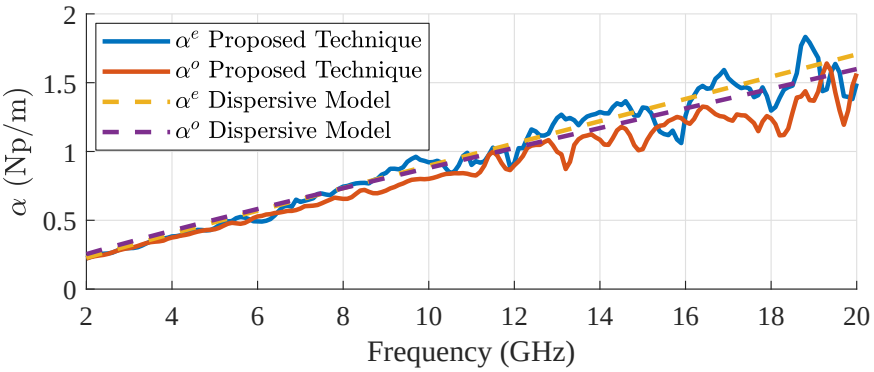

(b)

Figure A.3: Propagation constant of the even and odd modes applying the proposed method to electromagnetic simulated results, in comparison to analytical models. (a) Effective dielectric constant. (b) Attenuation constant.

eleventh in Fig. A.5). Each of the circuits was measured using a two-port network analyzer, as shown in Fig. A.5.

From the measurement of the S-parameters, the reflection coefficients Γ^e and Γ^o are extracted using (9) in order to apply the proposed method. Fig. A.6 shows the measured propagation constants using the experimental data compared with the full-wave-simulated results of Section A.2.2. In this case, the relative error in $\varepsilon_{r_{eff}}$ is about $\pm 3\%$ for the even and odd modes, and the precision on the determination of the attenuation constant, α, has worsened significantly.

As aforementioned, the statistical procedure is capable of providing a measure of the error in the determination of the propagation constant through the standard deviation σ of the outlier-free solutions of (A.3). In this case, Fig. A.7 shows the experimental results with error bars denoting the $\pm\sigma$ values. The error bars are too large for the effective permittivities and in the attenuation constants the negative values are not

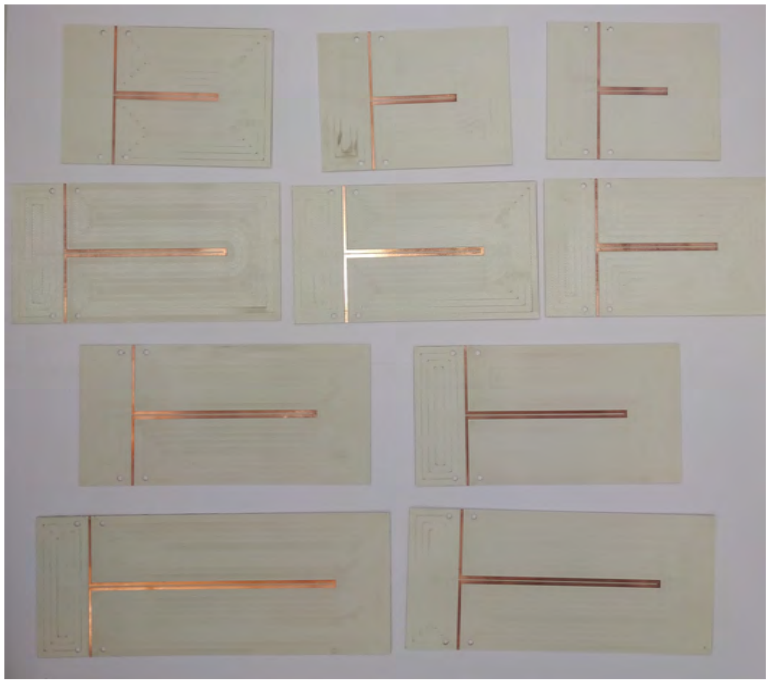

Figure A.4: Manufactured circuits.

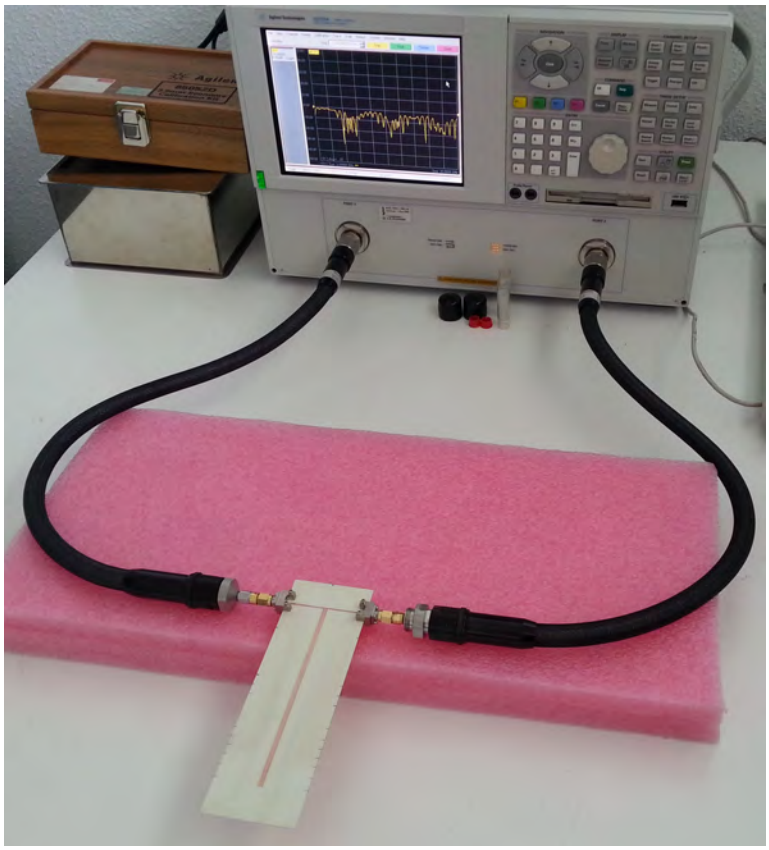

Figure A.5: Measurement process of one of the manufactured circuits.

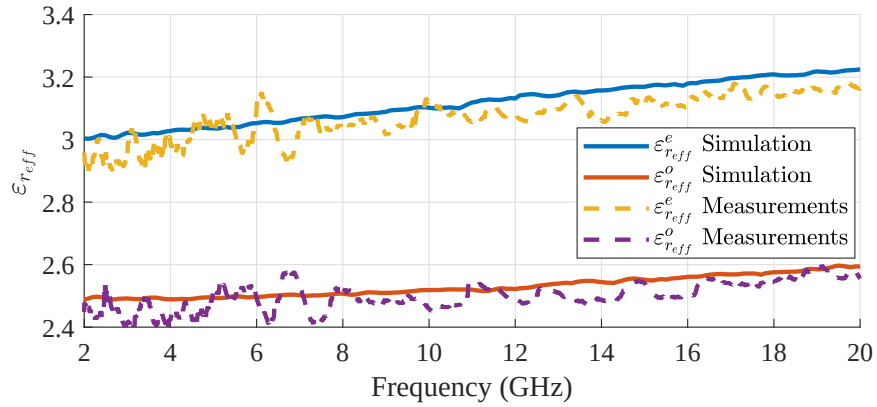

(a)

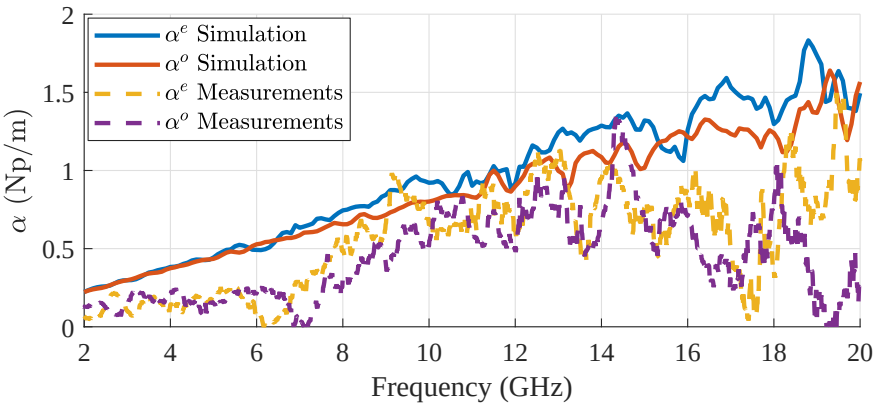

(b)

Figure A.6: Experimental determination of the propagation constants of the even and odd modes using the proposed method with 11 line lengths in comparison to electromagnetic simulation results. (a) Effective dielectric constants. (b) Attenuation constants.

statistically discardable. The high degree of inaccuracy certainly leaves room for improvement.

One of the prime suspects of the inaccuracies presented in the measured case stem from the differences between the feeding networks of each of the 11 circuits. These differences can be attributed to fabrication errors and some lack of repeatability in the interconnection with the measurement equipment and connectors. The proposed technique is not capable to deal with these differences since it relies on the invariance of the four-port access of Fig. A.1a. To increase the precision of the method, all the circuits used for the characterization should be identical but in the length of the coupled lines.

An alternative measurement procedure is proposed. This method lies in measuring

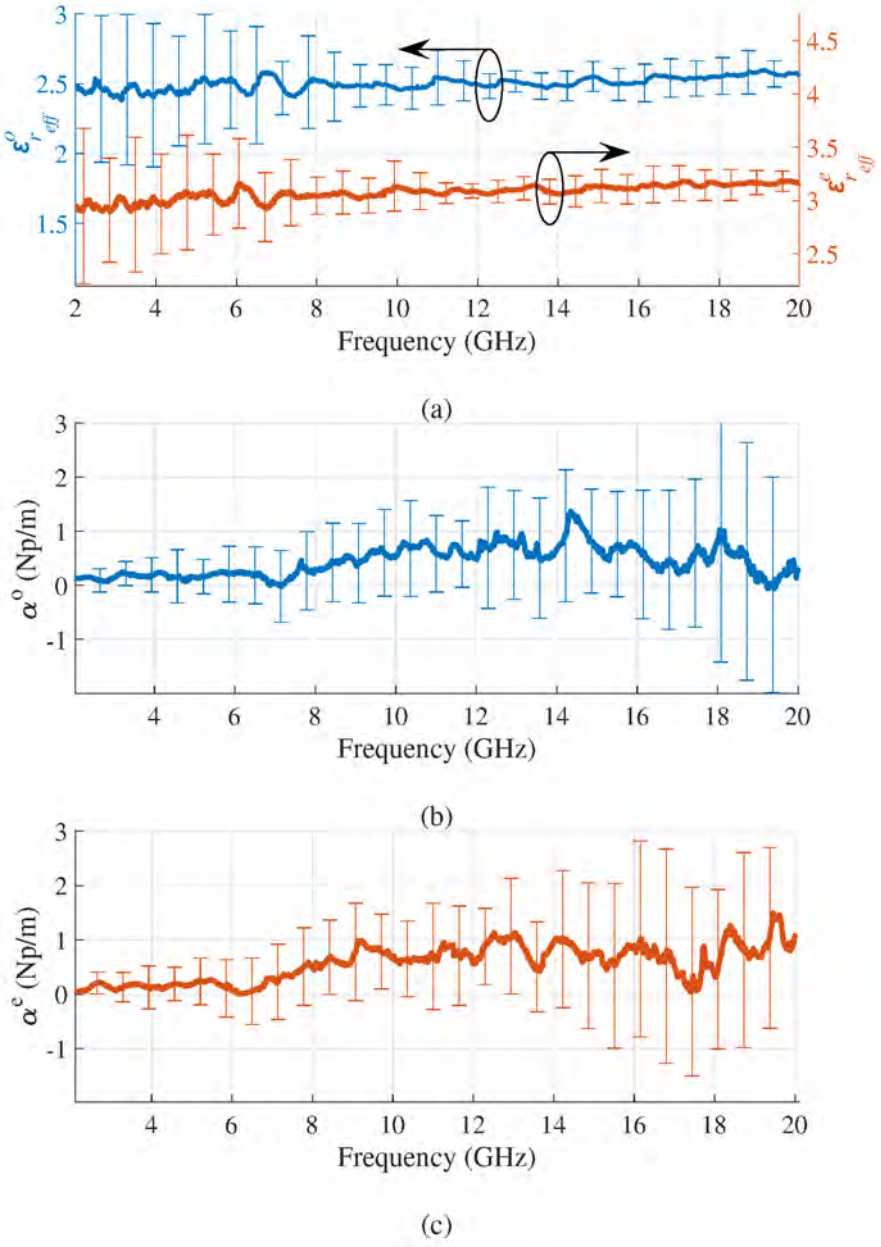

Figure A.7: Even- and odd-mode experimental results of the proposed procedure using 11 line lengths with $\pm\sigma$ error bars. (a) Effective dielectric constants. (b) Odd-mode attenuation constant. (b) Even-mode attenuation constant.

the circuit corresponding to the longest line and then getting the smaller lines by cutting this one in the appropriate length. After each cut, measurements are performed to collect the S-parameters data for each of the lines. This way, it is possible to obtain the measurement of coupled lines of different lengths by using a single circuit and, thus, removing possible differences between the feeding networks. Applying this *destructive* method implies that the coupled lines must be terminated in open-circuit both for the even and for the odd mode, whereas in the previous case the lines were terminated in

an open circuit for the even mode and in a short circuit for the odd mode. Fig. A.8 shows the final state of the destroyed circuit used in this particular case.

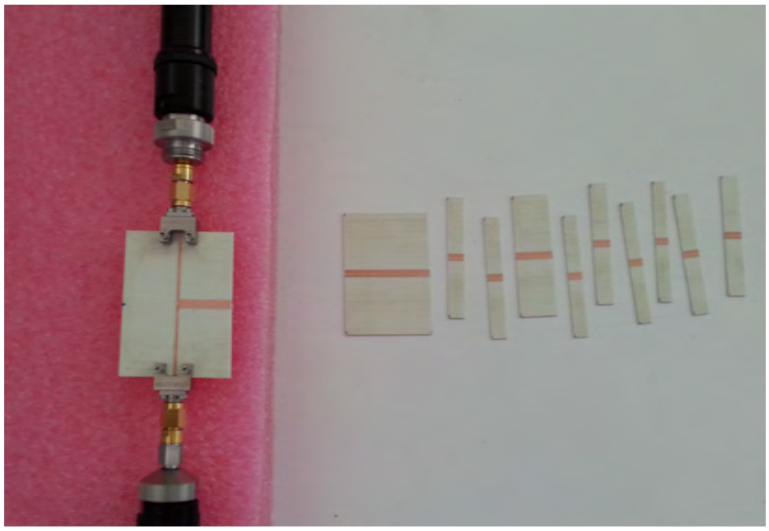

Figure A.8: Final state of the circuit using the destructive method.

After processing the measurements obtained with the destructive method, a new set of propagating constants is found. These results are plotted in Fig. A.9, which also shows the results obtained from the full-wave electromagnetic simulation of 11 lines terminated in an open circuit, in the same way as in Section A.2.2. Unlike the results of measuring 11 different circuits, now the level of accuracy is equivalent to the one obtained from simulations, which confirms the relevance of the repeatability of the line accesses. The differences in the values of $\varepsilon_{r_{eff}}$ are within the specification of the manufacturer for the substrate permittivity, which is ± 0.05. For comparison Fig. A.10 shows the results with error bars denoting the $\pm\sigma$ values. With this measurement strategy, the destructive procedure, the errors are significantly lower than in the previous one, using 11 different circuits (see Fig. A.7). Note the remarkable difference in the y-axis scales of Figs. A.7a and A.10a, and the fact that the results for the attenuation constants are now constrained to positive and significant values.

In Fig. A.9b it seems as if the values of α^e and α^o erratically increase from 12 GHz on, which is in agreement with the larger error bars in Figs. A.10b and A.10c for $f > 12$ GHz. This has been attributed to the presence of radiation in the circuit, which significantly increases around that frequency. Unavoidably, the circuit radiates differently depending on the length of the coupled line sections, which implies losses that cannot be attributed to the attenuation constant. Therefore, when radiation plays a meaningful role, it is not possible to measure an accurate value of α with any method. Even so, the results for both the attenuation constants and effective permittivities by

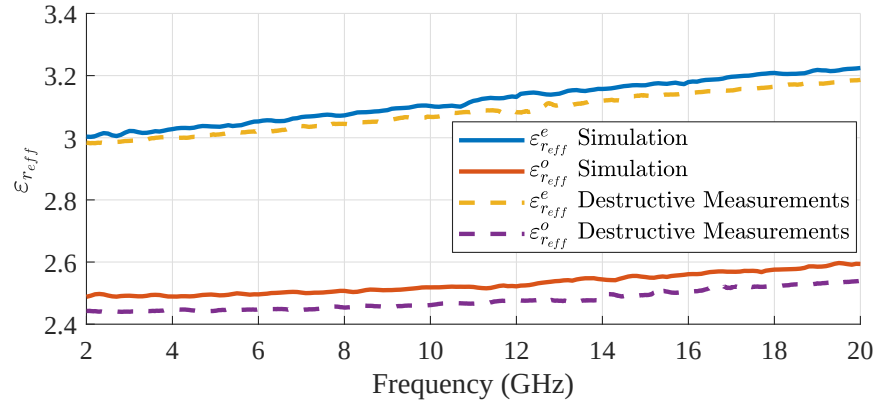

(a)

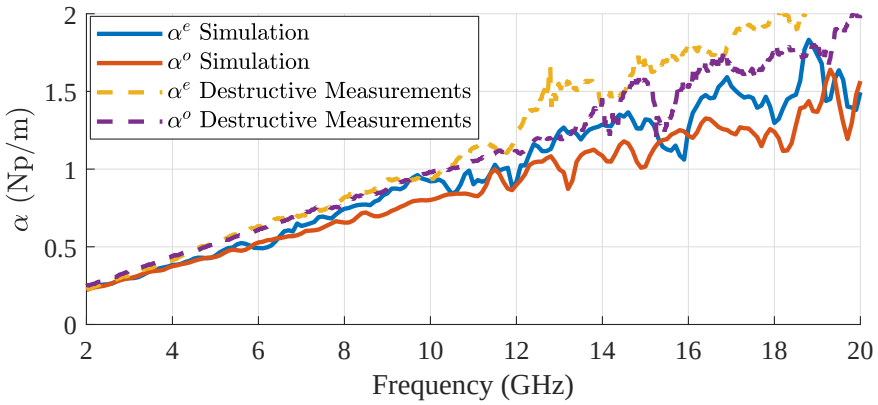

(b)

Figure A.9: Experimental determination of the propagation constants of the even and odd modes applying the proposed destructive method in comparison to electromagnetic simulation results. (a) Effective dielectric constants. (b) Attenuation constants.

means of the proposed procedure show an outstanding accuracy in a broad frequency band.

A.3 Conclusion

A relatively simple method for the accurate experimental determination of the propagation constants of symmetrical coupled lines is introduced. It is a useful method in broadband characterization, as evidenced by the decade-bandwidth (2-20 GHz) results obtained for the even and odd modes of microstrip coupled lines. Excellent results have been obtained for the effective dielectric constants, and good results have been achieved for their attenuation constants, even when these values are considerably low. This experimental characterization has been corroborated using the commercial full-

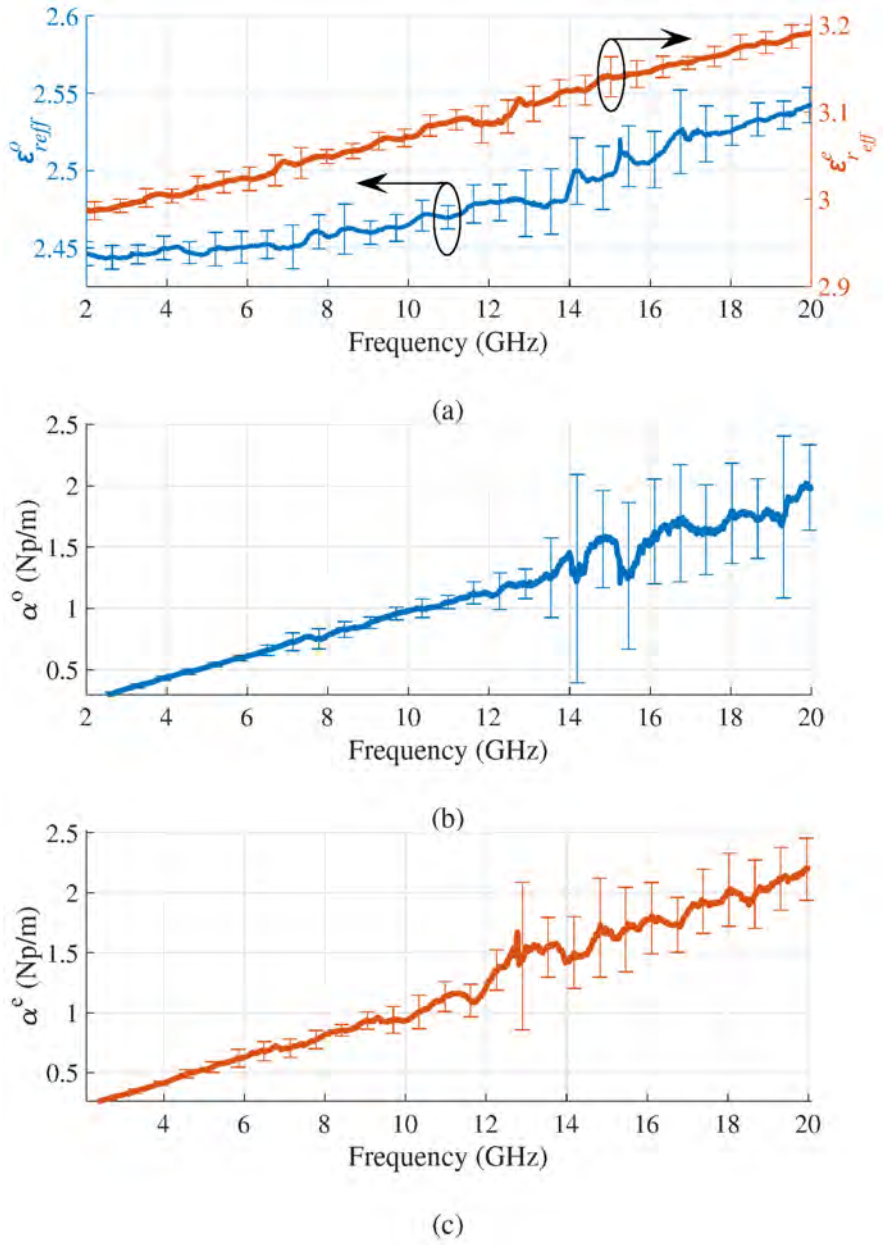

Figure A.10: Even- and odd-mode experimental results of the destructive procedure with $\pm\sigma$ error bars. (a) Effective dielectric constants. (b) Odd-mode attenuation constant. (b) Even-mode attenuation constant.

wave electromagnetic solver HFSS.

Two issues have proved to be particularly relevant. First, the results can be significantly better if special attention is paid to the repeatability of the launcher. Second, the ability to measure attenuation constants of open transmission lines at higher frequencies is constrained by the radiation of the coupled line sections. However, the proposed method has displayed a certain capacity to extract accurate results even in such a situation. Therefore, the proposed procedure has demonstrated to be an advantageous

alternative to the state-of-the-art methods for simple broadband characterization of the propagation constants of symmetrical coupled lines.

Appendix B

An Equivalent-Circuit Topology for Lossy Non-Symmetric Reciprocal Two-Ports

There is a growing interest in the modeling of lossy non-symmetric reciprocal two-port electromagnetic structures by means of equivalent circuits. This interest has been fostered, to a great extent, by periodic Leaky-Wave Antennas (LWAs), since it has been shown that the introduction of certain asymmetries in their unit cell can mitigate the so-called open-stopband effect at broadside [87, 88]. The performance of the LWA is indeed governed by the asymmetries of the unit cell and their control can lead to improved LWA design strategies and behavior. Having a proper equivalent circuit can, in general, help provide some physical insight into the involved electromagnetic phenomena [89], and can, in the particular case of LWAs, be crucial for extracting the propagation constant that determines the performance of such antennas [90].

From a purely mathematical point of view, three complex parameters are necessary for the complete specification of a dissipative reciprocal two-port structure, so the equivalent circuit must contain at least three lossy circuit elements or their equivalents [91]. A given equivalent circuit is characterized by its constituent elements or components (mainly immittances, transformers, and transmission line sections or reference plane shifts) and its topology (the way the elements are interconnected). In the case of nondissipative two-ports there is a wide variety of available equivalent circuits (see, for instance, [91, 92]). However, there is not such a variety of choices for the case of dissipative reciprocal two-ports.

One of the problems with dissipative reciprocal two-ports is that, depending on the topology of the equivalent circuit, immitances with negative real parts may appear, which is not a desirable characteristic, although it does not compromise energy conservation in the two-port as a whole. This modeling problem (the appearance of negative real parts in the immittances of the equivalent circuits) was already addressed in the early days of microwave technology. For instance, Felsen and Oliner [93] further elaborated on an original idea from Weissfloch [94] and proposed to separate the dissipative equivalent circuit into lossy and lossless portions. In doing so, they obtained what they called *canonical* networks or equivalent circuits composed by two transmission line sections (or two reference plane shifts), one reactance or susceptance, one ideal transformer with real turns ratio, and two non-negative resistors (a total of six elements, although only two of them are lossy). The idea of separating the dissipative two-port into lossy and lossless portions has reached our days and, very recently, Zappelli [95] has proposed equivalents circuits for dissipative reciprocal two-port devices based on this separation approach. These equivalent circuits contain non-negative resistors and, in its simpler form (*compact configuration*), has seven (real) elements and an intricate extraction procedure.

In the case of dissipative symmetric (certainly reciprocal) two-ports, the lattice network can be considered as the optimum equivalent circuit, since it guarantees the realizability of the two immittances required to model the response of any realizable symmetric network. Moreover, the lattice network provides a profound physical insight into the circuit behavior, since any response can be considered as a linear combination of the two *eigenstates* (even- and odd-mode excitations) of the structure. Because of this, in recent years, the spotlight has been put on the quest for lossy non-symmetric equivalent circuits that mimic, to some extent, the properties of the lattice network. Unfortunately, equivalent circuits based on the lattice-network topology require the structure to be symmetric, and the derivation of an extension of this topology for non-symmetric circuits has proved not to be straightforward.

In an attempt to elaborate on some design methodology to choose the degree of asymmetry needed to cancel the broadside effect in LWAs, an equivalent circuit based on the symmetric lattice network was proposed in [88]. Although this equivalent circuit was useful for the purpose of [88], this circuit lacked the main aforementioned properties of the lattice networks which might limit its application to other problems. An alternative to this circuit is the equivalent circuit proposed in [96]. The latter follows an eigenstate formulation approach [97] and, unlike the circuit in [88], it preserves the

property of symmetric lattice networks of being decomposable in eigenstates. This property of decomposition has been satisfactorily exploited very recently in [98] to propose the design flow of a modified microstrip Franklin unit cell for its use in LWAs.

Although the benefits of the equivalent circuit proposed in [96] have been already proved in specific LWA designs [98], this model has revealed to have two main problems. The first one is that the real parts of their immittances can be negative unless power orthogonality between the eigenstates is enforced by adding a frequency-dependent shift in the reference planes. This is an undesirable behavior for an equivalent circuit of a passive network. The second problem is that, when the two ports are isolated (y_{12} or z_{12} is zero or close to zero), the equivalent circuit is not able to properly degenerate into this limit case.

Based on the eigenstate decomposition proposed in [96], a novel equivalent circuit for non-symmetric structures is proposed here, which overcomes the main drawbacks of the equivalent circuits proposed there. The proposed circuit consists of two immittances and two transformers with a single complex turns ratio (i.e., three complex parameters, the minimum number of parameters required) as in [96], but with a different topology that has a dramatic effect on the immittances: their values are the eigenvalues of the immittance matrix of the structure. As an important consequence of this, the real parts of these two immittances are always positive (regardless of the real or complex character of the turns ratio or the choice of reference planes). Additionally, the circuit is able to gracefully degenerate into the limit case defined by $y_{12} = 0$ or $z_{12} = 0$, which broadens its applicability and usefulness. Even more, the extraction procedure is absolutely straightforward, with simple explicit equations for all the circuit elements. Obviously, the equivalent circuit degenerates into the sought lattice network in the case of symmetric two-ports. The performance evaluation of the equivalent circuit is addressed by extracting its element values for three two-port cases: one based on the circuit simulation of an artificial CRLH unit cell, one based on the full-wave electromagnetic simulation of a series-fed coupled patch unit cell of a LWA, and one based on the measurements of a complementary strip-slot. The last two cases include an analysis of the influence on the equivalent circuit elements of the two-port degree of asymmetry.

This appendix is structured as follows. Section B.1 shows the eigenstate decomposition of a generic two-port. Section B.2 proposes the new topology for both the admittance and impedance parameters. Section B.3 shows three examples of the application of the proposed equivalent circuit to model non-symmetric structures. Finally,

Section B.4 summarizes the main conclusions.

B.1 Theoretical Background

In [96], it was found that a non-symmetric reciprocal two-port network can be decomposed using an eigenstate formulation. For the sake of completeness, this argument is summarized here. Two decompositions were proposed, one of them using the admittance parameters and the other using the impedance parameters. From the admittance matrix of the network (the reasoning for the impedance matrix is analogous),

$$[Y] = \begin{bmatrix} y_{11} & y_{12} \\ y_{12} & y_{22} \end{bmatrix} \tag{B.1}$$

its eigenvalues can be obtained as

$$\lambda_1 = \frac{y_{11} + y_{22} + \sqrt{(y_{11} - y_{22})^2 + 4y_{12}^2}}{2} \tag{B.2a}$$

$$\lambda_2 = \frac{y_{11} + y_{22} - \sqrt{(y_{11} - y_{22})^2 + 4y_{12}^2}}{2} \tag{B.2b}$$

and their associated normalized eigenvectors can be obtained as

$$\overrightarrow{v_1} = \frac{1}{\sqrt{|p|^2 + 1}} \begin{bmatrix} p \\ 1 \end{bmatrix} \tag{B.3a}$$

$$\overrightarrow{v_2} = \frac{1}{\sqrt{|p|^2 + 1}} \begin{bmatrix} -1 \\ p \end{bmatrix}, \tag{B.3b}$$

where

$$p = \frac{y_{11} - y_{22} + \sqrt{(y_{11} - y_{22})^2 + 4y_{12}^2}}{2y_{12}}. \tag{B.4}$$

By the definition of the eigenvalues and eigenvectors, it is possible to write, then,

$$[Y]\overrightarrow{v_1} = \lambda_1 \overrightarrow{v_1} \tag{B.5a}$$

$$[Y]\overrightarrow{v_2} = \lambda_2 \overrightarrow{v_2} \tag{B.5b}$$

and, by interpreting these expressions in terms of circuits, the eigenvector $\overrightarrow{v_i}$ can be seen as applied voltages in each of the ports that produce the current $\lambda_i \overrightarrow{v_i}$ $(i = 1, 2)$. Unifying the expressions (B.5a) and (B.5b) and separating the result into the sum of two matrices, it can be written as

$$[Y][\overrightarrow{v_1} \;\; \overrightarrow{v_2}] = [\lambda_1 \overrightarrow{v_1} \;\; \overrightarrow{0}] + [\overrightarrow{0} \;\; \lambda_2 \overrightarrow{v_2}]. \tag{B.6}$$

Then, it is possible to split the $[Y]$ matrix into two other admittance matrices, $[Y^a]$ and $[Y^b]$, as

$$[Y] = [\lambda_1 \overrightarrow{v_1} \;\; \overrightarrow{0}][\overrightarrow{v_1} \;\; \overrightarrow{v_2}]^{-1} + [\overrightarrow{0} \;\; \lambda_2 \overrightarrow{v_2}][\overrightarrow{v_1} \;\; \overrightarrow{v_2}]^{-1} \tag{B.7a}$$

$$[Y] = [Y^a] + [Y^b]. \tag{B.7b}$$

Their values are given by

$$[Y^a] = \lambda_1 \begin{bmatrix} \frac{p^2}{p^2+1} & \frac{p}{p^2+1} \\ \frac{p}{p^2+1} & \frac{1}{p^2+1} \end{bmatrix} \tag{B.8a}$$

$$[Y^b] = \lambda_2 \begin{bmatrix} \frac{1}{p^2+1} & \frac{-p}{p^2+1} \\ \frac{-p}{p^2+1} & \frac{p^2}{p^2+1} \end{bmatrix}. \tag{B.8b}$$

Analogously, for the impedance formulation, the separation into submatrices is the following:

$$[Z] = [Z^a] + [Z^b] \tag{B.9a}$$

$$[Z^a] = \frac{1}{\lambda_1} \begin{bmatrix} \frac{p^2}{p^2+1} & \frac{p}{p^2+1} \\ \frac{p}{p^2+1} & \frac{1}{p^2+1} \end{bmatrix} \tag{B.9b}$$

$$[Z^b] = \frac{1}{\lambda_2} \begin{bmatrix} \frac{1}{p^2+1} & \frac{-p}{p^2+1} \\ \frac{-p}{p^2+1} & \frac{p^2}{p^2+1} \end{bmatrix}. \tag{B.9c}$$

Since the admittance matrix is the inverse matrix of the impedance matrix, by the properties of the eigenvalues, the impedance-matrix eigenvalues are the inverse of the admittance-matrix eigenvalues and their eigenvectors are the same. For this reason, in this derivation, the same eigenvalues of the immittance matrix, λ_1 and λ_2, and the same relation between the coefficient of their eigenvectors, p, have been used, regardless of whether the admittance or impedance matrix is considered.

Several circuit topologies for the subnetworks $[Y^a]$, $[Y^b]$, $[Z^a]$ and $[Z^b]$ were proposed

in [96]. However, they were the cause of its two main problems. The first one is that a frequency-dependent shift in the reference planes must be added to obtain positive real parts for the circuit immitance. The second problem is that when ports 1 and 2 are isolated from each other (y_{12} or z_{12} are close to zero), none of the topologies in [96] is capable to reproduce simultaneously the input impedances at the two circuit ports.

B.2 Proposed Equivalent Circuit

A new circuit topology for the subnetworks is proposed which solves the aforementioned drawbacks. The key point is to place a complex-turns-ratio transformer between two identical admittances, as depicted inside the dashed rectangles of Fig. B.1, which has a dramatic impact on the performance of the equivalent circuit.

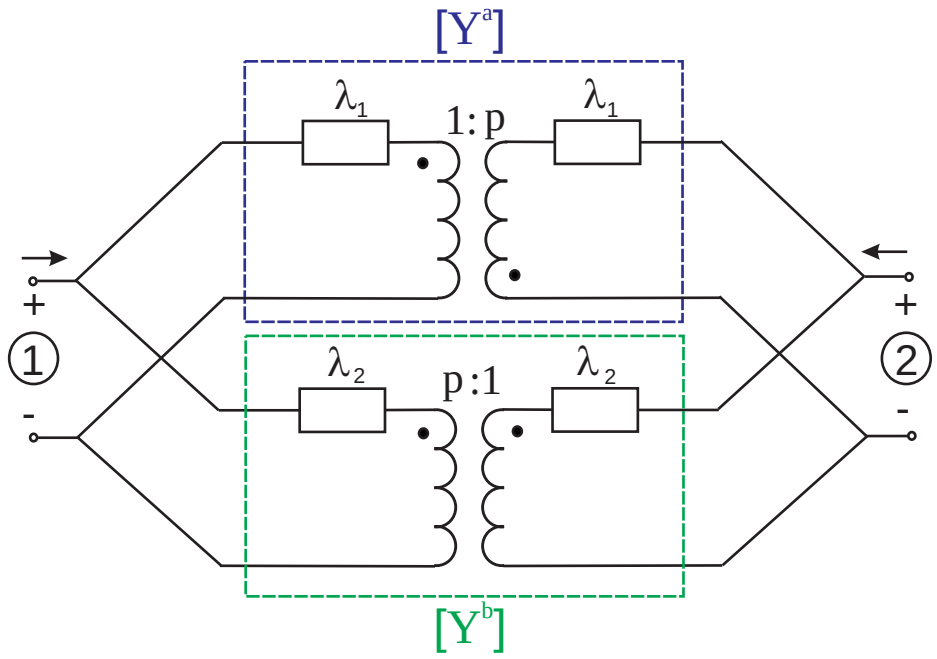

Figure B.1: Proposed eigenstate-based equivalent circuit using the admittance matrix.

A suitable analogous topology for the impedance matrix case is also proposed and it is shown inside the dashed rectangles of Fig. B.2. Note that, in both cases, the equivalent circuit is defined by three complex parameters, namely λ_1, λ_2, and p. The extraction of these parameters over frequency is straightforward, since they are, respectively, the eigenvalues of the admittance matrix and the relation between the coefficients of its eigenvectors.

A relevant characteristic of these topologies is that the values of the immittances are

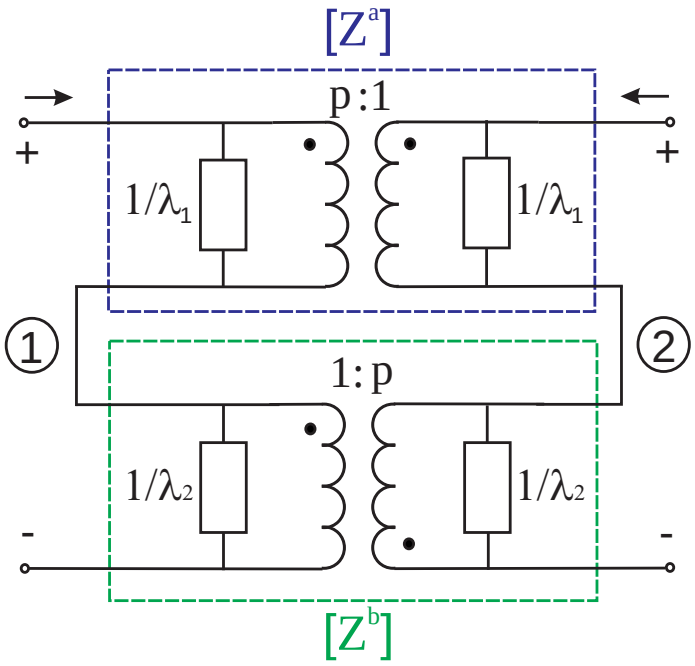

Figure B.2: Proposed eigenstate-based equivalent circuit using the impedance matrix.

the same as the eigenvalues of the admittance/impedance matrices. It can be proved that the real parts of the eigenvalues of the admittance matrix of a lossy reciprocal network are always positive or zero. Thus, every admittance of the equivalent circuit will never have negative real parts, provided the two-port is passive and reciprocal. Regarding the impedance-matrix-based equivalent circuit, the real parts of its impedances are always positive, since the inverse of a complex number with a positive real part will also have a positive real part.

Note that the turns ratios of the transformers are defined by a single parameter p, which is, in general, a complex number. It is important to note that complex-turns-ratio transformers are elements used in the synthesis of networks [99]. It is also important to realize that these transformers are two-ports that, depending on the load conditions at their ports, can be lossy or active. If the turns ratio is real, the transformer is lossless. The role played by these two transformers in the equivalent circuit is clearly illustrated by computing the dissipated power in the two-port under arbitrary excitation. This power is given by:

$$P_{dis} = \frac{1}{2}Re\{V_1^* I_1 + V_2^* I_2\} = \frac{1}{2}|A|^2 Re\{\lambda_1\} + \frac{1}{2}|B|^2 Re\{\lambda_2\} + \\ + \frac{1}{2}Re\left\{\frac{(p-p^*)(A^*B\lambda_2 - AB^*\lambda_1)}{|p^2|+1}\right\}, \quad \text{(B.10)}$$

which leads to:

$$P_{dis} = |A|^2 P_{dis}^a + |B|^2 P_{dis}^b + \frac{Im\{p\}}{|p^2|+1} Im\{AB^*\lambda_1 - A^*B\lambda_2\}, \tag{B.11}$$

where A and B are the complex amplitudes of the linear combination of eigenvectors that describe an arbitrary excitation, i.e.,

$$\begin{bmatrix} V_1 \\ V_2 \end{bmatrix} = \frac{1}{\sqrt{|p^2|+1}} \Big\{ A \begin{bmatrix} p \\ 1 \end{bmatrix} + B \begin{bmatrix} -1 \\ p \end{bmatrix} \Big\}. \tag{B.12}$$

The first and second terms of (B.11) are, respectively, the powers dissipated (P_{dis}^a and P_{dis}^b) in each subcircuit when only the corresponding eigenmode is excited. It is important to highlight that P_{dis}^a and P_{dis}^b are always positive or zero as $Re\{\lambda_1\}$ and $Re\{\lambda_2\}$ are non-negative. It is straightforward to prove that, when only one of the eigenmodes is excited, the voltages at both ports of the corresponding transformer are zero (virtual short-circuit) and, thus, the dissipated power in the transformer is zero, even if the turns ratio is complex. The third term of (B.11) is the so-called interaction term and accounts for the non-orthogonality of the eigenmodes. Note that this term is zero if the turns ratio is real, i.e., the eigenmodes are orthogonal. On the contrary, if the turns ratio is complex, the eigenmodes are non-orthogonal and the interaction term is non zero (positive or negative). In this case the complex-turns-ratio transformers are active or lossy and provide the required power to account for the energy conservation. The physical origin of the non-orthogonality of the eigenmodes is the asymmetry of the two-port. However, the asymmetry of the circuit does not necessarily imply the non-orthogonality of the eigenmodes. In particular, if the two-port is either resistive or lossless, the resulting turns ratios are real, which implies that the eigenmodes are orthogonal although the two-port is asymmetric.

Two limit cases should be mentioned, because of the capacity of the proposed circuit to properly represent both situations. The first one is when $y_{12} = 0$ ($z_{12} = 0$) and the ports are isolated. The turn ratios of the transformers tend either to zero or infinity ($p = 0$ or $p \to \infty$) and therefore, the two transformers exhibit an open circuit and a short circuit in their ports, which isolates the two ports of both subnetworks. As a result, the input admittance seen at each port will be λ_1 and λ_2, which are the theoretical values of the input admittances of the isolated two-port. Given the value of p, the interaction term of (B.11) vanishes, which corresponds to the fact that there is no interaction between one port and the other.

The second limit case is the symmetric network, with $p = 1$. The transformers then act either as a direct connection or as a crossover, and the resulting circuit topology becomes the classic lattice network with series admittances of value λ_2 and cross admittances of value λ_1. Once again, the interaction term of (B.11) vanishes (in this case because p is real). An expected result, since the modes of the lattice network are always orthogonal. Consequently, the lattice network becomes a particular case of the proposed equivalent circuit.

B.3 Case Studies

In this section, the performance of the proposed equivalent circuit is evaluated by extracting its component values, over a wide frequency band, for three different electromagnetic structures.

B.3.1 Artificial Composite Right/Left-Handed Transmission Line

The first analyzed structure is the unit cell of an artificial Composite Right/Left-Handed (CRLH) transmission line. This first theoretical analytical case has been chosen to avoid any spurious phenomena coming from either simulation numerical noise or measurement uncertainties. Specifically, the chosen unit cell is one of the two third-order artificial lossless CRLH transmission lines presented in [100]: the #6 unit cell in the taxonomy of [100, Table 1]. Like any other CRLH transmission line, it is said to be *balanced* [101] when the distributed series impedance and the distributed shunt admittance have exactly the same critical frequencies (poles and zeros). The need for an exact match seems to be the main reason for the difficulties to achieve a perfect *balance* in actual implementations and in avoiding the appearance of a stopband in the transition from left-handed to right-handed frequency bands.

To check the capability of the proposed circuit to analyze the asymmetries and imbalances of a real implementation of this unit cell, losses and asymmetries in the branches of the circuit have been considered. The losses have been included through a different finite quality factor for each element of the circuit (all quality factors around $Q \approx 50$). The asymmetries of the branches by means of slight modifications ($\approx \pm 10\%$) of the values of the elements of the circuit, which modify the resonance and anti-resonance frequencies of its immitances. The resulting circuit and element values are

reproduced in Fig. B.3.

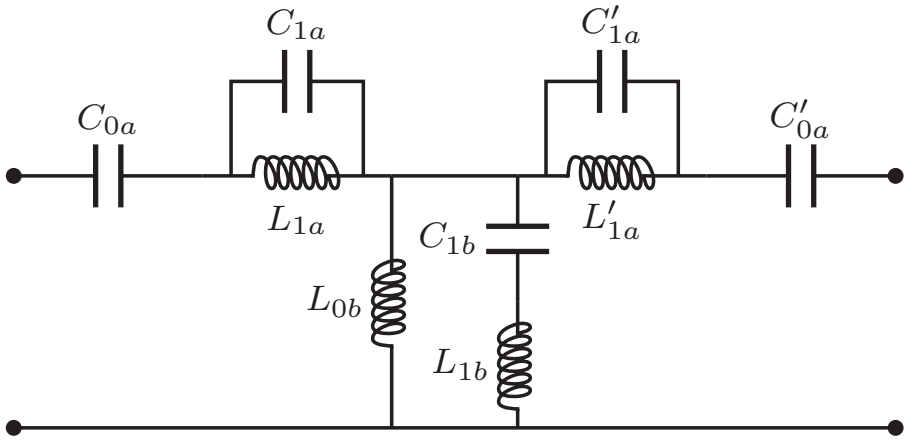

Figure B.3: Artificial CRLH transmission line unit cell. $C_{0a} = 7.45$ pF, $L_{1a} = 3.09$ nH, $C_{1a} = 1.86$ pF, $C'_{0a} = 5.59$ pF, $L'_{1a} = 2.55$ nH, $C'_{1a} = 2.05$ pF, $L_{0b} = 15.38$ nH, $L_{1b} = 6.21$ nH, $C_{1b} = 1.23$ pF

Fig. B.4 shows the values of the components of the proposed equivalent circuit up to 4 GHz. The analyzed structure has a stopband in the 1.8-2.2 GHz frequency band. At these frequencies, the y_{12} parameter is almost negligible and, thus, p is also close to zero. Even at this band, the admittances of the proposed equivalent circuit have positive real parts, and the change over frequency of the values of its circuit parameters is natural and well-behaved. Therefore, the capability of the proposed equivalent circuit to model structures that can have, over some bandwidths, decoupled ports is highlighted. Note that the transition between this stopband and the rest of the analyzed bandwidth is perfectly smooth.

B.3.2 Series-Fed Coupled Patch

The second analyzed structure is the so-called Series-Fed Coupled Patch (SFCP) [88], which is studied through electromagnetic simulations using the commercial software HFSS. The SFCP consists of an on-top-stacked patch with gap coupling to the feeding line, as shown in Fig. B.5, and its dimensions are the same as in [88]. In this case, the target of the study is how the parameters change when increasing its degree of asymmetry, which results from moving the patch along the feeding line axis a distance d. For this purpose, several unit cells with different degrees of asymmetry have been simulated and their equivalent circuit extracted.

Fig. B.6 shows the circuit parameters obtained when using the proposed equivalent

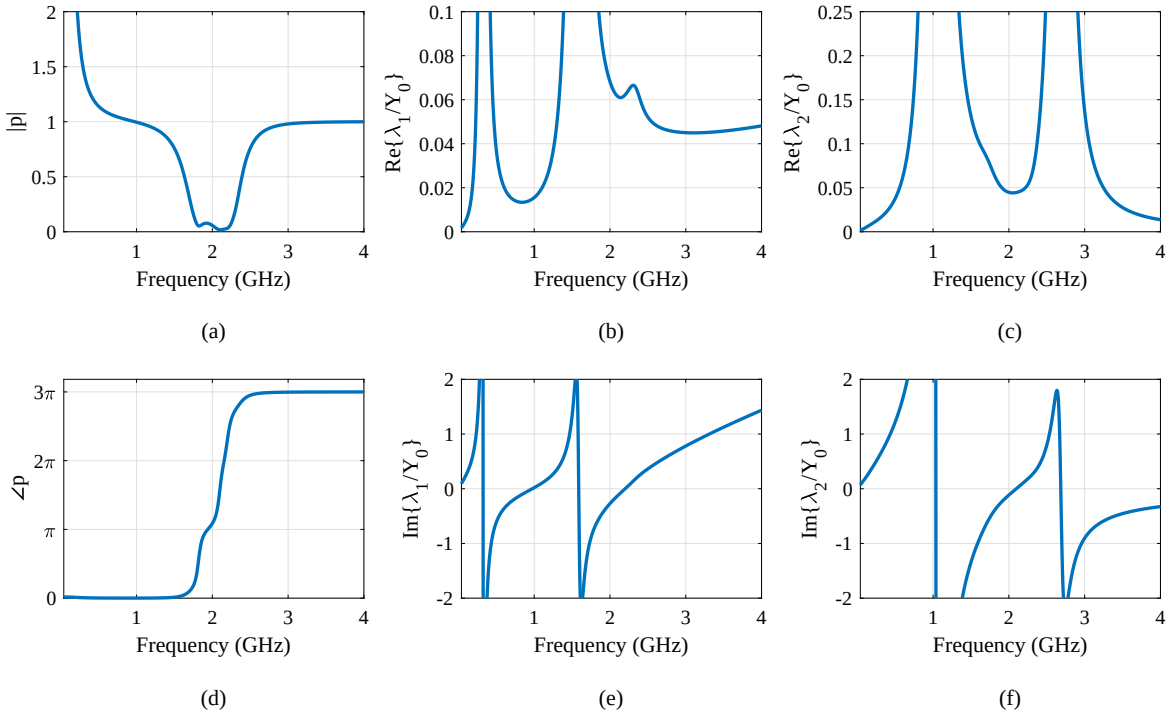

Figure B.4: Circuit parameters of the artificial CRLH transmission line unit cell using the proposed equivalent circuit. (a) Magnitude of p. (b) Real part of the normalized λ_1. (c) Real part of the normalized λ_2. (d) Phase of p. (e) Imaginary part of the normalized λ_1. (f) Imaginary part of the normalized λ_2. ($Z_0 = 1/Y_0 = 50\ \Omega$)

circuit for several degrees of asymmetry. To have a reference for the degrees of asymmetry analyzed, if the value of d were $d = 1650\,\mu m$ the patch and microstrip would have no overlapping area in one of the sides, whereas $d = 0$ corresponds to the symmetric case. In all cases, even with the numerical errors expected from a simulation, the real parts of the admittances are positive, and the equivalent circuit behaves smoothly also at lower frequencies, where the y_{12} is low for this structure. Additionally, it can be seen that the values of the immittances barely change when the level of asymmetry is changed. The information about the asymmetry of the structure is mainly in the magnitude of the turns ratio of the transformers. This makes the new equivalent circuit a powerful tool to design LWAs using this unit cell.

B.3.3 Complementary Strip-Slot

In order to validate the previous results with actual measurements, the so-called *complementary strip-slot* has been chosen as the last case study. This structure was proposed in [1] as a planar radiating element with outstanding broadband matching. It consists of a slot etched on the ground plane of a microstrip line. The complementary

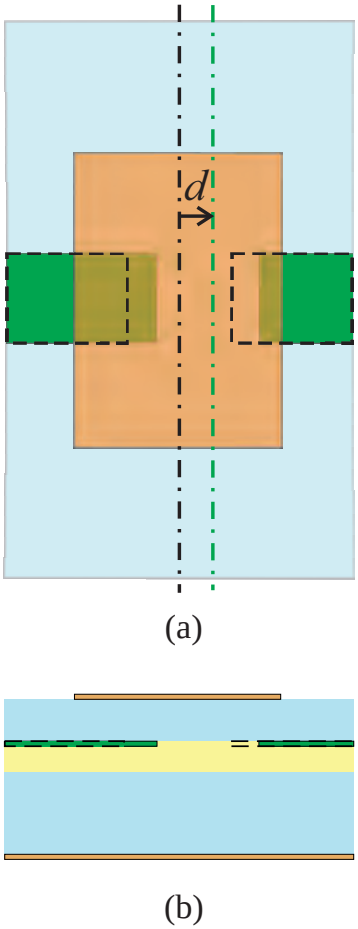

Figure B.5: The SFCP unit cell. (a) Top view. (b) Side view.

stub (strip) of the slot is placed on the microstrip layer, symmetrically aligned to the slot, as a matching element. This structure is especially interesting for the present analysis because the contribution of the strip is associated with the even mode, and that of the slot, with the odd mode. A consequence of the eigenstate separation property of the proposed equivalent circuit is that it can separate the contribution of these two modes even if some asymmetry is added to the structure. This introduction of asymmetry to the structure was proposed in [2] to reduce the broadside open-stopband effect when building an LWA with this element.

Several prototypes of the strip-slot element with different degrees of misalignment d have been fabricated. Fig. B.7 shows a partially backlit photograph of one of them. This misalignment is introduced by moving the strip and the slot a distance $d/2$ towards Port 2 and Port 1, respectively. In this case, the element values of the equivalent circuit have been extracted from the measured S-parameters with respect to $Z_0 = 50\,\Omega$, and the reference planes have been symmetrically placed 0.7 mm away from the center of the slot. To have a reference for the degrees of misalignment analyzed, the case of

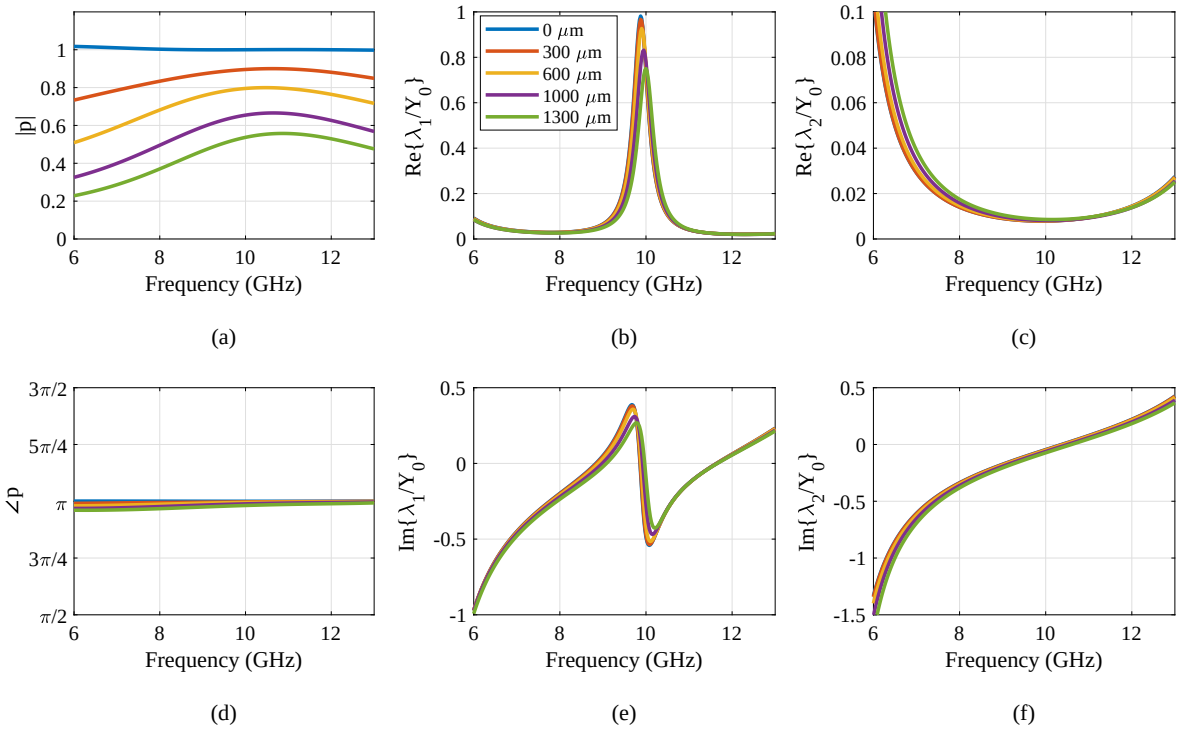

Figure B.6: Circuit parameters of the artificial SFCP unit cell for several asymmetries (d parameter) using the proposed equivalent circuit. (a) Magnitude of p. (b) Real part of the normalized λ_1. (c) Real part of the normalized λ_2. (d) Phase of p. (e) Imaginary part of the normalized λ_1. (f) Imaginary part of the normalized λ_2. ($Z_0 = 1/Y_0 = 50\,\Omega$)

$d = 540\,\mu m$ corresponds to the minimum value for which the strip and the slot have no overlapping area (they are adjacent elements loading the microstrip), whereas $d = 0$ corresponds to the symmetric case. The lengths of the strip and the slot are such that their first resonant frequencies (total length equal to $\lambda/2$) appear around 5.4 GHz. The structure is fabricated on GML 1032 substrate with $\epsilon_r = 3.2$ and 30 mil thickness. The TRL calibration technique was used to obtain the measurements. The calibration kit consisted of three "Lines" to cover the whole band of interest. Some anomalies occurred at the frequencies where the calibration changed from one "Line" to another, with the largest errors between 9.4 and 9.8 GHz.

Fig. B.8 shows the equivalent circuit of the measured structures. In this case, the values of p are greater than one and, in order to keep the shown results in the $0 - 1$ range, $1/p$ is plotted instead. Using the proposed circuit the real parts of the admittances are positive in all the frequency range, but between 9.4 GHz and 9.8 GHz. At these frequencies, the circuit do not behave as a passive circuit as a consequence of the anomalies introduced by the calibration kit. As in the previous case, the variation of the admittances with the asymmetry is small, taking into account that these are

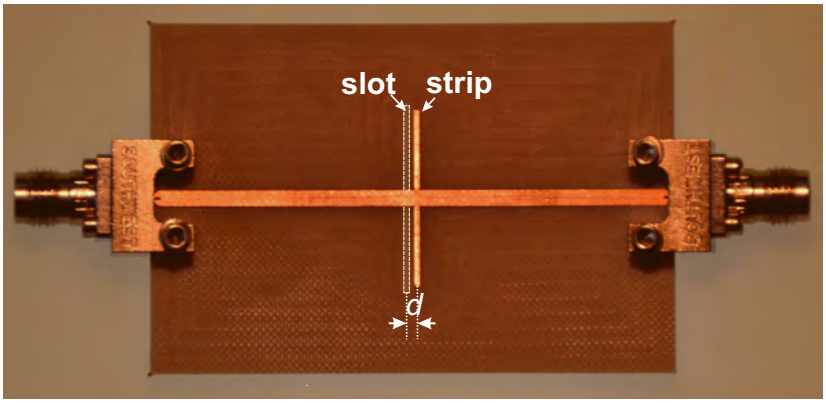

Figure B.7: Backlit photograph of a prototype of the complementary strip-slot with certain misalignment d.

different physical structures. Thus, they still represent properly the slot and the strip admittances, separately, with the transformation ratio of the transformer absorbing the effect of the asymmetry. With this case study, the eigenstate-separation capabilities of the equivalent circuit are illustrated, in addition to its robustness in the presence of errors and inaccuracies from measurements.

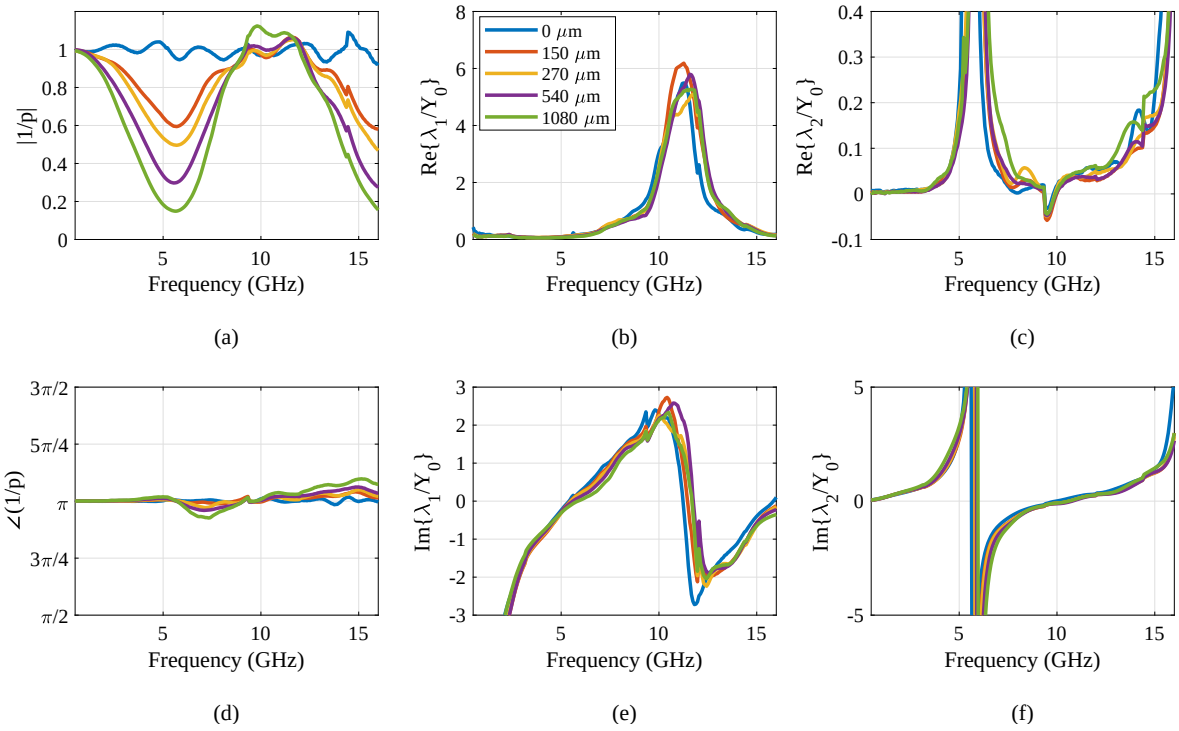

Figure B.8: Circuit parameters of the measured strip-slot unit cells for several asymmetries (d parameter) using the proposed equivalent circuit. (a) Magnitude of $1/p$. (b) Real part of the normalized λ_1. (c) Real part of the normalized λ_2. (d) Phase of $1/p$. (e) Imaginary part of the normalized λ_1. (f) Imaginary part of the normalized λ_2. ($Z_0 = 1/Y_0 = 50\ \Omega$)

B.4 Conclusion

In this appendix, a general eigenstate-based equivalent circuit for lossy non-symmetric reciprocal two-ports is proposed. It is general in the sense that it can be applied to any reciprocal lossy two-port regardless of its physical structure, since it does not rely on any physical aspect of the two-port. The circuit has only three complex parameters, namely two lossy immittances and the complex turns ratio of the transformers. It has been rigorously proved that the proposed circuit topology guarantees immittances with non-negative real parts. Moreover, the proposed equivalent circuit can efficiently handle two-ports with isolated ports ($y_{12} = 0$ or $z_{12} = 0$). Explicit and simple equations for the straightforward extraction of the equivalent circuit element values are provided.

The equivalent circuit has been validated by analyzing three different structures. In all cases, the results have proved and illustrated its capabilities and robustness against numerical and measurement uncertainties in a very broad band. An important feature of the proposed equivalent circuit is that it is capable of displaying the structure asymmetry explicitly. As a consequence, it is most convenient when the two-port has two identifiable eigenstates, since it easily models the underlying physics of the structure. This capability has been illustrated by two of the analyzed cases; in both, the turns ratio practically absorbs the asymmetry of the network leaving the immittances almost unperturbed. This is a desired feature when designing electromagnetic structures in which slight asymmetries of the unit cell play an important role, as is, for instance, the case of the mitigation of the stopband in LWAs.

The excellent simplicity, eigenstate-based derivation and extraordinary behavior in modelling structures of different nature makes the proposed equivalent circuit a good candidate for modelling lossy non-symmetric reciprocal two-ports, especially when physical insight is pursued. Indeed, the highlighted capabilities of the proposed network suggest that it can be regarded as a generalization of the symmetric lattice network for lossy non-symmetric two-ports.

Appendix C

Publications Derived From This Thesis

Journals

[1] A. Hernández-Escobar, E. Abdo-Sánchez, P. Mateos-Ruiz, J. Esteban, T.M. Martín-Guerrero, and C. Camacho-Peñalosa, "An Equivalent Circuit Topology for Lossy Non-Symmetric Reciprocal Two-Ports," submitted for publication.

[2] A. Hernández-Escobar, E. Abdo-Sánchez, J. Esteban, T.M. Martín-Guerrero, and C. Camacho-Peñalosa, "Broadband Determination of the Propagation Constant of the Slot Mode of a Rectangular Waveguide," *IEEE Antennas and Wireless Propagation Letters*, vol. 19, no. 12, pp. 2423–2427, Dec. 2020.

[3] A. Hernández-Escobar, E. Abdo-Sánchez, J. Esteban, T.M. Martín-Guerrero, and C. Camacho-Peñalosa, "Broadband determination of the even- and odd-mode propagation constants of coupled lines based on two-port measurements," *IEEE Transactions on Microwave Theory and Techniques*, vol. 68, no. 2, pp. 648–654, Feb. 2020.

[4] A. Hernández-Escobar, E. Abdo-Sánchez, and C. Camacho-Peñalosa, "A Wideband Equivalent Circuit for Stripline-Fed Cavity-Backed Slot Radiating Elements," *IEEE Access*, vol. 7, pp. 166428–166434, Nov. 2019.

[5] A. Hernández-Escobar, E. Abdo-Sánchez, and C. Camacho-Peñalosa, "A Broadband Cavity-Backed Slot Radiating Element in Transmission Configuration,"

IEEE Transactions on Antennas and Propagation, vol. 66, no. 12, pp. 7389–7394, Dec. 2018.

Conferences

[1] A. Hernández-Escobar, E. Abdo-Sánchez, J. Esteban, T.M. Martín-Guerrero, and C. Camacho-Peñalosa, "Broadband determination of the propagation constant of the slot mode of a rectangular waveguide," in *Proceedings of the XXXV Simposium Nacional de la Unión Científica de Radio (URSI 2020)*, Málaga, Sep. 2020. *Received a *URSI Young Researchers Secondary Award*.

[2] A. Hernández-Escobar, E. Abdo-Sánchez, J. Esteban, T.M. Martín-Guerrero, and C. Camacho-Peñalosa, "Measuring odd- and even-mode propagation constants of coupled-lines by means of the lattice network," in *Proceedings of the Encuentro Ibérico de Electromagnetismo Computacional*, Potes, Oct. 2019.

[3] A. Hernández-Escobar, E. Abdo-Sánchez, and C. Camacho-Peñalosa, "On the matching of stripline-fed cavity-backed slots as a series-fed array element," in *Proceedings of the IEEE-APS Topical Conference on Antennas and Propagation in Wireless Communications*, Granada, Sep. 2019.

[4] A. Hernández-Escobar, E. Abdo-Sánchez, and C. Camacho-Peñalosa, "Ranura de banda ancha en doble T sobre cavidad para arrays alimentados en serie," in *Proceedings of the XXXIV Simposium Nacional de la Unión Científica de Radio (URSI 2019)*, Seville, Sep. 2019.

[5] A. Hernández-Escobar, E. Abdo-Sánchez, and C. Camacho-Peñalosa, "A broadband bow-tie cavity-backed slot for traveling-wave arrays in the millimeter-wave band," in *Proceedings of the 12th European Conference on Antennas and Propagation (EuCAP)*, Krakow, Apr. 2019.

[6] A. Hernández-Escobar, E. Abdo-Sánchez, and C. Camacho-Peñalosa, "Elemento radiante de banda ancha en microstrip cerrada para arrays alimentados en serie," in *Proceedings of the XXXIII Simposium Nacional de la Unión Científica de Radio (URSI 2018)*, Granada, Sep. 2018.

[7] A. Hernández-Escobar, E. Abdo-Sánchez, and C. Camacho-Peñalosa, "Novel implementation for a broadband cavity-backed slot fed in transmission configura-

tion," in *Proceedings of the 11th European Conference on Antennas and Propagation (EuCAP)*, London, Apr. 2018.

[8] A. Hernández-Escobar, E. Abdo-Sánchez, and C. Camacho-Peñalosa, "Análisis preliminar del strip-slot complementario en tecnología stripline," in *Proceedings of the XXXII Simposium Nacional de la Unión Científica de Radio (URSI 2017)*, Cartagena, Sep. 2017.

Appendix D

Summary in Spanish

D.1 Introducción

D.1.1 Marco contextual

Ahora más que nunca, el mundo necesita estar completamente interconectado por medios digitales. Los esfuerzos de los últimos años han permitido reducir lo que antes era inevitable movilidad e interacción física, además de incrementar la eficiencia del trabajo en los países desarrollados. Sin embargo, se debe hacer aún más para lograr comunicaciones globales en tiempo real que sean accesibles a todos. Para este objetivo, se requieren tasas de bits extremadamente altas, también en enlaces inalámbricos.

En las últimas tendencias en comunicaciones inalámbricas, esto es, en la quinta generación de comunicaciones móviles (5G), se propone el uso de bandas de mayor frecuencia para aumentar la tasa de bits, ya que se dispone de más ancho de banda en esas bandas. Por esta razón, la banda de milimétricas (30 GHz - 300 GHz) ha ganado atención recientemente. El enfoque inicial ha estado en torno a 24, 28 y 39 GHz, pero ahora se están considerando incluso la banda E (60 GHz) y la banda V (70/80 GHz). Los pronósticos más optimistas incluyen la banda W (100 GHz) y la banda D (150 GHz). Este es solo un ejemplo de cómo se está renunciando a las comunicaciones inalámbricas tradicionales de banda estrecha en favor de los sistemas de banda ancha a alta frecuencia.

A pesar de que el diseño de antenas en el contexto de los sistemas de comunicaciones es uno de los desafíos más clásicos en la ingeniería de telecomunicación, las antenas para

nuevas aplicaciones y servicios de reciente aparición pueden requerir especial atención en su desarrollo o investigación adicional. Estas funcionalidades mejoradas pueden incluir ancho de banda amplio, alta eficiencia, alta directividad, tamaño pequeño, bajo coste y fácil integración.

Las ranuras radiantes han sido tradicionalmente buenas candidatas para diseñar antenas pequeñas de alto rendimiento debido a sus muchas ventajas, como ligereza, alta discriminación de polarización cruzada, escaso volumen y bajo coste de fabricación. Además, se pueden implementar utilizando diferentes tecnologías como microstrip o waveguide. Por estas razones, pueden ser una buena solución para las antenas de los futuros sistemas de comunicación.

Sin embargo, aunque el ancho de banda de estos radiadores es suficiente para aplicaciones de banda estrecha, podrá ser insuficiente para sistemas más exigentes y de alta tasa de bits. Los elementos radiantes de ranura tienen una naturaleza muy resonante que compromete considerablemente su ancho de banda de impedancia. Existen algunas técnicas para ampliar levemente su ancho de banda de impedancia, como utilizar ranuras anchas o descentrar el elemento con respecto a su alimentación. Sin embargo, todos presentan serios inconvenientes. El primero empeora sus características de radiación y el segundo hace que la ranura radie menos potencia en un ancho de banda aún más estrecho.

En [1], se propuso un nuevo método para aumentar el ancho de banda de las ranuras alimentadas por microstrip. El método consiste en añadir un strip en la línea microstrip que anula por completo la reactancia de la ranura y, por tanto, aumenta su ancho de banda. En realidad, si las dimensiones del strip se eligen correctamente, el ancho de banda de impedancia del elemento radiante resultante puede ser teóricamente ilimitado. Esta solución no solo no presenta nuevos inconvenientes, sino que también es simple, fácil de implementar y su diseño es sencillo. Este nuevo elemento ha demostrado ser sólido para la construcción de arrays, como los arrays de onda de fuga [2] o arrays log-periódicos [3].

Las ranuras alimentadas por microstrips, sin embargo, radian hacia ambas mitades del espacio, ya que consisten en una ranura impresa en un solo plano conductor. Esto significa que habrá al menos dos haces principales cuando se construya un array hecho con este elemento. Por lo tanto, pueden ser una mala elección cuando se desea un único haz directivo que no desperdicie energía en un haz adicional. Para eliminar uno de los haces, es posible utilizar un plano reflector detrás de la ranura, como en

[3]. Sin embargo, la distancia óptima entre el reflector y el radiador depende de la frecuencia, lo que reduce el ancho de banda del elemento. Además, esta solución aumenta significativamente el tamaño de la antena y elimina su perfil plano, que era una de las principales ventajas de utilizar una antena microstrip.

Una solución alternativa es el uso de una ranura sobre una cavidad (CBS). Estas ranuras están impresas en la superficie de una cavidad cerrada en lugar de en un plano de tierra de una sola capa. Su radiación es unidireccional porque la cavidad bloquea la radiación hacia una mitad del espacio. Los CBS han sido estudiados hace ya varias décadas [4] y su uso ha aumentado recientemente debido a su buen rendimiento y capacidad de fabricación utilizando SIW [5]. A pesar de esto, sus análisis previos no proporcionaron comprensión física sobre cómo funciona el elemento radiante, y sus ecuaciones de diseño eran demasiado complejas para su uso práctico o la elaboración de un circuito equivalente. Por supuesto, el problema del ancho de banda no se había resuelto para los CBS con tanta elegancia como en [1], y la presencia de la cavidad puede hacer que la antena sea bastante voluminosa a frecuencias más bajas en comparación con las ranuras alimentadas por microstrip. Aún así, aplicar la misma técnica de adaptación a los CBS es muy interesante para obtener un elemento radiante similar a una ranura unidireccional de banda ancha.

En consecuencia, la búsqueda de nuevas técnicas de adaptación para aumentar el ancho de banda del CBS parece ser un tema atractivo para la comunidad de antenas. Aplicar la técnica de adaptación de [1] a este tipo de ranuras puede resultar muy interesante desde un punto de vista práctico. Además, para hacer esto, la comprensión y el conocimiento de la física que hay detrás de estas ranuras, más complejas, pueden ayudar a su diseño y a mejorar aún más sus propiedades de radiación.

D.1.2 Génesis

El núcleo de esta tesis doctoral surgió al intentar obtener un nuevo elemento radiante que pudiera ser útil para diseñar arrays de antenas para sistemas de comunicación 5G y, para ello, era necesario un elemento radiante unidireccional. Se pretendió solucionar el problema de la radiación bilateral de la ranura alimentada por microstrip utilizando stripline. De esta manera, se aplicó el concepto de strip-slot complementario de [1] para diseñar una ranura adaptada con un stub y alimentada por strip que obtuviera radiación unidireccional. Sin embargo, se descubrió que paredes metálicas de la stripline actuaban como una cavidad, y la ranura era, entonces, un CBS. En este tipo de ranura,

el tamaño de la cavidad tiene un impacto significativo en su comportamiento.

A pesar de ello, se demostró que ajustando adecuadamente el tamaño de la cavidad era posible obtener adaptación en banda ancha. En cuanto al equivalente circuital para la estructura, no se encontró un modelo simple y útil en la literatura y, por lo tanto, se necesitó más investigación sobre el CBS. Se halló que el modo que se propaga dentro de la cavidad es el modo ranura de una guíaonda rectangular, que tiene frecuencia de corte. Partiendo de esa información, fue posible extraer un circuito equivalente de línea de transmisión para la ranura que obtuviera resultados precisos.

Este peculiar modo que se estaba propagando por la estructura despertó nuestro interés y, así, también se desarrolló un método para obtener su constante de propagación. Nuestro grupo tenía una amplia experiencia en la aplicación de una versión mejorada del método propuesto por Bianco y Parodi [6] a diferentes estructuras. De esta forma se obtuvo un método especializado para obtener más información sobre el modo slot.

D.1.3 Objetivos

El primer objetivo de esta tesis fue obtener un elemento radiante unidireccional para arrays alimentados en serie, basado en el concepto del strip-slot complementario. Dado que para lograr el primer objetivo se utilizó un CBS y su modelo no era sencillo, objetivos adicionales incluyeron la comprensión del CBS lo suficiente como para elaborar un modelo basado en línea de transmisión. Luego, se tuvo que desarrollar un circuito equivalente y un procedimiento de diseño para el nuevo elemento radiante.

Una vez que el elemento se caracterizó por completo, el siguiente objetivo fue utilizar las configuraciones de arrays exploradas con el strip-slot complementario para obtener arrays con un solo haz. Debido a la alimentación en serie de elementos, la atención se centró en arrays alimentados en serie.

Un requisito autoimpuesto fue la verificación de las conclusiones extraídas de la teoría y las simulaciones electromagnéticas mediante la fabricación de prototipos en cada fase de la investigación.

El objetivo final de este trabajo de investigación fue diseñar antenas de altas prestaciones utilizando un CBS alimentado en serie de banda ancha y resaltar el potencial de esta técnica de adaptación para obtener elementos radiantes no resonantes.

D.1.4 Estructura de los contenidos

El ***Capítulo 2*** comienza con la descripción del modo de ranura de una guía de ondas rectangular. A continuación, se presentan formas de caracterizar el modo. Una forma deriva del método propuesto por Bianco y Parodi en [6] y utiliza varias longitudes de ranura para obtener el valor de la constante de propagación del modo en un ancho de banda muy amplio. Se propone y fabrica una estructura sencilla para aplicar el método y se obtienen las medidas.

El modo antes estudiado se utiliza para explicar el funcionamiento del CBS proponiendo un circuito equivalente en el ***Capítulo 3***. La parte principal del circuito equivalente está compuesta por una línea de transmisión con la constante de propagación del modo slot y una longitud igual a la del slot. Además, se tiene en cuenta el efecto del extremo de la ranura y su distancia a la strip de alimentación.

En el ***Capítulo 4***, el concepto de strip-slot complementario se aplica a un CBS para aumentar significativamente su ancho de banda. Se estudia su procedimiento de diseño y circuito equivalente. Además, se fabrican y miden dos prototipos utilizando diferentes tecnologías. El método propuesto para mejorar el ancho de banda se compara con uno más clásico para resaltar sus ventajas. Por último, dos formas de aumentar aún más el ancho de banda del elemento radiante se ilustran mediante dos diseños adicionales.

Una vez que se ha estudiado el elemento, se exploran las aplicaciones en arrays. Debido a la alimentación del elemento, se consideran solo arrays alimentados en serie. La primera parte del ***Capítulo 5*** contiene el primer concepto de array inmediato, construido mediante la conexión en cascada de varios elementos CBS alimentados por una strip. Con un prototipo simple, se fabrica y mide una LWA con capacidad de escaneo. La segunda parte del ***Capítulo 5*** trata sobre el diseño de un array log-periódico basado en el CBS de banda ancha. El desafío aquí es modificar el elemento radiante para reducir la distancia entre ellos a pesar de la cavidad. Además, el acoplamiento mutuo entre los elementos tuvo que reducirse. Se construyó un prototipo para probar el concepto.

Finalmente, el ***Capítulo 6*** resume los resultados más importantes y destaca las contribuciones más significativas derivadas de la tesis. Concluye con una propuesta de líneas futuras para continuar con este trabajo de investigación.

Adicionalmente se incluyen otros apéndices para ampliar los contenidos propor-

cionados. El Apéndice A muestra la medida de las constantes de propagación de líneas microstrip acopladas utilizando un método similar al propuesto en el Capítulo 2. En el Apéndice B se estudia una nueva topología de circuito para estructuras asimétricas. La configuración del circuito separa los modos par e impar como lo hace la red de celosía para las estructuras simétricas. Finalmente, las publicaciones derivadas de esta tesis se enumeran en el Anexo C.

D.2 El modo slot de la guíaonda rectangular

La presencia de una ranura longitudinal en una guía rectangular clásica permite la propagación del modo slot. La distribución del campo eléctrico de este modo se muestra en la Fig. 2.1. Se puede observar que esta distribución de campo se parece mucho a la del modo TEM de una slotline ordinaria. Sin embargo, el modo slot de la guía rectangular tiene frecuencia de corte, ya que solo hay un conductor en la estructura. Esta frecuencia de corte, f_c, sin embargo, depende en gran medida del ancho de la ranura y las dimensiones de la sección transversal de la guía y, hasta donde llega el conocimiento de los autores, su expresión analítica aún no se ha obtenido en la literatura.

El modo slot de una guía rectangular tiene una naturaleza de tipo transversal eléctrico [16]. Además, incluso en presencia de conductor eléctrico perfecto y dieléctricos sin pérdidas solamente, existen pérdidas debido a la radiación de la estructura. Por estas razones, para modelar el comportamiento en frecuencia de su constante de propagación e impedancia, se considerará un modo TE con pérdidas. Estos, como se muestra en [17], están dados por

$$\gamma_{CBS} = j\frac{2\pi f\sqrt{\varepsilon_r' - j\varepsilon_r''}}{c}\sqrt{1-\left(\frac{f_c}{f}\right)^2\frac{\varepsilon_r'}{\varepsilon_r' - j\varepsilon_r''}} \tag{D.1}$$

$$Z_0 = \frac{Z_m}{\sqrt{\varepsilon_r' - j\varepsilon_r''}\sqrt{1-\left(\frac{f_c}{f}\right)^2\frac{\varepsilon_r'}{\varepsilon_r' - j\varepsilon_r''}}}, \tag{D.2}$$

donde c es la velocidad de la luz en el vacío, y la permitividad eléctrica del medio, ε_r, se divide en sus partes real e imaginaria de la siguiente manera:

$$\varepsilon_r = \varepsilon_r' - j\varepsilon_r''. \tag{D.3}$$

El valor de la impedancia Z_m depende de la impedancia del espacio libre, la geometría de la sección de la estructura, la ε_r del material dentro de la cavidad y la definición de voltaje. Por lo tanto, todos estos parámetros solo dependerán de las dimensiones de la sección transversal de la estructura mostrada en la Fig. 2.1 y del medio dentro de la cavidad. Si bien estas expresiones solo son válidas para estructuras cerradas, muestran una gran concordancia con los resultados obtenidos.

Para caracterizar el modo, se ha simulado una guía de ondas rectangular ranurada utilizando el software comercial HFSS. Los puertos de onda dan problemas en este tipo de estructuras, así que se han elegido puertos concentrados. A partir de los parámetros S del segmento simulado, los parámetros imagen se pueden obtener usando, como se muestra en [19],

$$\gamma_{im} = \cosh^{-1}\left(\frac{1 - S_{11}^2 + S_{21}^2}{2S_{21}}\right) \tag{D.4}$$

$$Z_{im} = Z_{0,ref}\sqrt{\frac{(1+S_{11})^2 - S_{21}^2}{(1-S_{11})^2 - S_{21}^2}}, \tag{D.5}$$

donde $Z_{0,ref}$ es la impedancia de referencia utilizada para obtener los parámetros-S. Luego, a partir de la definición de los parámetros de la imagen, la impedancia del modo, Z_0, es igual a Z_{im}, y la constante de propagación, γ, es γ_{im}/l, donde l es la longitud del segmento de guía simulado. La Fig. 2.4 y la Fig. 2.5 muestran, respectivamente, las γ y Z_0 obtenidas para tres longitudes de guía de ondas diferentes, 40, 80 y 120 mm. Se puede ver que si la línea es muy larga aparecen muchas resonancias, mientras que las líneas cortas no dan resultados precisos.

Como los resultados no eran satisfactorios, se propone un nuevo método de medida de la constante de propagacación del modo slot basado en [6]. Consiste en la medida del coeficiente de reflexión a la entrada de cuatro guías idénticas e igualmente terminadas de diferentes longitudes. Usando la invariancia de la relación cruzada de números complejos bajo una transformación bilineal, es posible extraer la constante de propagación, γ. La relación cruzada Γ_{1234} se puede definir utilizando los cuatro coeficientes de reflexión medidos, Γ_1, Γ_2, Γ_3 y Γ_4 como:

$$\Gamma_{1234} = \frac{(\Gamma_1 - \Gamma_2)(\Gamma_3 - \Gamma_4)}{(\Gamma_1 - \Gamma_3)(\Gamma_2 - \Gamma_4)} \tag{D.6}$$

y, entonces, se puede escribir:

$$\Gamma_{1234} = \frac{\left(1 - e^{-2\gamma\delta_{21}}\right)\left(e^{-2\gamma\delta_{31}} - e^{-2\gamma\delta_{41}}\right)}{\left(1 - e^{-2\gamma\delta_{31}}\right)\left(e^{-2\gamma\delta_{21}} - e^{-2\gamma\delta_{41}}\right)} \tag{D.7}$$

donde δ_{ij} es la diferencia entre las longitudes de las guías i y j. Resolviendo (D.7) en cada punto en frecuencia, es posible obtener el valor de γ en un ancho de banda amplio. Con una mejora estadística propuesta, es posible aumentar la precisión del método usando un mayor número de líneas terminadas. Para medir únicamente la constante de propagación del modo slot, se toman las medidas de dos puertos y se le aplica el método al coeficiente de reflexión del modo impar. Este método es insensible a la terminación utilizada, la impedancia característica de la guía de ondas y la red de alimentación.

Para no tener que fabricar numerosas guías, se propone una estructura capaz de tener diferentes longitudes para la ranura. Su modelo 3D se muestra en la Fig. 2.6, y su fabricación en la Fig. 2.7. Fig. 2.9 muestra la constante de propagación del modo slot desde su frecuencia de corte hasta 10 GHz, comparados con la constante de propagación de (D.1). La concordancia entre simulaciones y medidas es excelente para la constante de fase y muy buena para la constante de atenuación hasta 5 GHz. La concordancia entre el modelo, la simulación y las mediciones indican que la dependencia de la frecuencia de los resultados extraídos es la esperada. Además, el valor de la constante dieléctrica efectiva del modelo tiene el valor esperado para un modo de ranura cuasi-TEM. Se realiza, además, un caso adicional con la guía rellena de teflón. La Fig. 2.10 muestra la constante de propagación del modo después de aplicar la misma técnica a los resultados medidos y simulados, comparada nuevamente con el modelo. De nuevo, a pesar de que la determinación de las pérdidas es difícil, la constante de propagación se comporta como se esperaba con la frecuencia.

D.3 El elemento radiante de ranura sobre cavidad alimentado por strip

El problema de encontrar un circuito equivalente para el CBS alimentado por líneas de banda se aborda modelando tres partes diferentes de la estructura en orden. La primera es la caracterización del modo que se propaga a lo largo de un segmento de la línea CBS, la segunda consiste en agregar a la línea de transmisión propuesta el conocido efecto final de la ranura y la tercera parte agrega el efecto de alimentar la

ranura por una línea de franjas. Una vez que se agregan los tres efectos al circuito equivalente, se aplica a las mediciones.

La sección de la línea CBS, que se muestra en la Fig. 3.1, corresponde con la sección de una guía de ondas ranurada y, entonces, el modo que se propaga a lo largo de esta estructura es el modo slot estudiado en el Capítulo 2. Por lo tanto, el circuito equivalente propuesto de la sección de la ranura es una línea de transmisión cuya constante de propagación, γ_{CBS}, y la impedancia característica, Z_0, están definidas, respectivamente, por (D.1) y (D.2). Los parámetros de esas ecuaciones solo dependerán de las dimensiones de la sección transversal de la estructura y del medio dentro de la cavidad. Simulando un segmento de línea CBS, es posible encontrar los valores de los parámetros de la línea de transmisión. La frecuencia de corte, f_c, se define como la frecuencia cuando $\alpha(f_c) = \beta(f_c)$, donde α es la constante de atenuación y β la constante de fase [17] y, entonces, se puede extraer directamente de los resultados simulados. La ε_r' se puede ajustar para que tanto la β obtenida de la simulación como el circuito equivalente tengan el mismo comportamiento asintótico para frecuencias más altas. El valor de ε_r'' puede elegirse como dependiente de la frecuencia o constante, dependiendo de su idoneidad para modelar el fenómeno de pérdidas. Como también se muestra en la Fig. 3.2, la concordancia entre la simulación y el circuito equivalente es muy buena cerca de la frecuencia de corte y por debajo. Como era de esperar, las inexactitudes de las γ_{CBS} y Z_{im} simuladas alrededor de las frecuencias de resonancia de la línea dificultan la verificación del modelo con la simulación en esas frecuencias. Sin embargo, se puede ver que el comportamiento asintótico es similar.

La discontinuidad en el extremo corto de una ranura se modela con un inductor y una resistencia dependiente de la frecuencia conectados en serie. El efecto inductivo hace que la línea de ranura parezca eléctricamente más larga de lo que realmente es, mientras que la resistencia representa el efecto de la radiación en la discontinuidad. La strip de alimentación está debajo de la ranura, a una cierta distancia del fondo de la cavidad, d, y alimenta la ranura atravesando su centro. La Fig. 3.3 muestra la geometría de esta estructura. La transición entre la línea de alimentación y la ranura ha sido tradicionalmente modelada por un transformador ideal, donde la relación de transformación, n, representa la cantidad de acoplamiento entre los campos de la strip y la ranura. Cuando la distancia entre la ranura y la strip, $h-d$, es pequeña, ambos están fuertemente acoplados y n es mayor. A medida que aumenta la distancia entre ellos, se reduce el valor de n. Sin embargo, la frecuencia de resonancia de la ranura también cambia. Este efecto se modela utilizando una capacidad, C, colocada en paralelo con el

resto del circuito y su valor es mayor a medida que aumenta la distancia entre la strip y la ranura. La Fig. 3.5 muestra el circuito equivalente propuesto para la estructura completa. Los valores de n, C, R_{end} y L_{end} pueden hallarse a partir de la simulación usando mínimos cuadrados.

Para verificar el circuito equivalente propuesto también con resultados experimentales, se ha aplicado a un caso diferente con un prototipo disponible, que se muestra en la Fig. 3.8. La Fig. 3.9 muestra los valores de la impedancia de la estructura CBS a partir de los resultados de las medidas y utilizando el circuito equivalente propuesto. Los parámetros del circuito equivalente son: $f_c = 2.418$ GHz, $\varepsilon'_r = 1.75$, $tan\delta = 0.004$, $Z_m = 132\ \Omega$, $R_{end} = 4.3\ \Omega$, $L_{end} = 0$, $n = 0.86$ y $C = 0$. Se puede observar que la concordancia con el circuito equivalente es excelente hasta 6.5 GHz.

D.4 Ranura sobre cavidad de banda ancha alimentada por una strip

En este capítulo se estudia un nuevo elemento radiante CBS compacto alimentado por strip. De manera similar a [1], se introduce un stub complementario debajo de la ranura para mejorar el ancho de banda de impedancia considerablemente. La configuración de transmisión de dos puertos también se adopta aquí y la cavidad se implementa utilizando tecnología SIW. Este elemento radiante puede verse como una transformación del *strip-slot complementario* para obtener radiación unidireccional. Esto se logra reemplazando la línea microstrip por una estructura cerrada (stripline o microstrip cerrada), evitando que la estructura radie hacia un semiespacio. Estas modificaciones en la geometría conllevan varios desafíos: el CBS se comporta de manera diferente al de una ranura convencional y el plano de masa adicional dificulta la obtención de la adaptación de impedancia. Gracias al circuito equivalente del CBS obtenido en el Capítulo 2, es posible entender cómo diseñar la cavidad para aliviar estos problemas y además obtener un circuito equivalente basado en la red en celosía. Este circuito se muestra en la Fig. 4.3, donde el valor de sus impedancias se corresponden aproximadamente con las de modelos en línea de transmisión del stub y la ranura por separado, como se muestra en la Fig. 4.4. La metodología de diseño es sencilla. Primero, deben elegirse el tamaño de la cavidad y la anchura de la ranura para obtener una frecuencia de corte del modo slot bajo, que permita su propagación, mientras que la frecuencia de resonancia del modo TE_{101} debe ser alta y estar fuera de la banda de funcionamiento del elemento. Después, deben diseñarse las longitudes de la ranura y el stub para que sus resonancias

coincidan en frecuencia y así se anulen. Por último, hay que jugar con la anchura del stub y la distancia entre la ranura y la línea de alimentanción para conseguir el nivel de impedancia deseado.

Se han construido dos prototipos en distintos tecnologías para verificar el concepto. El primer prototipo se implementa utilizando una configuración de stripline suspendida (Fig. 4.6). Para mitigar las deficiencias de esta primera configuración, posteriormente se propuso el uso de una microstrip cerrada (Fig. 4.12). Los resultados muestran que, efectivamente, esta estructura consigue un ancho de banda considerable (las Figs. 4.7 y 4.13 muestran los parámetros S de cada prototipo). Además, se verifica que el circuito equivalente propuesto permite modelar la estructura de forma apropiada. Asimismo, se corrobora que el diagrama de radiación del elemento es unidireccional (Figs. 4.11 y 4.16).

La forma de ampliar el ancho de banda del CBS propuesto se compara con una más tradicional, que consiste en descentrar la posición de la strip de alimentación respecto a la ranura, como se muestra en Fig. 4.18(a). En las Figs. 4.21 y 4.12, se proporcionan los resultados de la simulación de ambas formas para adaptar la misma ranura. Se puede observar que, usando la técnica de descentrar la alimentación, cuanto mayor es el ancho de banda, más se reduce la potencia radiada por el elemento. Por esto, la adaptación mediante el stub se puede usar en un ancho de banda más amplio de manera efectiva, pero, en este caso, una stripline asimétrica o una microstrip cerrada son la única opción para alimentar el CBS.

Una forma de aumentar el ancho de banda del elemento es aumentar la frecuencia de resonancia de la cavidad. Sin embargo, el comportamiento de la ranura se ve fuertemente afectado por las dimensiones de la cavidad, y al reducirlas, también aumentará considerablemente la frecuencia a la que la ranura comienza a radiar. En lugar de reducir el ancho de la cavidad para aumentar la frecuencia de resonancia del modo TE_{101}, que también aumenta la frecuencia de corte del modo slot, el enfoque seguido consiste en reducir la longitud de la cavidad, ya que también aumenta la frecuencia de resonancia, como se muestra en (4.1). La longitud mínima de la cavidad, sin embargo, está limitada por la longitud de la ranura y, por tanto, se utilizan dos técnicas diferentes para reducir su tamaño longitudinal. La primera consiste en utilizar una ranura con forma de doble T, como se muestra en la Fig. 4.23. En la Fig. 4.26 se puede ver cómo la ranura empieza a radiar a frecuencias más bajas utilizando esta configuración, mientras que tanto sus parámetros S como diagrama de radiación no han sido modificados apreciablemente (Figs. 4.24 y 4.27). La segunda, en usar una

ranura bow-tie, se muestra en la Fig. 4.28 y se verifica con un diseño a frecuencias de milimétricas. Fig. 4.30 muestra los resultados de la simulación de los parámetros S, Fig. 4.31 la relación de potencia radiada respecto a la potencia introducida y Fig. 4.32 su diagrama de radiación. Con este diseño, se ilustra que modificando la forma de la ranura se puede conseguir no solo un ancho de banda más amplio sino también un nivel de potencia radiada más estable. Además, esta es la primera vez que se propone este elemento en frecuencias de ondas milimétricas, con resultados prometedores.

D.5 Arrays lineales basados en el CBS de banda ancha

Dada la alimentación en serie del CBS de banda ancha diseñado en el capítulo anterior, es inmediato construir arrays cargando la strip de alimentación con varios elementos. Se proponen dos arquitecturas de array distintas, un array de onda progresiva con todos los elementos idénticos, como se muestra en la Fig. 5.1, y un array log-periódico, Fig. 5.15. Para fabricar estos arrays, se han tenido que usar cavidades más estrechas, que permitan diseñar con libertad la distancia entre elementos. Para que esto no impida el correcto funcionamiento del elemento, se hacen las cavidades más altas. Además, en lugar de usar tornillos como hasta ahora para las paredes mecánicas laterales, se emplea una pieza de aluminio fresada, cubierta con el sustrato con la ranura y la línea de alimentación impresas. En el caso del array de onda progresiva, además, se rellena la cavidad de un material impreso en 3D.

De acuerdo a la teoría de armónicos espaciales, el array de onda progresiva es capaz de hacer un escaneo en frecuencia desde atrás hacia adelante en dos bandas distintas. Los resultados corroboran esta predición (Fig. 5.12), aunque también ponen de manifiesto una desadaptación en las frecuencias en las que la estructura radia en dirección broadside. Este fenómeno se conoce como *open-stopband* y es un problema clásico en este tipo de estructuras. No obstante, se emplea el elemento ligeramente desalineado entre la strip y la ranura para mejorar el funcionamiento en broadside. En la Fig. 5.8 se presenta la comparación del coeficiente de reflexión simulado del array con 10 elementos alineados perfectamente y ligeramente desalineados, donde se observa que, con la versión desalineada, las desadaptaciones en broadside desaparecen. Por tanto, se consigue un array capaz de hacer escaneo del haz en frecuencia desde atrás hacia adelante, pasando por broadside.

Los arrays log-periódicos son antenas de banda ancha construidas a partir de elementos resonantes que siguen una progresión geométrica logarítmico-periódica (ver esquema en la Fig. 5.14). A pesar de que estos arrays suelen ser fabricados con elementos resonantes, un elemento de banda ancha como el aquí propuesto es propio para construir este tipo de arrays de forma sencilla, por lo que su uso en estas antenas resulta de interés. Se ha seguido la metodología de diseño del strip-slot complementario para elementos no resonantes. Puesto que, además de estar adaptado en todo el ancho de banda, la eficiencia de radiación del elemento no es resonante, sino paso alto, el factor de escala entre elementos adyacentes puede ser más bajo que en los arrays clásicos. Esto implica que se puede cubrir el mismo ancho de banda con menos elementos. Además, la adaptación del array en banda ancha está asegurada, puesto que todos los elementos están adaptados en todo el ancho de banda de diseño. Esto no ocurre en los arrays clásicos, en los cuales es necesario introducir un desfasaje adicional de 180° entre elementos, para conseguir la cancelación de las reflexiones provenientes de los elementos que no están próximos a su frecuencia de resonancia y, por tanto, no están adaptados. Además, se propone como novedad alternar la dirección de los stubs para reducir el acomplamiento entre elementos adyacentes.

Para verificar las conclusiones extraídas anteriormente, se ha realizado un diseño con 15 elementos y un factor de escala de 0.95. Las ranuras y cavidades siguen la progresión log-periódica mientras que las strips están diseñadas individualmente para que cada elemento esté adaptado en banda ancha. El prototipo resultante se muestra en la Fig. 5.16. En la Fig. 5.17 se representa el coeficiente de reflexión medido y simulado. Se observa que el array presenta una muy buena adaptación en el ancho de banda de diseño. La Fig. 5.18 muestra los diagramas de radiación a distintas frecuencias. Se observa que el array mantiene razonablemente el apuntamiento del único haz en el ancho de banda de diseño, hacia atrás pero con un ángulo entorno a los $-50°$.

D.6 Conclusiones y líneas futuras

En esta tesis doctoral se ha estudiado una estructura radiante de banda ancha basada en el CBS. Consiste en una guíaonda rectangular con una ranura longitudinal en su parte superior y cortocircuitada en sus extremos. La ranura es alimentada por una strip transversal y, por lo tanto, es especialmente adecuada para construir arrays alimentados en serie.

Para comprender completamente el mecanismo de radiación del CBS y poder desar-

rollar un circuito equivalente de línea de transmisión, se ha estudiado y caracterizado el modo slot de una guíaonda rectangular. Utilizando un simulador electromagnético comercial, se ha obtenido la impedancia característica del modo y su constante de propagación en una frecuencia muy amplia, aunque sea aproximadamente. Además, se ha propuesto un método muy robusto y preciso para obtener la constante de propagación del modo slot. El método consiste en simular o medir ranuras de diferentes longitudes para obtener resultados en banda súper ancha. Se ha propuesto, fabricado y medido una estructura específica para aplicar el método a este modo.

También se ha propuesto un circuito equivalente completo pero simple para un CBS alimentado por strip. El componente principal del circuito equivalente es una línea de transmisión con constante de propagación e impedancia característica las del modo slot de la guía. La precisión del circuito equivalente se verificó con éxito mediante simulación y medida.

Después, se estudió un método de mejora del ancho de banda para el CBS. El método es una aplicación directa del 'strip-slot complementario' a esta estructura. Se ha proporcionado un estudio teórico de la estructura que separa los modos par e impar y un circuito equivalente de sencillo basado en la red en celosía. Sin embargo, la resonancia de la cavidad puede impedir que el elemento radiante funcione en algunas frecuencias y debe tenerse muy en cuenta. Se han fabricado y medido dos prototipos en distintas configuraciones de fabricación. La principal ventaja sobre el 'strip-slot complementario' es que su diagrama de radiación es unidireccional. Se han simulado otros dos diseños para encontrar modificaciones que aumenten el ancho de banda del elemento radiante. Uno de ellos, la ranura en 'bow-tie', fue diseñado para la banda de milimétricas con resultados prometedores para construir arrays a 60 GHz o más.

Finalmente, se ha utilizado el elemento radiante en dos arquitecturas de arrays. El primero ha sido un array lineal de onda progresiva construido cargando la strip con varios CBS de banda ancha iguales. Se ha logrado un escaneo en frecuencia del único haz desde atrás hacia adelante. La medición de un prototipo verificó lo que predecía la teoría de diseño de arrays de onda progresiva. La segunda arquitectura que se ha utilizado es el array log-periódico. Los tamaños de las ranuras y cavidades siguen una progresión logarítmica, mientras que los stubs se diseñaron para optimizar la adaptación de impedancia. El acoplamiento mutuo se redujo alternando la dirección de los stubs. Este sencillo diseño ha obtenido un coeficiente de reflexión muy bajo (menos de -12 dB) en un ancho de banda amplio (más del 60 % de ancho de banda porcentual). La dirección del único haz ha sido de unos 50^{o} hacia atrás. Los resultados

fueron nuevamente verificados mediante medidas.

D.6.1 Contribuciones originales

La principal contribución de esta tesis es el uso de un stub de adaptación para diseñar CBS de banda ancha alimentados por strip, el análisis teórico para explicar su funcionamiento y metodología de diseño. Estos se lograron a partir de un circuito equivalente en red en celosía, que es otra contribución significativa que, además, explica el comportamiento del elemento radiante.

También es destacable el trabajo relacionado con la medida de las constantes de propagación. La aplicación de un método sólido y establecido para extraer las constantes de propagación a los modos par e impar por separado ha permitido proponer una forma de medir las constantes de propagación de los modos de líneas acopladas. Aplicar esto a un tema muy relacionado con este trabajo ha permitido obtener un método novedoso para extraer la constante de propagación del modo slot en una guíaonda rectangular.

Otra contribución significativa de esta tesis es un punto de vista diferente en el análisis de un CBS alimentado por strip. Considerar el modo slot de una guía rectangular como el modo de propagación en la estructura no se había encontrado antes en la literatura. Ver la ranura como una línea de transmisión de este modo terminado en cortocircuito permitió comprender el elemento radiante de una manera simple pero efectiva. Basándose en eso, también se propuso un circuito equivalente novedoso.

En cuanto a las aplicaciones de array del CBS de banda ancha propuesto, aunque las topologías son clásicas y ya se usaban con el 'strip-slot complementario', la presencia de la cavidad limitaba la distancia mínima entre elementos, y se han tenido que considerar formas de reducir su tamaño. Además, para el diseño de array de onda progresiva, se utilizó un relleno hecho mediante impresión 3D, demostrando que podría ser una idea interesante para, por ejemplo, reducir el tamaño de cavidades de antenas o aumentar su robustez de una forma muy flexible. Una contribución significativa del diseño de la matriz logarítmica periódica es la forma de reducir el acoplamiento mutuo. Se ha descubierto que el acoplamiento mutuo ha sido causado principalmente por los stubs y, por tanto, alternar su dirección ha mejorado significativamente el coeficiente de reflexión de la antena.

D.6.2 Trabajo futuro

Para continuar con este trabajo de investigación, se proponen las siguientes líneas de trabajo:

- **Caracterización de la impedancia del modo slot**

  Aunque se propuso un método muy preciso para obtener la constante de propagación del modo slot, la forma de obtener su impedancia sigue siendo muy inexacta a algunas frecuencias. Puede ser interesante para aumentar la precisión del circuito equivalente el encontrar otra forma de obtener esta impedancia de forma precisa en un ancho de banda amplio.

- **Incluir todas las dimensiones de la estructura en el circuito equivalente**

  Para encontrar el circuito equivalente del CBS, una sección de guía ranurada debe ser simulada previamente. Por tanto, el circuito equivalente debe realizarse a posteriori, y los valores de todos sus parámetros no se pueden predecir a partir de las dimensiones de la estructura. Evidentemente, esto no es lo ideal. Se podría trabajar en el futuro para encontrar cómo cambian los parámetros con las dimensiones de la cavidad, el ancho de la ranura y el relleno dieléctrico. Sería especialmente interesante descubrir cómo cambian las pérdidas de radiación, ya que son esenciales en el diseño de arrays.

- **Implementar el elemento radiante mediante otras tecnologías de sistemas de transmisión**

  El strip-slot complementario ha sido aplicado en este trabajo a estructuras cerradas como la stripline o la microstrip cerrada para obtener radiación unidireccional. Sin embargo, podría ser interesante aplicar el mismo concepto a otros sistemas de transmisión cerrados como la guía rectangular o la guía ridge gap.

- **Reducir el tamaño de la cavidad**

  Algunas limitaciones de los arrays diseñados se debieron al tamaño de la cavidad. La solución adoptada aquí fue hacer la cavidad más alta, lo que empeora el perfil plano de la antena. Se podrían emplear técnicas de reducción a la cavidad para facilitar el diseño o la implementación del array. El aumento de la permitividad eléctrica podría ser una opción, pero se debe explorar cómo esto puede cambiar las propiedades de radiación de la ranura.

- **Implementación de otras topologías de array**

  En este trabajo se han analizado dos conceptos de array. Sin embargo, el elemento radiante propuesto se puede utilizar en otras topologías. En principio, cualquier configuración de array alimentado en serie puede construirse utilizando el CBS propuesto. Además, la simulación de la ranura tipo bow-tie ha mostrado resultados prometedores en la banda de milimétricas y, por lo tanto, un array para la banda de 60 GHz sería muy interesante y podría tener un gran impacto en el estado del arte de antenas.

Bibliography

[1] E. Abdo-Sánchez, J. Page, T. Martín-Guerrero, J. Esteban, and C. Camacho-Peñalosa, "Planar broadband slot radiating element based on microstrip-slot coupling for series-fed arrays," *IEEE Transactions on Antennas and Propagation*, vol. 60, no. 2, pp. 6037–6042, Dec. 2012.

[2] E. Abdo-Sánchez, T. M. Martín-Guerrero, J. Esteban, and C. Camacho-Peñalosa, "Short dual-band planar leaky-wave antenna with broadside effect mitigation," *IET Microwaves, Antennas and Propagation*, vol. 10, no. 5, pp. 574–578, May 2016.

[3] E. Abdo-Sánchez, J. Esteban, T. Martín-Guerrero, and C. Camacho-Peñalosa, "A novel planar log-periodic array based on the wideband complementary strip-slot element," *IEEE Transactions on Antennas and Propagation*, vol. 62, no. 11, pp. 5572–5580, Nov. 2014.

[4] J. Galejs, "Admittance of a rectangular slot which is backed by a rectangular cavity," *IEEE Transactions on Antennas and Propagation*, vol. 11, no. 2, pp. 119–126, Mar. 1963.

[5] Z. Chen, H. Liu, J. Yu, and X. Chen, "High gain, broadband and dual-polarized substrate integrated waveguide cavity-backed slot antenna array for 60 ghz band," *IEEE Access*, vol. 6, pp. 31 012–31 022, 2018.

[6] B. Bianco and M. Parodi, "Measurement of the effective relative permittivities of microstrip," *Electronics Letters*, vol. 11, no. 3, pp. 71–72, Feb. 1975.

[7] P. Liu, Y. Li, Z. Zhang, S. Wang, and Z. Feng, "A fixed-beam leaky-wave cavity-backed slot antenna manufactured by bulk silicon mems technology," *IEEE Transactions on Antennas and Propagation*, vol. 65, no. 9, pp. 4399–4405, Sep. 2017.

[8] J. W. Holloway, L. Boglione, T. M. Hancock, and R. Han, "A fully integrated broadband sub-mmwave chip-to-chip interconnect," *IEEE Transactions on Microwave Theory and Techniques*, vol. 65, no. 7, pp. 2373–2386, Jul. 2017.

[9] Y. J. Cheng, W. Hong, K. Wu, and Y. Fan, "Millimeter-wave substrate integrated waveguide long slot leaky-wave antennas and two-dimensional multibeam applications," *IEEE Transactions on Antennas and Propagation*, vol. 59, no. 1, pp. 40–47, Jan. 2011.

[10] J. A. G. Malherbe and J. Joubert, "Radiation properties of a long slot in the broad wall of a waveguide," *Electronics Letters*, vol. 34, no. 6, pp. 568–570, Mar. 1998.

[11] J. Zehentner, J. Mrkvica, and J. Machac, "Flat waveguide with a longitudinal slot," in *Proceedings IEEE MTT-S International Microwave Symposium Digest*, Jun. 2005.

[12] J. Liu and Y. Long, "A full-wave numerical approach for analyzing rectangular waveguides with periodic slots," *IEEE Transactions on Antennas and Propagation*, vol. 60, no. 8, pp. 3754–3762, Aug. 2012.

[13] J. Joubert and J. A. G. Malherbe, "Moment method calculation of the propagation constant for leaky-wave modes in slotted rectangular waveguide," in *IEE Proceedings - Microwaves, Antennas and Propagation*, vol. 146, no. 6, 1999, pp. 411–415.

[14] P. J. B. Clarricoats, P. E. Green, , and A. A. Oliner, "Slot-mode propagation in rectangular waveguide," *Electronics Letters*, vol. 2, no. 8, pp. 307–308, Aug. 1966.

[15] A. Sutinjo, M. Okoniewski, and R. H. Johnston, "Suppression of the slot-mode radiation in a slitted waveguide using periodic slot perturbations," *IEEE Antennas and Wireless Propagation Letters*, vol. 8, pp. 550–553, 2009.

[16] R. Garg, I. Bahl, and M. Bozzi, *Microstrip Lines and Slotlines*, 3rd ed., ser. Microwave & RF. Artech House, 2013.

[17] J. E. Page, *Propagación de ondas guiadas*, 4th ed. ETSIT UPM, 1983.

[18] P. A. Rizzi, *Microwave engineering passive circuits*. Prentice-Hall, Inc., 1988.

[19] G. Matthaei, L. Young, and E. M. T. Jones, *Microwave filters, impedance-matching networks, and coupling structures.* McGraw-Hill, 1964.

[20] B. Bianco and M. Parodi, "Determination of the propagation constant of uniform microstrip lines," *Alta Frequenza*, vol. 45, pp. 107–110, Feb. 1976.

[21] Y. Yoshimura, "A microstrip slot antenna," *IEEE Transactions on Microwave Theory and Techniques*, vol. 20, no. 11, pp. 760–762, Nov. 1972.

[22] D. M. Pozar, "A reciprocity method of analysis for printed slot and slot-coupled microstrip antennas," *IEEE Transactions on Antennas and Propagation*, vol. 34, no. 12, pp. 1439–1446, Dec. 1986.

[23] A. Axelrod, M. Kisliuk, and J. Maoz, "Broadband microstrip-fed slot radiator," *Microwave Journal*, pp. 81–94, Jun. 1989.

[24] A. K. Bhattacharyya, Y. M. M. Antar, and A. Ittipiboon, "Full wave analysis for the equivalent circuit of an inclined slot on a microstrip ground plane," in *IEE Proceedings-H Microwave, Antennas and Propagation*, vol. 139, Jun. 1992, pp. 245–250.

[25] M. Himdi and J. Daniel, "Analysis of printed linear slot antenna using lossy transmission line model," *Electronics Letters*, vol. 28, no. 6, pp. 598–601, 1992.

[26] H. G. Akhavan and D. Mirshekar-Syahkal, "Approximate model for microstrip fed slot antennas," *Electronics Letters*, vol. 30, no. 23, pp. 1902–1903, 1994.

[27] J. P. Kim and W. S. Park, "Network modeling of an inclined and off-center microstrip-fed slot antenna," *IEEE Transactions on Antennas and Propagation*, vol. 46, no. 8, pp. 1182–1188, Aug. 1998.

[28] J. E. Ruyle and J. Bernhard, "A wideband transmission line model for a slot antenna," *IEEE Transactions on Antennas and Propagation*, vol. 61, no. 3, pp. 1407–1410, Mar. 2013.

[29] R. M. van Schelven, D. Cavallo, and A. Neto, "Equivalent circuit models of finite slot antennas," *IEEE Transactions on Antennas and Propagation*, vol. 67, no. 7, pp. 4367–4376, Jul. 2019.

[30] W. Li, K. D. Xu, X. Tang, Y. Yang, Y. Liu, and Q. Liu, "Substrate integrated waveguide cavity-backed slot array antenna using high-order radiation modes

for dual-band applications in K-band," *IEEE Transactions on Antennas and Propagation*, vol. 65, no. 9, pp. 4556–4565, Sep. 2017.

[31] Q. Wu, J. Yin, C. Yu, H. Wang, and W. Hong, "Broadband planar SIW cavity-backed slot antennas aided by unbalanced shorting vias," *IEEE Antennas and Wireless Propagation Letters*, vol. 18, no. 2, pp. 363–367, Feb. 2019.

[32] S. A. Long, "A mathematical model for the impedance of the cavity-backed slot antenna," *IEEE Transactions on Antennas and Propagation*, vol. 25, no. 6, pp. 829–833, Nov. 1977.

[33] A. Hadidi and M. Hamid, "Aperture field and circuit parameters of cavity-backed slot radiator," in *IEE Proceedings-H Microwave, Antennas and Propagation*, vol. 136, no. 2, Apr. 1989, pp. 139–146.

[34] H. Dashti and M. H. Neshati, "Input impedance of rectangular substrate integrated waveguide (SIW) cavity backed slot antennas," in *Proceedings 25th Iranian Conference on Electrical Engineering*, May 2017.

[35] R. O. E. Lagerlöf, "Stripline fed slots," in *Proc. 2nd European Microwave Conference*, Aug. 1971.

[36] D. J. Sommers, "Slot array employing photoetched tri-plate transmission lines," *IEEE Transactions on Microwave Theory and Techniques*, vol. 3, pp. 157–162, Mar. 1955.

[37] A. G. Roederer, "A log-periodic cavity-backed slot array," *IEEE Transactions on Antennas and Propagation*, vol. 16, no. 6, pp. 756–758, Nov. 1968.

[38] R. S. Robertson and R. S. Elliott, "The design of transverse slot arrays fed by the meandering strip of a boxed stripline," *IEEE Transactions on Antennas and Propagation*, vol. 35, no. 3, pp. 252–257, Mar. 1987.

[39] Q. Li and Z. Shen, "Inverted microstrip-fed cavity-backed slot antennas," *IEEE Antennas and Wireless Propagation Letters*, vol. 1, pp. 98–101, 2002.

[40] M. Imbert, J. Romeu, M. Baquero-Escudero, M. T. Martinez-Ingles, J. M. Molina-Garcia-Pardo, and L. Jofre, "Assessment of LTCC-based dielectric flat lens antennas and switched-beam arrays for future 5G millimeter-wave communication systems," *IEEE Transactions on Antennas and Propagation*, vol. 65, no. 12, pp. 6453–6473, Dec. 2017.

[41] A. Hernández-Escobar, E. Abdo-Sánchez, and C. Camacho-Peñalosa, "A broadband cavity-backed slot radiating element in transmission configuration," *IEEE Transactions on Antennas and Propagation*, vol. 66, no. 12, pp. 7389–7394, Dec. 2018.

[42] S. Hashemi-Yeganeh and C. Birtcher, "Theoretical and experimental studies of cavity-backed slot antenna excited by a narrow strip," *IEEE Transactions on Antennas and Propagation*, vol. 41, no. 2, pp. 236–241, Feb. 1993.

[43] J. Hirokawa, H. Arai, and N. Goto, "Cavity-backed wide slot antenna," in *IEE Proceedings-H Microwave, Antennas and Propagation*, vol. 136, no. 1, Feb. 1989, pp. 29–33.

[44] N. L. VandenBerg, L. P. B. Katehi, J. A. Lick, and G. T. Mooney, "Characterization of strip-fed cavity-backed slots," *IEEE Transactions on Antennas and Propagation*, vol. 40, no. 4, pp. 405–413, Apr. 1992.

[45] D. Shahani and B.Bhat, "Network model for strip-fed cavity-backed printed slot antenna," *Electronics Letters*, vol. 14, no. 24, pp. 767–769, 1978.

[46] K. Sato, M. Komeya, and H. Shimasaki, "Studies on the equivalent circuit of the excitation to a cavity-backed slot antenna," in *Proceedings Asia-Pacific Microwave Conference*, Nov. 2013.

[47] K. Yoshimatsu, L. Sato, T. Kubo, and H. Shimasaki, "Equivalent circuit of the excitation to a slot antenna and the matching to a complex impedance," in *Proceedings Asia-Pacific Microwave Conference*, Nov. 2013.

[48] H. Yang and N. G. Alexopoulos, "A dynamic model for microstrip-slotline transition and related structures," *IEEE Transactions on Microwave Theory and Techniques*, vol. 36, no. 2, pp. 286–293, Feb. 1988.

[49] A. Hernández-Escobar, E. Abdo-Sánchez, and C. Camacho-Peñalosa, "Novel implementation for a broadband cavity-backed slot fed in transmission configuration," in *Proceedings 12th European Conference of Antennas and Propagation*, vol. 36, no. 2, Apr. 2018, pp. 286–293.

[50] D. M. Pozar, "Reciprocity method of analysis for printed slot and slot-coupled microstrip antennas," *IEEE Transactions on Antennas and Propagation*, vol. 34, pp. 1439–1446, Dec. 1986.

[51] J. Galejs, "Admittance of rectangular slot which is backed by a rectangular cavity," *IEEE Transactions on Antennas and Propagation*, vol. 11, no. 2, pp. 119–126, Mar. 1963.

[52] S. A. Long, "Experimental study of the impedance of cavity-backed slot antennas," *IEEE Transactions on Antennas and Propagation*, vol. 23, no. 1, pp. 1–7, Jan. 1975.

[53] G. Q. Luo, Z. F. Hu, L. X. Dong, and L. L. Sun, "Planar slot antenna backed by substrate integrated waveguide cavity," *IEEE Antennas and Wireless Propagation Letters*, vol. 7, pp. 235–239, 2008.

[54] L. Ge, Y. Li, J. Wang, and C. Sim, "A low-profile reconfigurable cavity-backed slot antenna with frequency, polarization, and radiation pattern agility," *IEEE Transactions on Antennas and Propagation*, vol. 65, no. 5, pp. 2182–2189, May 2017.

[55] S. Mukherjee, A. Biswas, and K. V. Srivastava, "Broadband substrate integrated waveguide cavity-backed bow-tie slot antenna," *IEEE Antennas and Wireless Propagation Letters*, vol. 13, pp. 1152–1155, 2014.

[56] E. Abdo-Sánchez, D. Palacios-Campos, C. Frías-Heras, F. Y. Ng-Molina, T. Martín-Guerrero, and C. Camacho-Peñalosa, "Electronically steerable and fixed-beam frequency-tunable planar traveling-wave antenna," *IEEE Transactions on Antennas and Propagation*, vol. 64, no. 4, pp. 1298–1306, Apr. 2016.

[57] M. van Rooyen, J. W. Odendaal, and J. Joubert, "High-gain directional antenna for wlan and wimax applications," *IEEE Antennas and Wireless Propagation Letters*, vol. 16, pp. 286–289, 2017.

[58] D. J. Sommers, "Slot array employing photoetched tri-plate transmission lines," *IRE Transanctions on Microwave Theory and Techniques*, vol. 3, no. 2, pp. 157–162, Mar. 1955.

[59] R. Shavit and R. Elliott, "Design of transverse slot arrays fed by a boxed stripline," *IEEE Transactions on Antennas and Propagation*, vol. 31, no. 4, pp. 545–552, Jul. 1983.

[60] S. Hashemi-Yeganeh and C. Birtcher, "Theoretical and experimental studies of cavity-backed slot antenna excited by a narrow strip," *IEEE Transactions on Antennas and Propagation*, vol. 41, no. 2, pp. 236–241, Feb. 1993.

[61] C. Löcker, T. Vaupel, and T. F. Eibert, "Radiation efficient unidirectional low profile slot antenna elements for x-band application," *IEEE Transactions on Antennas and Propagation*, vol. 53, no. 8, pp. 2765–2768, Aug. 2005.

[62] Y. P. Huang and X. Z. Zhang, "A low cross-polarization stacked slot antenna backed by substrate integrated cavity," in 15^{th} *International Symposium on Antenna Technology and Applied Electromagnetics*, 2012.

[63] M. E. V. Valkenburg, *Introduction to Modern Network Synthesis.* Ed. New York: John Wiley & Sons Inc., 1960.

[64] P. Brachat and J. M. Baracco, "Dual-plarization slot-coupled printed antennas fed by stripline," *IEEE Transactions on Antennas and Propagation*, vol. 43, no. 7, p. 738–742, Jul. 1995.

[65] A. Sangster, "Optimisation of radiation efficiency for a transverse ground-plane slot in boxed-stripline," *IEE Proceedings-Microwwave on Antennas and Propagation*, vol. 141, no. 6, pp. 509–516, Dec. 1994.

[66] X. Bai, S. Qu, K. Ng, and C. H. Chan, "Sinusoidally modulated leaky-wave antenna for millimeter-wave application," *IEEE Transactions on Antennas and Propagation*, vol. 64, no. 3, pp. 849–855, Mar. 2016.

[67] P. J. Soh, S. Yan, H. Xu, and G. A. E. Vandenbosch, "A dual-band cavity antenna embedded within multiple metallic enclosures," *IEEE Transactions on Antennas and Propagation*, vol. 64, no. 5, pp. 1587–1594, May 2016.

[68] E. García-Marín, E. Márquez-Segura, P. Sánchez-Olivares, J. L. Masa-Campos, J. A. Ruiz-Cruz, and C. Camacho-Peñalosa, "Ink-jet imple-mentation of stacked-patch antenna for wireless applications," in *IEEE MTT-S International Microwave Workshop Series on Advanced Materials and Processes for RF and THz Applications (IMWS-AMP)*, 2019.

[69] R. Johnson, H. Jasik, and H. Crawford, *Antenna Engineering Handbook*, ser. McGraw-Hill handbook. McGraw-Hill, 2009.

[70] Q. Wu, R. Jin, and J. Geng, "A single-layer ultrawideband microstrip antenna," *IEEE Transactions on Antennas and Propagation*, vol. 58, no. 1, pp. 211–214, 2010.

[71] T. Ma, J. Ai, M. Shen, and W. T. Joines, "Design of novel broadband endfire dipole array antennas," *IEEE Antennas and Wireless Propagation Letters*, vol. 16, pp. 2935–2938, 2017.

[72] X. Wei, J. Liu, and Y. Long, "Printed log-periodic monopole array antenna with a simple feeding structure," *IEEE Antennas and Wireless Propagation Letters*, vol. 17, no. 1, pp. 58–61, 2018.

[73] G. Zhai, X. Wang, R. Xie, J. Shi, J. Gao, B. Shi, and J. Ding, "Gain-enhanced planar log-periodic dipole array antenna using nonresonant metamaterial," *IEEE Transactions on Antennas and Propagation*, vol. 67, no. 9, pp. 6193–6198, 2019.

[74] X. Lv, W. Yu, J. Wu, X. Luo, and Y. Ge, "Analysis and modeling of GaAs-based coupled microstrip lines," in *IEEE International Conference on Microwave Technology and Computational Electromagnetics*, May 2011, pp. 136–139.

[75] J. Kim, D. Oh, and W. Kim, "Accurate characterization of broadband multiconductor transmission lines for high-speed digital systems," *IEEE Transactions on Advanced Packaging*, vol. 33, no. 4, pp. 857–867, Nov. 2010.

[76] I. Piekarz, J. Sorocki, K. Wincza, and S. Gruszczynski, "Microwave sensors for dielectric sample measurement based on coupled-line section," *IEEE Transactions on Microwave Theory and Techniques*, vol. 65, no. 5, pp. 1615–1631, May 2017.

[77] J. G. Richings and B. Easter, "Measured odd- and even-mode dispersion of coupled microstrip lines," *IEEE Transactions on Microwave Theory and Techniques*, vol. 23, no. 10, pp. 826–828, Oct. 1975.

[78] V. Rizzoli, "Resonance measurement of single- and coupled-microstrip propagation constants," *IEEE Transactions on Microwave Theory and Techniques*, vol. 25, no. 2, pp. 113–120, Feb. 1977.

[79] T. M. Winkel, L. S. Dutta, H. Grabinski, and E. Groteluschen, "Determination of the propagation constant of coupled lines on chips based on high frequency measurements," in *Proceedings IEEE Multi-Chip Module Conference*, Feb. 1996, pp. 99–104.

[80] T. M. Winkel, L. S. Dutta, and H. Grabinski, "An accurate determination of the characteristic impedance matrix of coupled symmetrical lines on chips based

on high frequency S-parameter measurements," in *IEEE MTT-S International Microwave Symposium Digest*, vol. 3, Jun. 1997, pp. 1769–1772.

[81] U. Arz, D. F. William, D. K. Walker, and H. Grabinski, "Asymmetric coupled CMOS lines-an experimental study," *IEEE Transactions on Microwave Theory and Techniques*, vol. 48, no. 12, pp. 2409–2414, Dec. 2000.

[82] J. G. Nickel, D. Trainor, and J. E. Schutt-Aine, "Frequency-domain-coupled microstrip-line normal-mode parameter extraction from S-parameters," *IEEE Transactions on Electromagnetic Compatibility*, vol. 43, no. 4, pp. 495–503, Nov. 2001.

[83] M. Wojnowski, V. Issakov, G. Sommer, and R. Weigel, "Multimode TRL calibration technique for characterization of differential devices," *IEEE Transactions on Microwave Theory and Techniques*, vol. 60, no. 7, pp. 2220–2247, Jul. 2012.

[84] J. van der Merwe, H. C. Reader, and J. H. Cloete, "S-parameter measurements yielding the characteristic matrices of multiconductor transmission lines," *IEEE Transactions on Electromagnetic Compatibility*, vol. 40, no. 3, pp. 249–256, Aug. 1998.

[85] J. C. Tippet and R. A. Speciale, "A rigorous technique for measuring the scattering matrix of a multiport device with a 2-port network analyzer," *IEEE Transactions on Microwave Theory and Techniques*, vol. 30, no. 5, pp. 661–666, May 1982.

[86] D. E. Muller, "A method for solving algebraic equations using an automatic computer," *Mathematical Tables and Other Aids to Computation*, vol. 10, no. 56, pp. 208–215, 1956. [Online]. Available: http://www.jstor.org/stable/2001916

[87] S. Otto, A. Al-Bassam, A. Rennings, K. Solbach, and C. Caloz, "Radiation efficiency of longitudinally symmetric and asymmetric periodic leaky-wave antennas," *IEEE Antennas Wirel. Propag. Lett.*, vol. 11, pp. 612–615, Jun. 2012.

[88] ——, "Transversal asymmetry in periodic leaky-wave antennas for Bloch impedance and radiation efficiency equalization through broadside," *IEEE Trans. Antennas Propag.*, vol. 62, no. 10, pp. 5037–5054, Oct. 2014.

[89] F. Mesa, R. Rodriguez-Berral, and F. Medina, "Unlocking complexity using the ECA: The equivalent circuit model as an efficient and physically insightful tool

for microwave engineering," *IEEE Microw. Mag.*, vol. 19, no. 4, pp. 44–65, Jun. 2018.

[90] ——, "On the computation of the dispersion diagram of symmetric one-dimensionally periodic structures," *Symmetry*, vol. 10, p. 307, Aug. 2018.

[91] C. G. Montgomery, R. H. Dicke, and E. M. Purcell, *Principles of Microwave Circuits*. MIT Radiation Lab series, 1948.

[92] N. Marcuvitz, *Waveguide Handbook*, ser. IEE electromagnetic waves series. The Institution of Engineering and Technology, 1986.

[93] L. B. Felsen and A. A. Oliner, "Determination of equivalent circuit parameters for dissipative microwave structures," in *Proc. IRE*, vol. 42, no. 2, 1954, pp. 477–483.

[94] A. Weissfloch, *Elek. Nach. Tech.* vol. 19, 1942.

[95] L. Zappelli, "Equivalent circuits of lossy two-port waveguide devices," *IEEE Trans. Microw. Theory Techn.*, vol. 67, no. 10, pp. 4095–4106, Oct. 2019.

[96] E. Abdo-Sánchez, C. Camacho-Peñalosa, T. M. Martín-Guerrero, and J. Esteban, "Equivalent circuits for nonsymmetric reciprocal two ports based on eigenstate formulation," *IEEE Transactions on Microwave Theory and Techniques*, vol. 65, no. 12, pp. 4812–4822, 2017.

[97] S. Wane and D. Bajon, "Broadband equivalent circuit derivation for multi-port circuits based on eigen-state formulation," in *IEEE MTT-S Int. Micro. Symp. Dig.*, 2009, pp. 305–308.

[98] J. Lu, H. J. Ng, D. Kissinger, C. F. Jou, and L. Wu, "Design of a novel microstrip Franklin leaky-wave antenna using the eigenstate approach," *IEEE Trans. Antennas Propag.*, vol. 67, no. 7, pp. 4484–4494, Jul. 2019.

[99] L. P. Huelsman, *Circuits, Matrices and Linear Vector Spaces*, ser. Dover Books on Electrical Engineering. Dover Publications, 2013.

[100] C. Camacho-Peñalosa, T. Martín-Guerrero, J. Esteban, and J. Page, "Derivation and general properties of artificial lossless balanced composite right/left-handed transmission lines of arbitrary order," *Progress In Electromagnetics Research B*, no. 13, pp. 151–169, Jan. 2009.

[101] C. Caloz and T. Itoh, *Electromagnetic Metamaterials, Transmission Line Theory and Microwave Applications.* Wiley, New York, 2005.